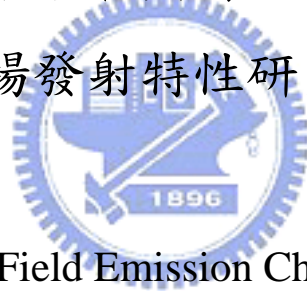# 國立交通大學

電子工程學系 電子研究所

博 士 論 文

低溫合成之奈米碳管與薄膜側向場發射子之
場發射特性研究

Study on the Field Emission Characteristics of

Low-Temperature-Synthesized Carbon Nanotubes and Thin Film Edge

Field Emitters

研 究 生：林高照

指導教授：鄭晃忠 教授

中 華 民 國 九 十 七 年 七 月

低溫合成之奈米碳管與薄膜側向場發射子之場發射特性研究

Study on the Field Emission Characteristics of Low-Temperature-Synthesized Carbon Nanotubes and Thin Film Edge Field Emitters

研 究 生：林高照　　　　　Student：Kao-Chao Lin

指導教授：鄭晃忠　　　　　Advisor：Huang-Chung Cheng

國 立 交 通 大 學

電子工程學系 電子研究所

博 士 論 文

中華民國九十七年七月

低溫合成之奈米碳管與薄膜側向場發射子之場發射特性研究

研究生：林高照　　　　　指導教授：鄭晃忠 博士

國立交通大學電子工程學系暨電子研究所博士班

摘要

在本論文中，我們主要研究標的為場發射材料與場發射元件的低溫製作方法與其場發射特性研究。為了可以均勻且低成本的將奈米碳管應用於場發射顯示器上，熱化學氣相沈積比起其他方法具有簡單且低成本的優勢，因此被認為是最有潛力的碳管成長方法之一。藉由多層結構催化金屬的使用，我們可利用熱化學氣相沈積在低溫下於玻璃基板上合成奈米碳管。多層結構催化金屬的組成包含支撐層、中間層與催化金屬，其中支撐層可以有效幫助催化金屬均勻分散避免其聚合成過大的粒子，而中間層除了幫助催化金屬保持均勻分散外還可以促進碳原子的析出進而形成石墨層結構，由實驗結果可以發現，當中間層材料為鉻與鈦時，奈米碳管的型態是最佳的，同時其表現出絕佳的場發射特性：當所施加的電場強度為 6 V/μm 時，其場發射電流密度分別可達到 18.24 與 28.60 mA/cm^2，遠超過應用上所需的數值。除此之外，碳管的場發射特性與外觀也會受到製程條件的影響，如反應氣體流量。藉由逐步改變與控制製程氣體的流量比例，我們得到一組最佳的成長參數，當製程氣體乙烯、氫氣與氮氣分別為 125、10 與 1000 sccm 時，奈米碳管具有最好的電性表現：。實驗結果也說明場發射特性與碳管的結晶性有

相當程度的關係，隨碳管結晶性增加其場發射電流的穩定性也跟著增加。同時，碳管成長的活化能圖說明多層結構催化金屬具有較低的成長活化能，因此相較於其他催化金屬可以有效於低溫下催化碳管成長。

接下來，為有效改善電子束發散的現象，我們提出一基於低溫成長奈米碳管的自聚焦場發射元件，此一元件結構不需要額外的聚焦閘極而是採用將電極設計成一雙條狀電極且平行於場發射區域旁，不同於傳統元件結構具有被閘極包圍的場發射區域，自聚焦閘極結構因為條狀電極只鄰近單一邊的碳管，因此會造成異於傳統的非對稱的場發射區，結合此兩個非對稱場發射區域，場發射電子將於陽極板上形成一重疊的顯示區塊。從實驗結果來看，此一新穎閘極結構可以有效控制電子束軌跡且於陽極板上形成較小的發光區。模擬結果說明相較於傳統沒有聚焦結構的元件，當採用自聚焦閘極結構時陽極板上的場發射區域可由 622 微米縮小至 232 微米，同時實際螢光版上的發亮區域也顯示出相同的實驗結果，因此證明自對焦閘極結構可簡單且有效地控制電子束於陽極板上的大小。

最後，我們提出兩種形成次微米間距的方法並將其應用於製作具有低超作電壓的薄膜側向場發射子。元件可藉由薄膜沈積與濕式蝕刻完成，且電極間距可由蝕刻時間來控制，次微米間距形成於射極與集極間，當其間距為 200 奈米時，元件的啟始場發射電壓可以降低到 48 伏特。此外，為了進一步更可靠地製作此一次微米間距，我們提出一類平面側向場發射元件結構，此元件的電極間距可以藉由薄膜的厚度來調變，不同的膜厚將形成不同的間距大小。另外，經由一形成製程改變場發射子的表面型態，形成較高的表面粗糙度，元件的場發射特性可明顯的改善。當控制電極間距此一膜層的厚度為 200 奈米時，經過形成製程處理的元件，其場發射啟始電壓值可降低到 9 伏特。

Study on the Field Emission Characteristics of Low-Temperature-Synthesized Carbon Nanotubes and Thin Film Edge Field Emitters

Student: Kao-Chao Lin   Advisor: Dr. Huang-Chung Cheng

Department of Electronics Engineering & Institute of Electronics

College of Electrical Engineering and Computer Science

National Chiao Tung University

ABSTRACT

In this thesis, low-temperature synthesis processes of emitter materials and devices as well as their field emission characteristics were investigated. For their application in field emission displays, carbon nanotubes (CNTs) should be employed uniformly on glass substrates in order to reduce the manufacture cost. Thermal chemical vapor deposition (t-CVD) had the merits of simplicity and cost efficiency in fabrication and large scalability as compared with other techniques. Therefore, it seemed to be a potential method for synthesizing nanotubes on glass substrates. Multilayer catalysts utilized in thermal CVD systems showed a remarkable catalytic ability for growth of CNTs at low temperatures. The multilayer catalysts were composed of supporting layer, interlayer, and catalytic metal. A supporting layer had the functionality in uniformly distribution of catalytic nanoparticles, meanwhile preventing their agglomeration. Besides improving the uniformity of catalytic particles, interlayers were able to enhance the precipitation of carbon atoms, thus

iii

resulting in the formation of graphite sheets. According to the results of experiment, while the interlayers were chromium (Cr) and titanium (Ti), carbon nanotubes showed the better morphologies and field emission performances: field emission current density of 18.24 and 28.60 mA/cm^2 for Cr and Ti, respectively, at the electric field of 6 V/µm. Moreover, field emission characteristics of nanotubes can be improved by optimizing the synthesis conditions, i.e. reaction gas flow rates. According to the results of experiments, an optimal synthesis condition formed of reaction gases was 125, 10, and 1000 sccm for C_2H_4, H_2, and N_2, respectively. The morphology and field emission performance also showed a significant relationship corresponding to the crystallinity of nanotubed analyzed by Raman Spectra. A high stability of emission current was correlative with a better crystallinity. The growth activation energy calculated based on the dependence of nanotube length versus temperature revealed the fact that CNTs synthesized with a multilayer catalyst displayed a lower value than single or binary catalysts.
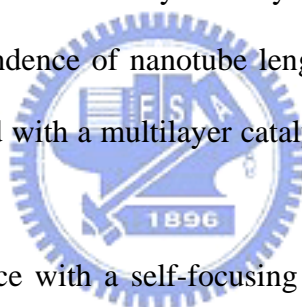
Next, a CNT-based device with a self-focusing gate structure was proposed to obviate the issue of electron beam divergence. Without additional focusing electrodes, the self-focusing gate structure employed a pair of gate electrodes parallel with the vicinity of emitters, which resulted in an asymmetric emission area as compared with the conventional gate structure. Therefore, electrons emitted from the emitters gave rise to an overlapping region on the anode plate so that a reduction of spot size had been achieved. According to the simulation results and luminescent images, this self-focusing gate structure had a well controllability on the trajectory of electrons, and therefore showed a smaller luminescent spot size than the conventional one. Because of the overlapping of electron beams, the luminescent spot sizes could be remarkably reduced to 232 µm in x direction as compared with 622 µm for the conventional gate structure which had a serious issue of beam divergence. As a result,

the self-focusing gate structure manufactured with a simple process can produce well-focused electron beams for the application in FEDs.

Finally, two simple techniques of creating sub-micron gaps were proposed for thin film edge emitters in order to realize the feasibility in low-voltage operation and simplicity in fabrication. A lateral field emitter was manufactured by thin film deposition and wet etching processes. The spacing was determined by the lateral etching distance formed during etching stage. By controlling the duration of etching, the distances between emitters and collectors were well defined in submicron ranges. Device performance showed a low turn-on voltage of 48 V at an emission current of 100 nA as the emitter-collector spacing was 200 nm. In addition, for creation of submicron gaps in a more robust way, a novel quasi-planar thin film field emitter was proposed and fabricated utilizing the similar idea. The spacing between the emitter and collector could be well controlled via the thickness of Cr layers, which created submicron gap. A forming process caused an increased surface roughness of emitters and resulted in a higher field enhancement factor, which showed better field emission characteristics. The quasi-planar field emission diode with the first Cr layer of 200 showed a low turn-on voltage of 9 V at the current level of 100 nA.

Contents

Chapter 1   Introduction

Chapter 2　　Investigation of Carbon Nanotubes Synthesized at Low Temperatures Using Multi-layered Catalytic Films

Chapter 3　　Improvements of Morphologies and Field Emission Characteristics for Carbon Nanotubes by Modifying the Gas Flow Rate Ratios

Chapter 4   Fabrication and Characterization of Carbon Nanotube Field Emission Devices with a Self-Focusing Gate Structure

Chapter 5   Fabrication and Emission Characteristics of Chromium Thin Film Edge Emitters

Chapter 6   Summary and Conclusions

Chapter 7   Future Prospects

References

Tables

Figures

Vita

Publication Lists

Table Lists

Figure Captions

Chapter 1

xiv

Chapter 3

Chapter 4

Chapter 5

Chapter 1

Introduction

1.1 Overview of Vacuum Microelectronics

The emergence of vacuum tubes could trace back to the observation of emission current by the research team of Thomas Edison while they conducted the experiment of evacuated light bulb. The phenomenon that the filament in vacuum environment could induce emission current did not attract much attention because of no potential application until the invention of the vacuum tube diode by J. Ambrose Fleming in 1904. Afterward, the triode vacuum tube amplifier invented by Lee De Forest in 1906 launched the electronics industry since it marked the transition of the vacuum tube from a passive to an active device. With the combination of the control grid, the vacuum tube became the key element in the emerging discipline of electronics, especially for the radio stations, and the great quantity of requirement for vacuum tubes emerged in World War 1 owing to the military concern. In 1916, the tetrode, with an additional grid compared to triode, further made the remarkable advancement for the vacuum tube in the use of audio frequency power amplifier. In 1926, the pentrode tube, utilizing a third grid, was designed to overcome the problem of negative resistance characteristics caused by secondary emission from the anode being attracted to the positively charged screen in tetrode. The fact that the suppressor grid provided a means to prevent the secondary emissions from reaching the screen grid allowed the full capabilities of the vacuum tubes to be realized in the application of power amplifier. Despite its numerous applications in research and

communications, the vacuum tube had many drawbacks. It was extremely fragile, had a limited life, was fairly large, and required a lot of power to operate its heating element.

Recent development of vacuum microelectronics started in 1928, when R. H. Fowler and L. W. Nordheim published the theory of field emission, which described the relationship between the emission current density and the applied electric field based on electron tunneling through metal surfaces [1.1]. According to Fowler-Nordeim theory, a highly applied electric field of approximately 10^3 V/µm is necessary for electrons tunneling through the triangular barrier at the metal surfaces. Therefore, there was no remarkable advance in application until 1968, when C. A. Spindt published the work about a fabrication method to create small dimension metal cones by thin film vacuum deposition techniques [1.2]. Because of the outstanding properties of Spindt cathode, many researchers had devoted to the work on the refinement, characteristics, and applications of the Spindt emitters since the late 1960s.

In 1947, William Shockley, Walter Brattain, and John Bardeen successfully invented the first point-contact bipolar transistor in Bell Lab [1.3]. After that, the concepts of integrated circuits (ICs) subsequently proposed by Jack Kilby worked for Texas Instrument and Robert Noyce worked for Fairchild Semiconductor in 1960s. The invention of solid-state devices and concepts of ICs revealed the unpredictable potentials of solid-state electronics and, therefore, entered a new era [1.4-1.5]. In fact, "vacuum state" devices have potentially a number of outstanding advantages with respect to the presently much popular "solid state" devices, including fast drift velocity and associated transit time, radiation hardness and temperature insensitivity, and higher output power. For example, the saturation drift velocity is limited to less than 3×10^7 cm/sec in all solid-state devices whereas the saturation electron velocity in

vacuum is limited to 3×10^{10} cm/sec theoretically and practically to about 6-9×10^{8} cm/sec [1.6]. The faster drift velocity of vacuum devices as compared with the solid-state devices results from less scattering in the channel of vacuum devices. Additionally, because there is no medium in the channel of vacuum devices, temporary and permanent radiation effects should be neglected and the effects of temperature on performance are essentially none exists. The comparisons between vacuum microelectronics and solid state devices are shown in Table 1.1.

Because of the surging worldwide interest in vacuum microelectronics and their applications, the first International Vacuum Microelectronics Conference (IVMC) was held in 1988 for the scopes providing a meeting for researches to gather and exchange information about all aspects of the field, including emission device physics, materials, and fabrication processes, etc. So far, much effort had been put into the work about improving the characteristics of emitters, such as lower operation voltages, higher emission current density, and longer lifetimes. Different cathode materials and device structures also have been proposed for further advancing the technology.

1.2 Theory of Field Emission

In semiconductor physics, the thermionic-field emission and field emission are both important mechanisms for the transport of electrons over the potential barrier between the metal and the semiconductor. In Schottky barriers on highly-doped silicon crystal, the depletion region is so narrow that the electrons can tunnel through the barrier near the top where the barrier is small enough which is called thermionic-field emission. On the other hand, in a degenerate silicon crystal, the electrons can tunnel through the energy barrier even near the Fermi level which is

3

called field emission. It can be found that the tunneling in thermionic-field emission process requires electrons with higher energy than in field emission process. The emission of electrons from a surface of conductive material such as metal or semiconductor into a vacuum environment at an extremely high electric field is also a quantum mechanical tunneling phenomenon. The energy diagram of a metal-vacuum system without external electric field is displayed in Fig. 1.1(a). As shown in Fig. 1.1(b), the vacuum level is bent at extremely high electric field and the energy barrier between the surface of metal and the vacuum become so narrow that the electron can tunnel through it easily, even at very low temperature. Here W_0 is the energy difference between an electron at rest outside the metal and an electron at rest inside the metal, whereas W_F is the energy difference between the Fermi level and the bottom of conduction band. The work function Φ defined as $\Phi = W_0 - W_F$. When an external electric field is applied, the vacuum level is reduced and the energy barrier at the surface of conductive metal or semiconductor becomes thinner. Then an electron having energy "W" has a finite probability of tunneling through the surface barrier. Fowler and Nordheim derive the famous Fowler-Noedhiem equation (1.1) as below [1.7-1.8]:

$$J = \frac{aE^2}{\phi t^2(y)} \exp\left[\frac{-b\phi^{\frac{3}{2}}v(y)}{E}\right] \tag{1.1}$$

where J is the current density (A/cm^2), E is the applied electric field (V/cm), Φ is the work function (eV), $a = 1.56 \times 10^{-6}$, $b = -6.831 \times 10^{-7}$, $y = 3.7947 \times 10^{-4}E^{1/2}/\Phi$, $t^2(y) \doteqdot 1.1$ and $v(y)$ can be approximated as [1.9]

$$v(y) = \cos(0.5\pi y) \tag{1.2}$$

or

$$v(y) = 0.95 - y^2 \tag{1.3}$$

Typically, the field emission current is measured as a function of the applied voltage V.

4

Substituting relationships of J = I/α and E = βV into Eq. 1.1, where α is the emitting area and β is the local field enhance factor at the emitting surface, following equation can be obtained

$$I = \frac{A\alpha\beta^2 V^2}{\phi t^2(y)} \exp\left[\frac{-bv(y)\phi^{3/2}}{\beta V}\right]$$ (1.4)

Then take the log. Form of Eq. 1.4

$$\log\left(\frac{I}{V}\right) = \log\left[1.54\times10^{-6}\frac{\alpha\beta^2}{\phi t^2(y)}\right] - 2.97\times10^7\left(\frac{\phi^{3/2}v(y)}{\beta V}\right)$$ (1.5)

from Eq. 1.5, the slope of a Fowler-Nordhiem (F-N) plot is given by

$$S \equiv slope_{FN} = 2.97\times10^7\left(\frac{\phi^{3/2}}{\beta}\right)$$ (1.6)

The parameter β can be evaluated from the slope S of the measured F-N plot if the work function Φ is known

$$\beta \cong -2.97\times10^7\left(\frac{\phi^{3/2}}{S}\right)$$ (1.7)

Emission area α can be subsequently extracted from a rearrangement of Eq. 1.5

$$\alpha = \left(\frac{I}{V^2}\right)\frac{\phi}{1.4\times10^{-6}\beta^2}\exp\left(\frac{=9.89}{\sqrt{\phi}}\right)\exp\left(\frac{6.53\times10^7\phi^{3/2}}{\beta V}\right)$$ (1.8)

For example, electric field at the surface of a spherical emitter of radius r concentric with a spherical anode (or gate) of radius (r + d) can be represented analytically by

$$E = \frac{V}{r}\left(\frac{r+d}{d}\right)$$ (1.9)

Though a realistic electric field in the emitter tip is more complicated than the equation above, we can multiple Eq. 1.9 by a geometric factor β' to approximate the real condition.

$$E_{tip} = F(r,d) = \beta' \frac{V}{r} \left(\frac{r+d}{d} \right) \tag{1.10}$$

Where r is the tip radius of emitter, d is the emitter-anode (gate) distance, β' is a geometric correction factor [1.9], and F(r,d) is a function of r and d.

For a very sharp conical emitter tip, where d>>r, E_{tip} approached to β'(V/r). Moreover, for r>>d, E_{tip} approaches to β'(V/d) which is the solution for parallel-plate capacitor and for a diode operation in a small anode-to-cathode spacing.

As the tip radius of the gated field-emission array is very small, Eq. 1.10 can be approximated as:

$$E_{tip} = \beta' (\frac{V}{r}) \tag{1.11}$$

Combining E= β V and Eq. 1.11, we can obtain the relationship:

$$E_{tip} = \beta V = \beta' (\frac{V}{r}) \text{ and } \beta' = \beta r \tag{1.12}$$

The tip radius r is usually in the range from a few nm to 50 nm, corresponding to the parameter β' ranging from 10^{-1} to 10^{-2}.

Besides, transconductance g_m of a field emission device is defined as the change in anode current due to a change in gate voltage [1.10].

$$g_m = \frac{\partial Ic}{\partial Vg} \bigg|_{ve} \tag{1.13}$$

Transconductance of a field-emission device is a figure of merit that gives as an indication of the amount of current charge that can be accomplished by a given change in gate voltage. The transconductance can be increased by using multiple tips or by decreasing the cathode-to-gate spacing for a given cathode-to-anode spacing.

1.3 Applications of Vacuum Microelectronics

In past decades, vacuum electronic devices have been developed by reducing the device scale down to micro-size with the improved manufacturing technologies and equipments. Due to the outstanding properties of vacuum microelectronics, there are several potential applications attracting worldwide attention, including field-emission displays (FEDs) [1.11-1.15], microwave amplifiers and generators [1.16-1.18], ultra-fast switches, intense electron/ion sources [1.19-1.20], electron source of scanning electron microscope (SEM) and e-beam lithography, micro-sensors [1.21-1.22], and devices needed to work in hostile environment. Among these applications, FEDs seem most likely to have substantial commercial impact due to the emerging requirement in flat panel display industry.

1.4 Field Emission Displays
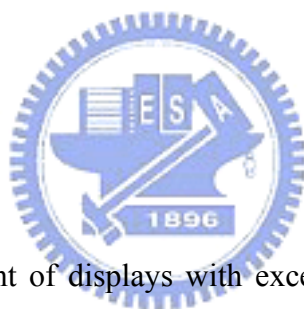
Owing to the requirement of displays with excellent image qualities and large image size, the development of flat-panel displays (FPDs) is one of the most important industries in the world now. Based on the operation physics of display devices, the flat panel displays generally can be categorized into two types: self-emissive and non-emissive types. The non-emissive type can not produce luminous light by itself, which should combine with other lighting elements for displaying images, such as active matrix-liquid crystal displays (AMLCD) which need a back light module. In contrast, the self-emissive type can produce graphic vision by itself, and there are many technologies announced worldwide, including plasma display panel (PDP), organic light Emission display (OLED), light emission diode (LED), polymer light emitting diode (PLED), electro-luminescence display (EL display), vacuum fluorescent display (VFD), Flat cathode-ray tube (CRT), and field

emission display (FED). Among these display technologies, FEDs were considered to be one of the most promising technologies that will be the major display technique in the near future due to its outstanding performance.

The idea of the field-emission display was first proposed and described in U.S. patent 3,500,102 issued in 1970 by Crost, Shoulders, and Zinn. However, the first monochrome prototype was demonstrated in Japan Display until 1986 by a group from LETI [1.23] and the first color display (6 inch) was demonstrated in 1993 by Pixel/LETI [1.24]. To know the history of field-emission displays better, more relative events of field-emission displays were listed in Table 1.2.

The operation of FED is similar to that of CRT, in which phosphor is excited by a stream of electrons traveling through a vacuum. In contrast with CRT which employed electron guns, FED is matrix-addressed by an array of emitters where electrons emitted to a phosphor anode plate that is located in close proximity (0.2-2 mm) to the cathode plate. It can provide an image with high resolution and avoid the distortion of image caused by external electric or magnetic field. The figures of field-emission displays and traditional CRTs shown in Fig. 1.2 illustrate the differences between these two displays schematically. The advantages of field-emission displays over other flat panel displays are higher brightness, better viewing angle, lower power consumption, less radiation, and larger operating range of temperature. The comparison of the characteristics for several flat-panel displays is listed in Table 1.3.

Generally, the field-emission displays could be classified into two main categories based on the operation configuration: diode and triode structures. As shown in Fig. 1.3(a), the field emission current is emitted from the cathode to the anode in the diode configuration, and the emission current is controlled by the voltage applied on the anode electrode. It has the merit of simple structure as compared with the

triode structure. However, the driving voltage required to show a grayscale is high so that it is costly and complex for the design of driving circuit. By comparison, the triode configuration, shown in Fig. 1.3(b), utilizes an extraction gate proximity to the emitter array so as to extract electrons from the cathode with a relative lower driving voltage. The emission current density from the cathodes to the anode is controlled by the voltage biased to the gate electrode. The electrons on the tip of emitters are extracted by the electric field induced from the gate voltage and parts of them are attracted by the electric field induced from the anode voltage. In the triode configuration, a much lower driving voltage is required to realize a grayscale than the diode structure. In addition, the field emission device with a triode structure has the merits of luminous efficiency, emission stability, and uniformity over large areas compared with diode one [1.25].
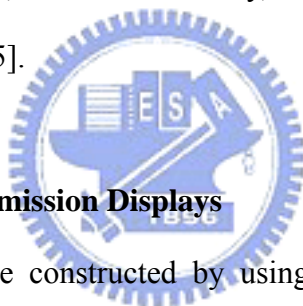
1.4.1 Technologies of Field Emission Displays

Fundamentally, FEDs are constructed by using three elemental technologies: micro-fabrication technology for the emitter arrays, optoelectronic technology for the anode plates, and vacuum technology for the packaging. Among these technologies, the performance of FEDs is determined by the technology of the cathode plates by which the electrons are generated. So far, researchers have put their attention to the development of new cathode structures for more robust in manufacture and application, such as Spindt-type field emitters, silicon tip field emitters, metal-insulator-metal (MIM), ballistic-electron surface-emitting device (BSD), ferroelectric emitters, and planar field emitters including surface conduction electron emitter (SCE) and edge field emitters. Besides, new cathode materials, such as diamond, diamond-like carbon, and carbon nanotubes, had been intensively studied for their potential as attractive electron sources. Many companies like Samsung of

Korea, ITRI of Taiwan, NEC of Japan, etc. have taken a lot of resources to research and develop the technology of field-emission display, and many amazing achievements had been announced in publications.

1.4.1.1 Cathode Structures

1.4.1.1.1 Spindt-Type Field Emitters

The original idea for the development of microfabricated field emitter array (FEA) came from Ken Shoulders and Dubley Buck at Massachusetts Institute of Technology (MIT) in the 1950s [1.26] but it was realized 40 years later beyond the reach of technology. The basic concepts were brought by Shoulders to the Stanford Research Institute (SRI) to develop the microfabricated vacuum integrated circuits [1.27] and he also proposed a thin display tube base on matrix-addressed arrays of microfabricated field emitters, the field-emission displays (FEDs) [1.28]. As part of Shoulder's program, Capp Spindt proposed a smart method to form the arrays of miniature metal field emitter cones in microsize cavities with an surrounded extraction gate [1.29]. The cathodes of Spindt field emitter arrays are fabricated by forming metal cones on the conducting cathode electrodes as electron emitters by using thin film deposition processes. The metal cone is surrounded by an accelerating grid electrode (gate) which is insulated from the conducting cathode electrode by a dielectric layer. The cathode array features like a source of electrons with a positive voltage bias applied to the surrounding gate electrode. The micrographs of Spindt field emitter arrays taken by SEM are shown in Fig. 1.4 [1.27]. Although the Spindt type field emitter array provide a method to realize sharp metal tips with extraction gate electrode, it still has some drawbacks of needing huge metal depositing equipment, complex processes, requirement of high driving voltage, and reliability issues.

1.4.1.1.2 Silicon Tip Field Emitters

Sharp silicon tips of field emitter array are fabricated from crystalline silicon wafer by using oxidation processes to obtain silicon tips with small radius [1.30]. The processing steps of forming the silicon tips can be realized via standard semiconductor processes. According to some researches, the emission current from silicon tips can reach as high as 10 µA/tip [1.31]. Furthermore, crystalline silicon is a good material for the investigation of field emission array because of its great electronic, crystalline, mechanical properties, and availability. With well-developed techniques and equipments for fabrication, the apex radii of fabricated silicon tips can be bellow 10 nm with small deviation. One of the methods to form silicon tips is utilizing the orientation-dependant etching (ODE) which can form a convex pyramids structure [1.32-1.33]. Another way of fabricating silicon tips array is the oxidation sharpening process which is also the most used method in creating sharp tips on silicon wafers [1.34]. However, the array of silicon tips still has the problem of local failure due to high emission current density. Local heating at the silicon tips due to high emission current passing through can result in a local evaporation of silicon tips to reduce its sharpness and, therefore, cause a gradual degradation in emission current. Moreover, the requirement of driving voltage is still too high for the applications of field-emission devices due to its high work function.

1.4.1.1.3 Metal-Insulator-Metal Emitters (MIM)

Metal-insulator-metal cathodes are a kind of thin film tunneling device proposed by Mead in early 1960s and has been studied by many researchers [1.35-1.40]. Due to the stack structure, the buried cathode of MIM devices is less contamination and the electrons tunnel through interfacial Schottky barriers instead of surface barriers. This

device consists of a thin insulating film (e.g. Al_2O_3) sandwiched between two metal electrodes, as shown in Fig. 1.5(a). The ultra-narrow insulating film allows the tunneling trough of electrons when a moderate electric field is applied across the layer. The energy diagram in Fig. 1.5(b) shows that the tunneling electrons are injected from the negative electrode (the emitter) through the insulating layer into the positive electrode (the gate) as hot electrons and are detected as diode current I_b. Part of the electrons have sufficient kinetic energy to overcome the surface energy of the Au and emit into the vacuum, which are collected as an emission current I_e. However, most of the tunneling electrons lose their kinetic energies while they pass through the structure due to scattering events in both the insulator and the gate metal. It is important to notice that the MIM structure requires a very precise control over the thickness of film to even atomic scale and the roughness of film is also very critical which can cause a very significant fluctuations in emission current and emission uniformity.
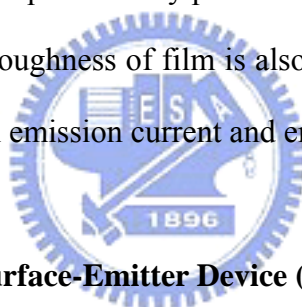
1.4.1.1.4 Ballistic Election Surface-Emitter Device (BSD)

In 1998, a novel cold-cathode technology based on a nanocrystallized polysilicon (NPS) layer was reported by the authors [1.41]. The electron emission characteristics strongly suggest that electrons injected into the NPS layer are transported quasi-ballistically [1.42]. It showed various excellent characteristics as compared with conventional FEDs [1.43] and it was termed a ballistic electron surface-emitting display (BSD). The device structure is schematically illustrated in Fig. 1.6. A non-doped polysilicon layer formed by a plasma-enhanced chemical vapor deposition (PECVD) technique was anodized in a solution of HF and ethanol under the illumination of tungsten lamp in order to form the NPS layer. After anodization, thin SiO_2 layers on the surface of Si nanocrystallites were created by an electrochemical oxidation (ECO) technique. It was also shown that the BSD had excellent thermal

stability and a frit sealed model was fabricated [1.44-1.45]. However, the oxide charging effect results in the degradation of device performance, and damage of thin oxide layer often takes place while the current density is large.

1.4.1.1.5 Ferroeletric Emitters

About 40 years ago, it has been observed that electrons emitted from the surfaces of ferroelectric materials during polarization reversal [1.46-1.47]. It was recognized that the polarization induces macroscopic charge separation on the two opposite surfaces of ferroelectric samples. As shown in Fig. 1.7, the screening charges are developed to compensate the net charges. A fast reversal (about sub-microseconds) of the polarization results a large electric field that ejects the electrons from the negative charged surface. By contrast, no external extraction field is required to overcome the surface work function to obtain electrons emission from ferroelectric emitters [1.48]. The emission depends on the polarization fields within the ferroelectric material and only excitation energies such as electrical, optical, thermal or mechanical energies are required to overcome the coercive fields. Ferroelectric emission is thus a transient unipolar effect generated from non-equilibrium charged ferroelectric surface. Ferroelectric cathodes have very robust surfaces that may be exposed to air and operated in poor vacuum conditions (up to 10^{-2} torr) or even in plasma. However, many issues in ferroelectric emissions such as polarization fatigue during multiple fast switching, emission current stability, and domain structure aging are still needed to be overcome before those envisioned devices could be realized.

1.4.1.1.6 Planar (Lateral) Field Emitters

Planar field emitters, small in device size, had the merits of design versatility and low operation voltage, and therefore showed a potential in vacuum microelectronics,

especially, for high frequency application. Besides, owing to the simplicity in device structure and operation in low voltage, the planar also attract much interest in the application of field emission displays, such as surface conduction electron emitter (SCE) and edge field emitters.

◆ **Surface Conduction Electron Emitters (SCE)**

Surface conduction emission is the phenomenon that electrons are emitted from a cathode when electric current flows through the cathode in parallel with the cathode surface [1.49]. It has attracted a great deal of attention since a 10-inch full color display incorporated a thin film PdO cathode based on the surface conduction emission mechanism was built by the researchers at Canon in Japan [1.50]. The device structure with two ultrafine PdO film as cathode and gate electrodes from top view is demonstrated in Fig. 1.8(a). The forming process of the gap between cathode and gate electrodes is to apply a voltage between two electrodes so that an electric current with high density flows through the PdO film in parallel with the surface. The thin film generates Joule heating when the electric current passing through and cause a fissure of nano scale between two electrodes. The fissure where be spatially discontinuous but electric continuous which causes field emissions because of high fields established across the cracks along the surface. The emitted electrons can be collected by the anode spaced apart from the surface of cathode after multiple scatterings on the cathode, as shown in Fig. 1.8(b). Due to the nanosize of the gap between cathodes and gates, the driving voltage can be greatly suppressed to several decades volt. The uniformity of emission current from device to device is also good resulting from the uniform PdO film. However, the emission current from cathode to anode is still low due to the fact that most of the emitted electrons are collected by the gate electrode merely 10 nm apart from the cathode.

◆ **Thin Film Edge Emitters**

In contrast to SCE formed by thick film techniques, the thin film edge emitters were fabricated mainly based on the thin film deposition process. Similar to the device structure of SCE, the emitter and collector electrodes were posited in the same horizon between which a submicron gap was created. So far, many techniques such as electron beam lithography (EBL), focus ion beam (FIB), and chemical mechanical polish (CMP) [1.51-1.53], were employed to form a small spacing across electrodes. Nevertheless, the throughput is poor and there is a lack of scalability for large area.

1.4.1.2 Cathode Materials

Fabricating field emission cathodes with low operation voltage, high emission current, excellent stability and good reliability is crucial to commercialize the field emission display. According to the F-N equation, the performance of emission devices could be improved with novel cathode materials in terms of aspects: the work function ϕ of the cathode material must be as low as possible and the field-enhancement factor β and emission area α should be as large as possible.

1.4.1.2.1 Diamond and Diamond-Like Carbon (DLC)

Diamond is one of the main crystalline allotropes of carbon, which is formed in an sp^3 tetrahedral bonded cubic structure. Due to its negative work function, diamond possesses a very small barrier for its electrons to leave the surface and emit into the vacuum environment. When the surfaces of diamond are terminated with hydrogen atoms, the electron affinity, which is a measured energy barrier that electrons must overcome to escape from the surfaces of diamond into vacuum, can become negative

[1.54]. Moreover, the diamond surfaces are chemically inert and mechanically strong. Therefore, diamond is considered a very promising material of the electron emitters in vacuum microelectronics. Unfortunately, the conductivity of diamond is not good, and thus the maximum emission current from the diamond surface to the vacuum environment is limited. Additionally, the process temperature for diamond to be deposited via chemical vapor deposition is also usually higher than 700 $^\circ$C. It makes the diamond electron emitters difficult to be fabricated on the glass substrates.

Diamond-like carbon (DLC) is another particular interesting material of three dimensional network of sp^3 and sp^2 bonded carbon atoms [1.55-1.57]. For its good field emission properties and lower deposition temperature than diamond, DLC attracted a lot of interesting from many researches. Depending on the deposition conditions, the ratio of hydrogen carbon (a-C:H) and hydrogen-free carbon (a-C) can be altered in the DLC. It also means that different portions of sp^3 and sp^2 bonding can be achieved to dictate the field emission properties [1.58-1.59]. It is interesting that the emission properties of these amorphous carbon or DLC improve with increasing sp^3 content, while those of diamond materials deteriorate. It suggests that there is an optimal ratio of sp^3 and sp^2 bonding in order to obtain emitters with lowest turn-on field. However, the process of synthesizing the DLC is complex and sensitive to the growth conditions. In addition, the emission site density of DLC is poor for the application in FEDs.

1.4.1.2.2 Carbon Nanotubes

Carbon nanotubes had attracted a great deal of attention since its first observation in 1991 by Iijima [1.60]. Generally, they can be classified into single-walled nanotubes (SWNTs) and multi-walled nanotubes (MWNTs) depending on their fine structures. Due to their high aspect ratio, strong mechanical strength, good thermal

conductivity, and inert chemical properties, CNTs are recognized as a very promising material of electron emitters. From the report of De Heer, the emission current density over 100 mA/cm^2 is measured from a partially aligned CNTs film prepared by drawing nanotube suspensions through 200 nm pore ceramic filters [1.61]. It has also been reported in many other researches that CNTs can provide a high emission current density [1.62-1.63].

So far, most nanotubes could be synthesized via three techniques, including arc discharge [1.64], laser ablation [1.65], and chemical vapor deposition (CVD) [1.66]. The arc discharge system employed two carbon electrodes kept in a close distance in helium (He) ambience for igniting the phenomenon of arc discharging, and thus CNTs could be grown inside the cathode electrode with the aids of carbon source evaporated form anode electrode. The CNTs synthesized by using arc discharge are usually in bundles and need to be released by ultrasonic cleaner and particular etching solution. The laser ablation system applied a laser source to vaporize a graphite target in a chamber, and small carbon molecules or atoms condense quickly to form large clusters and then react with the catalyst to form CNTs as the vaporized graphite cooled rapidly. However, the arc discharge and laser ablation systems have the drawbacks of high thermal budget, low throughput, and non-uniformity in synthesis. In contrast, CVD system appears to be a good technique in synthesis of CNTs for its simplicity and scalability. The process of synthesizing CNTs in chemical vapor deposition system includes heating a catalytic material at high temperature and flowing hydrocarbon gas through the reacting chamber for a period of time. With the aids of catalytic particles of transition metals, such as iron (Fe), nickel (Ni), or cobalt (Co), the carbon atoms precipitate from the super-saturated nanoparticles and form tubular carbon solids in sp^2 bonding. Therefore, recently many researchers have devoted themselves to the development of CVD techniques for synthesis of CNTs in

pure quality and high quantity.

1.5 Motivation

For the application of flat panel displays, large-area and cost-effective manufacture processes are essential for the profits of manufacturers. Glasses, naturally containing silica as a main component, could provide sufficient mechanical strength for fabrication processes, and seems to be a good candidate for supporting substrates. However, the softening point of glasses is about 580℃, which limits the fabrication processes that should be carefully designed so as to eliminate the issues of bending or cracking.

Carbon nanotubes (CNTs) having superior properties, such as high aspect ratio, high thermal and electrical conductivity, and chemical inertness, have been considered as potential cathode materials for field emission. Nowadays, nanotubes can be synthesized via three methods, including arc discharging, laser ablation, and chemical vapor depositions (CVD). The former two methods could not directly form nanotubes on the glass substrates due to their high temperature processes and poor uniformity. Therefore, CVD, which can directly and selectively grow nanotubes at designate area, is supposed to be a promising technique for the application of CNT-FEDs in large area. Current CVD systems could be divided into two categories: plasma-based CVD, and thermal CVD (t-CVD). The plasma-based CVD, including PECVD, MPCVD, and ECR-CVD, must be consisted of a vacuum environment for igniting and sustaining the plasma, and therefore the instruments is complex and costly in design. On the other hand, the thermal CVD system could be operated at atmospheric ambient, that is, cost effective and higher throughput. However, as compared with PECVD, t-CVD

could not provide sufficient growth rates of nanotubes at low temperatures because of the low reactivity of processing gases. Thus, the substrate typically was required to heated up to higher temperatures approximately $600°C$ or more to effectively synthesize nanotubes in thermal CVD system. Such high temperatures were not compatible with temperature-sensitive processes and materials, preventing the utilization of glass substrate. Therefore, we employ multilayer catalysts to provide high catalytic activity for synthesis of nanotubes at low temperatures in thermal CVD system and investigate the correlative growth mechanism. Furthermore, the morphologies and field emission characteristics are also improved by modifying process conditions comprising different flow rate ratios of reaction gases.

Because lower turn-on voltage is necessary to reduce the cost of driving circuits of field emission displays, the triode devices fabricated with an extraction interposed between cathode and anode plates is demonstrated to be an essential technique for realizing commercial products. Nevertheless, the divergence of electron beams is a serious problem as the field emission devices operate in triode configuration. For large distances that are generally necessary to avoid arcing phenomenon as phosphors are biased with high operation voltages at anode plates for high luminescent efficiency, the electron beams are easily spreading and cause inevitable cross-talking noises between neighboring pixels. Therefore, much effort has been made to introduce the focusing electrodes which are negatively biased with respect to the extraction gates for modifying the electrical potential around the emitters so as to control and focus the trajectory of the emitting electrons. These focusing electrodes utilized in combination with the triode structure gave rise to an increasing cost due to the complexity in manufacturing processes. In order to simplify the manufacture process, a new mechanism for controlling the beam trajectory is proposed, and the focusing structure was fabricated to characterize the device performance.

Additionally, planar field emitters have the low driving voltages as compared with other cathode structures due to the sub-micron spacing between emitters and collectors. Moreover, the device structure is simple and possesses the advantages in design versatility. However, most of planar field emitters are manufactured with complex processes, such as creation of sub-micron gaps via focus ion beam (FIB), or via electron beam lithography (EBL). Thus the throughput of fabrication is low, and the application is limited as well. For obviating the issue mentioned above, two kinds of manufacture processes are proposed for simplicity in fabrication of high performance planar field emitters.

1.6 Thesis Organization
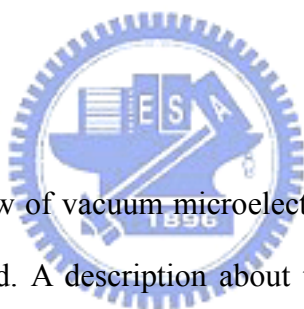
In chapter 1, the overview of vacuum microelectronics and basic theory of field emission were first introduced. A description about the field emission displays and their cathode technologies were briefly addressed in following sections. Finally, the motivation of this thesis was mentioned before the thesis organization.

Chapter 2 shows the synthesis of nanotubes at low temperatures via atmospheric thermal CVD system in combination with multi-layered catalysts, and the functionality of different components in the catalysts is also discussed in this chapter.

In chapter 3, the field emission characteristics of nanotubes synthesized with multi-layered catalysts is improved by modifying the ratios of flow rates of the reaction gases.

Chapter 4 discloses a novel self-focusing gate structure and related processes, which could resolve the issue of electron beam spreading as the FEDs operate in triode configuration.

In chapter 5, a simple fabrication process consisting of wet etching and lift-off is proposed to create a submicron gap for planar edge emitters. Additionally, a quasi-planar structure of submicron gaps controlled via thin film deposition process is also demonstrated, and the field emission characteristics are further improved by a forming process so as to reduce the operation voltages.

Finally, the conclusions and recommendations for future research are described in chapter 6 and 7, respectively.

Chapter 2

Investigation of Carbon Nanotubes Synthesized at Low Temperatures Using Multi-layered Catalytic Films

In this chapter, carbon nanotubes were synthesized at 550℃ using multilayer catalysts which were composed of supporting layer, interlayer, and catalytic metal. Supporting layer could effectively enhance the dispersion of catalytic nanoparticles and meanwhile avoid their agglomeration during the synthetic process. Interlayers not only promoted the distribution of nanoparticles but also function to enhance the precipitation of carbon atoms. Interlayers which had surface energy comparable to catalytic metal and positive of formation heat of carbide revealed to improve the growth of CNTs at low temperatures.

2.1 Introduction

Carbon nanotubes (CNTs), discovered by Iijima in 1991 [2.1], are promising candidates for emitter materials of cold cathodes due to their unique properties, such as high aspect ratio, high mechanical strength, chemical inertness and large current capability [2.2-2.4]. Wang et al. reported a low turn-on electric field of 0.8 V/μm from nanotube bundle emitters [2.5]; meanwhile, Zhu et al. demonstrated a very high current density of 4 A/cm^2 from CNT field emitters [2.6]. In addition, Samsung

announced a matrix-addressable diode display using CNTs as emitters, showing the potential for field emission displays (FEDs) [2.7]. Therefore, field emission displays based on CNTs have attracted much attention in recent years [2.8-2.10]. For FEDs to be cost competitive with existing display technologies, inexpensive glass is commonly used as the substrates. Nowadays, several methods have been well developed for preparing CNTs on glass substrates at low temperatures, including screen printing [2.11], electrophoresis [2.12], and chemical vapor deposition (CVD) [2.13-2.17]. Among these methods, CVD appears to be a superior one due to its good uniformity and pixel resolution. Numerous CVD systems have been employed to directly grow CNTs on glass substrates, and they can be categorized into two types of instruments based on the ways by which the hydrocarbon gases are decomposed: plasma-based CVD and thermal CVD. The plasma-based CVD systems, such as inductively coupled plasma CVD (ICP-CVD) [2.13], electron cyclotron resonance CVD (ECR-CVD) [2.14], and plasma-enhanced chemical vapor deposition (PECVD) [2.15], utilize a source of plasma to effectively decompose the hydrocarbon gases, thus enhancing the growth of nanotubes at low temperatures on glass substrates. In contrast, thermal CVD [2.16-2.17] imply that the decomposition of reaction gases is carried out with the aid of thermal energy supplied by the instrument. For the sake of different operation mechanism, the plasma-based systems revealed to be a better choice than thermal one due to the higher efficiency in synthesis of CNTs. It has been shown that the activation energy characterized for the growth of CNTs by PECVD was lower than that by thermal CVD [2.18-2.19] and that the growth limiting step was determined by the diffusion of carbon on catalysts: surface diffusion for PECVD and bulk diffusion for thermal CVD [2.20]. This indicates that effective decomposition of carbon precursors by plasma could enhance the growth rates at low temperatures due to a lower activation energy. Nevertheless, it is worth mentioning that a vacuum

environment is necessary for the purpose to ignite and sustain the plasma source. Thus an evacuation system should be equipped in plasma-based systems, that is, a higher cost for large area and low throughput. Moreover, it is not easy to well control the plasma source in large area because the parameters for sustaining plasma should be precisely provided to obviate a big issue in non-uniformity. Therefore, it is generally suggested that thermal CVD would be a favored method owing to its controllability and scalability. Despite the high feasibility, however, thermal CVD typically involves processing temperatures of over 600℃ to overcome the decomposition energy of carbon precursors, which is significantly higher than the softening point of glass substrates (580℃). Thus, in several studies, a two-zone electric furnace has been employed, which consists of a high temperature zone for preheating the reaction gas to enhance its reactivity [2.21-2.23], hence facilitating the growth of CNTs at low temperatures. With the similar ideas, there were work employing hot filament assisted systems [2.24], which consisted of a filament heated at high temperatures (~1600℃), to pre-decompose the precursors. These techniques are not only complicated in the manufacturing processes but also thermally inefficient because of the high thermal budget.

According to work published, the type of catalyst also plays an important role in the growth of CNTs because the process is a catalytic reaction. Kamada *et al.* indicated that a binary catalyst could synthesize CNTs well at low temperatures due to its high activity [2.25]. Park and coworkers also employed a ternary alloy as a catalyst for improving the crystallinity of CNTs synthesized at low temperatures [2.16-2.17]. Since thermal CVD utilizes thermal energy to assist the decomposition of carbon precursors, a highly active catalyst is essential for low-temperature synthesis of CNTs. However, it is difficult to prepare these catalysts because the composition of elements should be carefully synthesized. In this chapter, multilayer catalysts were employed to

synthesize CNTs by thermal CVD at atmospheric pressure, and the morphologies and emission characteristics were investigated based on the compositions of multilayer catalysts. The components of multilayer catalysts were formed by sputtering in a simple manner. The functionality of each component of multilayer catalysts is discussed, and a growth mechanism is also constructed for clarifying and modeling the synthesis of nanotubes at low temperatures.

2.2 Experimental Procedures

2.2.1 Sample Fabrication

Multiwalled carbon nanotubes (MWNTs) were grown on Cr-coated N-type (100) silicon substrates with multilayer catalysts at atmospheric pressure by thermal CVD. The multilayer catalysts formed of supporting layer, interlayer, and catalytic metal were sequentially deposited on Cr-coated substrates by magnetron sputtering (Ion Tech Microvac 450CB) at the pressure of 7.6×10^{-2} Torr at room temperature. Because the sputtering system consisted of three sputtering sources, the three components of multilayer catalysts could be sequentially prepared without breaking the vacuum environment. Cobalt and aluminum are used as the catalytic metal and supporting layer, respectively, while different kinds of metal were employed as interlayer, such as Ti, Cr, Pd, etc.

The atmospheric pressure thermal CVD system consists of a 2-in.-diameter horizontal quartz tube, an electric heating system, reaction gas supply and related mass flow controllers. Samples loaded into the quartz tube were heated to the predetermined temperature of 550℃ in a nitrogen flow for an oxygen-free ambience. Prior to the CNT growth, hydrogen gas with a flow rate of 50 sccm was fed into the reaction tube for 5 min to reduce the catalyst metal to the metallic phase, meanwhile

transforming into nanoparticles. Then, carbon nanotubes were grown at designated temperatures with reaction gas, ethylene, at a flow rate of 75 sccm for 30 min. After that, samples were furnace-cooled to room temperature in nitrogen flow to fully exhaust the reaction and byproduct gases.

2.2.2 Material Analysis

The morphologies of the samples were characterized by scanning electron microscopy (SEM; Hitachi S-4700I). The fine internal structures of nanotubes and catalytic elements of nanoparticles were examined by high-resolution transmission electron microscopy (HRTEM; JEOL JEM-2000EX) and X-ray energy dispersive spectroscopy (EDS), respectively. The surface property of multilayer catalysts was characterized by X-ray photoelectron spectroscopy (XPS) using Al Kα source.

Field emission characteristics of CNTs were measured with a parallel diode-type configuration in a high-vacuum chamber with the pressure of 5×10^{-6} Torr. A glass substrate coated with indium tin oxide (ITO) and P22 phosphor (ZnS: Cu, Al) was used as the anode plate, and the gap between the cathode and the anode plate was set to be 160 μm. The emitting area was well defined as 0.25 mm^2 by photolithography. Anode voltages up to 1000 V were applied at intervals of 5 V with a source measure unit (Keithley 237) for the verification of field emission characteristics while the cathode was biased at 0 V.

2.3 Morphologies and Field Emission Characteristics of CNTs

2.3.1 Effect of Supporting Layer

Figure 2.1 showed the plane view SEM images of samples with catalysts after pretreatment process. In Fig. 2.1(a), the surface morphology of the sample with a

single layer of catalytic metal (20Co) did not significantly reveal the formation of nanoparticles after pretreatment. In contrast, as the underlayer, either Cr or Al, was employed, the formation of nanoparticles was remarkably enhanced, shown in Figs. 2.1(b), 2.1(c), and 2.1(d). Moreover, it was clearly that the sample with multilayer catalysts (20Co/20Cr/100Al) showed a more uniform morphology than others. By increasing the thickness of supporting layer from 2 nm to 20 nm, the morphologies of nanoparticles shown in Fig. 2.2 indicated that there was a smallest particle size for the sample with Al supporting layer of the thickness of 10 nm.

After the process of CNT growth, the SEM images, displayed in Fig. 2.3, clearly showed that since the nanoparticles were small and uniformly distributed after pretreatment, the samples exhibited a better morphology of nanotubes, especially for the sample with multilayer catalysts. The corresponding field emission characteristics of each sample after CNT synthesis were shown in Fig. 2.4. There was manifest correlation between morphology and emission characteristics of CNTs; that is, the sample with multilayer catalysts (20Co/20Cr/100Al) represented a better performance that was a field emission current density of 8.28 mA/cm^2 at the electric field of 6 V/μm. The detail emission characteristics were summarized in Table 2.1.

According to the analysis of XPS examined on the sample surface which was conducted by growth process for 5 min (Fig. 2.5), there was information showing the formation of aluminum oxide. The spectrum revealed a significant 2p peak of oxidized-Al with a binding energy of 75.4 eV. It was conjectured that the thin aluminum layer transformed into aluminum oxide during the heating step due to the residual oxygen in the reaction chamber [2.26]. Jodin *et al.* [2.27] reported that catalysts combining with fumed alumina nanoparticles acting as a support could prevent agglomeration of catalytic particles during the CVD growth process; that is, the alumina support facilitated the uniform distribution of the catalytic nanoparticles

and preserved their small sizes for CNT growth. Moreover, as compared with a flat substrate coated with metal catalyst clusters, a buffer layer-supported catalyst had the advantage of a higher active surface area, thus more active sites for nucleation [2.28-2.29]. Accordingly, aluminum significantly revealed to be a good supporting layer for enhancing the growth of nanotubes.

2.3.2 Effect of Interlayer

As mentioned previously, the supporting layer of Al could effectively reduce the size of nanoparticles and resulted in a uniform dispersion of catalysts. However, there was a lack of information about the role interlayers played. In order to clarify the functionality of interlayer, various metallic metals were employed as interlayers interposed between supporting layer (Al) and catalytic metal (Co). The thickness of interlayer was determined to be 2 nm, while that of Al and Co were 10 nm and 2 nm, respectively. Figure 2.6 showed the SEM images of CNTs synthesized with different interlayer metals. It was obviously that the samples with interlayers of Cr and Ti exhibited the better morphologies as compared with other samples. The field emission characteristics of each sample were shown in Fig. 2.7, and the corresponding turn-on fields and current densities were listed in Table 2.2. Accordingly, the samples with Cr and Ti interlayers both had emission current density exceeding 10 mA/cm^2, which was suitable for the application of FEDs [2.30].

The effect of interlayer thickness on morphology of CNTs was also investigated via samples with different interlayer thickness of Ti and Cr as the thickness of supporting layer and catalytic metal were fixed with 10 and 2 nm, respectively. The thickness of Cr interlayer was modified from 1 nm to 100 nm, and the corresponding SEM micrographs of samples after CNT growth were illustrated in Fig. 2.8. As the ratio of Co over Cr was close to 1~2, the CNTs showed a better morphology than

others. Similar effect was manifest for Ti interlayer according to the SEM images shown in Fig. 2.9. In other words, the optimal catalytic metal over interlayer ratio should be chosen close to 1~2, which would give rise to better field emission characteristics. The detail data of emission current and turn-on field with different interlayer thickness were illustrated in Fig. 2.10 and Table 2.3 for Cr, while in Fig. 2.11 and Table 2.4 for Ti.

Figure 2.12(a) showed a high-resolution TEM image of nanotubes grown with the multilayer catalyst (20Co/30Ti/100Al) at 550℃, and revealed a closed tip filled with catalytic metal particles and a multiwalled structure consisting of the wavy graphite sheets aligned parallel to the tube axis. The inner and outer diameters were about 8 nm and 27 nm, respectively. The outer graphitic sheets were usually less crystalline than the inner ones, and more defects were shown in the outer surface of nanotubes. The corresponding EDS analysis of the catalytic particle was shown in Fig. 2.12(b), confirming that the particle was composed of cobalt. Neither Al nor Ti peak appeared in the figure, and the Cu signal originated from the TEM microgrid. By the same token, similar information was found in the sample with Cr interlayer. The TEM and corresponding EDS analysis of nanotubes synthesized with multilayer catalysts (20Co/30Cr/100Al) were illustrated in Figs. 2.13(a) and 2.13(b), respectively. This result was similar to those of other literature in which binary catalysts were employed [2.31-2.32], and indicated that only Co particles directly participate in the growth of nanotubes.

In order to study in more detail and possible reaction of interlayer, samples with multilayer catalysts was conducted with CNT growth process for 5 min and then cooled down for XPS analysis. When the sample using Ti as interlayer was performed, the C1s spectrum in Fig. 2.14(a) revealed two different peaks at 281.5 and 285 eV, respectively. The peak at 281.5 eV was close to the signal of titanium carbides [2.33],

while the other peak at 285 eV corresponded to the binding energy of free carbon or CNTs. The C1s spectrum of sample with Cr interlayer shown in Fig. 2.14(b) displayed two carbon forms: a major peak at 285 eV and a minor peak at 283 eV, which was characterized as chromium carbide phases [2.34]. Conclusively, it was conjectured that the interlayer played an important role in two aspects for the low-temperature synthesis of nanotubes. First, the interlayer interposed between supporting layer and catalytic metal could be considered as another supporting layer other than Al. From the view point of surface energy, the materials with a large surface energy tended to merge into a large agglomeration for reduction in the surface area. According to the data of surface energy shown in Fig. 2.15, the interlayers could be classified into three categories as compared with the surface energy of Co: (1) surface energy smaller than that of Co, (2) surface energy close to that of Co, and (3) surface energy larger than that of Co. Since the difference of surface energies between interlayer and catalytic thin films would give rise to different morphologies of catalytic nanoparticles, the growth of nanotubes would be influenced by interlayers as well. As shown in Fig. 2.16, while the surface energy of interlayers were smaller than that of Co, the catalytic nanoparticles tended to merge into large ones for reduction in surface area, thus a stable state. On the contrary, while the surface energy of interlayers were larger than that of Co, the catalytic nanoparticles tended to form a film-like morphologies covering on the surface of interlayers for reduction in surface area of interlayer thin films. Both conditions mentioned above could not result in an uniform distribution of small nanoparticles. For this reason, interlayers whose surface energy close to that of catalytic metal (Co) would had a positive effect on the formation of catalytic nanoparticles. Conclusively, Ti and Cr whose surface energies close to that of Co seemed to be good interlayer candidates for the growth of nanotubes. Second, it was generally known that growth of nanotubes should incorporate the step of carbon

precipitation. It is proposed that the precipitation sites of carbon existed in the region of particles which is super-cooled because of the large driving force for the super-saturation. Therefore, the super-saturated carbon would precipitate at these sites to reconstruct the equilibrium. As described previously, the interlayer metal transformed into carbide phase during processing. According to the formation heat of carbides for various metals listed in Table 2.5, the values of formation heat could be classified into two categories: H>0 and H<0. The positive formation heat of carbide indicated that the reaction of carbide would consume thermal energy supplied from environment, that is, an endothermic reaction. On the contrary, negative formation heat means an exothermic reaction. While transforming into carbide phase, the interlayer of positive formation heat would consume thermal energy in the neighborhood and give rise to a reduction in temperature, thus a preferred precipitation sites of carbon. Accordingly, the interlayer, such as Ti, Ta, Cr, and Hf, would have the positive effect on synthesis of nanotubes. In combination of the aspects mentioned above, only Ti and Cr interlayer revealed to be candidates appropriate for low-temperature synthesis of CNTs, and this was correspondent to the results of experiments.

2.4 Growth Mechanism

Although the real growth mechanism of CNTs was still at issue, a possible mechanism for nanotubes synthesis with the multilayer catalysts was proposed. Initially, the Co catalyst thin film broke up and transformed into nanoparticles, which minimized the surface energies during the heating process. These nanoparticles provided the nucleation and growth sites for nanotubes, and the size of these particles

dictated the diameter of nanotubes. From the results of experiment, the Al film acting as the supporting layer could remarkably enhance the formation of nanoparticles, and meanwhile improved the uniformity of catalytic particles by avoiding their mergence into large ones. Raw and decomposed carbon precursors absorbed on the surface of catalyst metal particles and dissociated into carbon atoms. The concentration of carbon in the catalyst particles increased until supersaturation was reached. Carbon atoms diffused along the concentration gradient via the surface and/or bulk of the metal particles and precipitated at the preferable nucleation sites to form the graphitic sheets. Since the incorporation of interlayer which had positive formation heat of carbides could enhance the precipitation of carbon, a positive driving force existed for the formation of graphite sheets, thus growth of nanotubes. Therefore, the multilayer catalysts showed an outstanding catalytic property for synthesis of CNTs at low temperatures.

2.5 Summary

Multilayer catalysts composed of trilayer structure were employed to enhance the growth of CNTs at a low temperature of 550℃ in the atmospheric-pressure thermal chemical vapor deposition system. The fact that CNTs could be deposited at low temperatures with the multilayer catalysts was ascribed to the aspect of nano-effect caused by the supporting layer and interlayers. The well-distributed small catalytic nanoparticles were attributed to the combination effect aided via the Al supporting layer and the interlayers, which held similar surface energy as that of catalytic metal. Moreover, the interlayers played an important role to enhance precipitation of carbon due to the positive formation heat of carbides. The optimal thickness for Al supporting

layer is about 10 nm, while the thickness ratio of interlayer over catalytic metal (2 nm Co) was suggested to be 1~2 both for Cr and Ti. CNTs grown at 550℃ with the multilayer catalysts exhibited a high emission current density of 18.24 mA/cm^2 and 28.60 mA/cm^2 for the samples employed with interlayers of Cr (30 nm) and Ti (30nm), respectively, as the electric field was applied at 6 V/μm.

Chapter 3

Improvements of Morphologies and Field Emission Characteristics for Carbon Nanotubes by Modifying the Gas Flow Rate Ratios

In this chapter, the effect of reaction gas flow rate on the growth of CNTs using thermal CVD at low temperatures was discussed. The morphology and field emission performance showed a significant relationship corresponding to the crystallinity of nanotubed analyzed by Raman Spectra. Moreover, the growth activation energy calculated based on the dependence of nanotube length versus temperature revealed the fact that CNTs synthesized with a multilayer catalyst (20Co/30Ti/100Al) displayed a lower value than single or binary catalysts. Finally, a growth mechanism for CNTs using multilayer catalysts is constructed for discussion.

3.1 Introduction

As mentioned in chapter 1, for the application of CNTs in field emission displays, reliable growth techniques capable of yielding high purity materials in large and designated area is crucial for the realization of the potential. Chemical vapor deposition (CVD), therefore, would be a promising method for their uniformity and scalability as compared with arc discharge and laser ablation. In order to produce the nanotubes in good quality and large quantity, a thorough understanding of growth

mechanism is necessary for optimization of synthesis conditions and manufacture concerns. The general growth process involves heating a catalyst material to high temperatures and flowing in a hydrocarbon gas for a period of time. The growth mechanism of nanotubes for CVD system are based on the following model first proposed by Baker [3.1]: the hydrocarbon molecules decompose at the catalyst surface, and the carbon atoms dissolve into the metal forming a solid solution. When this solution becomes supersaturated, carbon atoms diffuse through the bulk or surface of the particle and precipitate at its active sites in crystalline graphitic layers. In conjunction with the transition metals in CVD system, the proceeding of CNT growth is a catalytic process, and the synthesis conditions, therefore, should be well-designed for high quality material in large quantity. Accordingly, the key parameters in nanotube growth are the temperatures, catalysts, and hydrocarbon gas.

It is generally known that as the temperature increases, the activity of catalysts and reactivity of carbon precursors become higher, and thus the growth rates could be greatly enhanced. Therefore, more active nucleation sites could be formed at higher temperatures, resulting in higher densities of CNTs. A high nanotube nucleation density combined with fast growth rates would contribute to the vertical alignment of CNTs due to a steric effect (crowding effect): the confinement by neighboring nanotubes leads to a preferred growth direction perpendicular to the substrates [3.2]. According to the study published by C. P. Deck et al. [3.3], transition elements (Fe, Co, and Ni) were found to have some (~1 at.%) carbon solubility in the solid solution, and form few, if any, stable carbide phases. Elements with no carbon solubility or with multiple carbide phases did not produce nanotubes in vapor phase CVD process. Moreover, binary or ternary catalysts in conjunction with plural elements could provide the catalytic functionality for the growth of CNTs at low temperatures [3.4-3.5]. Additionally, much work indicated that the morphology of CNTs is

remarkably dependent upon the process conditions of reaction gases. M. P. Siegal reported that the site density of CNTs would be control in several orders of magnitude by selecting the appropriate chemically reactive hydrocarbon gas [3.6]. It is also proposed by other work that growth of the carbon nanotubes was strongly affected by gases introduced during the heat-up stage prior to the growth, which markedly affected the growth rate of carbon nanotubes by an order of magnitude and changed the crystallinity of carbon nanotubes [3.7].

In consideration of CNT-based FEDs, it is crucial to employ techniques in a simple manner for low-temperature synthesis of nanotubes on glass substrates. As discussed in chapter 2, the multilayer catalysts had the merits for low-temperature synthesis of nanotubes due to their high reactivity. In order to fully optimize the production of carbon nanotubes, the growth conditions involved in their synthesis must be completely understood. In this chapter, therefore, experiments designed with modification of the ratios of reaction gases were conducted to characterize the effect of gas flow rates on the morphology and field emission property of CNTs. Moreover, the investigation of the activation energy of CNTs grown with highly active catalysts in a thermal CVD system was also necessary for clarifying the growth mechanism.

3.2 Experimental Procedures

3.2.1 Sample Fabrication

Multiwalled carbon nanotubes (MWNTs) were grown on Cr-coated N-type (100) silicon substrates with a multilayer catalyst at atmospheric pressure by thermal CVD. The multilayer catalyst (20Co/30Ti/100Al) formed of Al (10 nm), Ti (3 nm), and Co (2 nm) were sequentially deposited on substrates by magnetron sputtering (Ion Tech

Microvac 450CB) at the pressure of 7.6×10^{-2} Torr at room temperature. Because the sputtering system consisted of three sputtering sources, the multilayer catalysts could be sequentially sputtered without breaking the vacuum environment.

The atmospheric pressure thermal CVD system consists of a 2-in.-diameter horizontal quartz tube, an electric heating system, reaction gas supply and related mass flow controllers. Samples loaded into the quartz tube were heated to the predetermined temperatures in the range from 500 to 650℃ in a nitrogen flow as an oxygen-free ambient. Prior to the CNT growth, hydrogen gas with a flow rate of 50 sccm was fed into the reaction tube for 5 min to reduce the catalyst metal to the metallic phase, meanwhile transforming into nanoparticles. Then, carbon nanotubes were grown at designated temperatures for 30 min with reaction gas mixture, including nitrogen, hydrogen, and ethylene. After that, samples were furnace-cooled to room temperature in nitrogen flow to fully exhaust the reaction and byproduct gases.
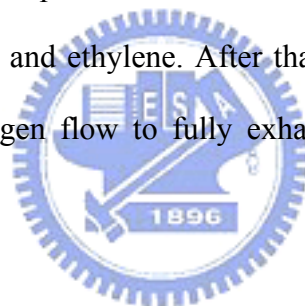
3.2.2 Material Analysis and Field Emission Measurement

The morphologies of the samples were characterized by scanning electron microscopy (SEM; Hitachi S-4700I). Typical Raman spectra are performed with a 514.5 nm Ar excitation laser to analyze the crystallinity of CNTs, which were determined by the relative intensity of the D-band to the G-band (I_D/I_G).

Field emission characteristics of CNTs were measured with a parallel diode-type configuration in a high-vacuum chamber evacuate to the pressure of 5×10^{-6} Torr. A glass substrate coated with indium tin oxide (ITO) and P22 phosphor (ZnS: Cu, Al) was used as the anode plate, and the gap between the cathode and the anode plate was set to be 160 μm. The emitting area was well defined as 0.25 mm^2 by

photolithography. Anode voltages up to 1000 V were applied at intervals of 5 V with a source measure unit (Keithley 237) for the verification of field emission characteristics while the cathode was biased at 0 V.

3.3 Morphology and Field Emission Characteristics of CNTs

3.3.1 Effect of Hydrogen

The effect of hydrogen gas flow rate on the growth of CNTs was investigated based on SEM images shown in Fig. 3.1. During the growth process, the total flow rates of N_2 and H_2 were kept with 1000 sccm, whereas the flow rate of C_2H_4 is fixed at 75 sccm. As the flow rate of H_2 was increased form 0 to 50 sccm, the morphology of as-grown samples changed remarkably. At the H_2/N_2 ratio of 10/990, nanotubes revealed to be vertically aligned with respect to the substrates. Poor morphologies were observed while the H_2 flow rates were larger or smaller than 10 sccm. It had been reported that the hydrogen gas introduced during process could be an important factor for activate the catalytic particles [3.8]. The hydrogen atoms could react with carbon atoms to form hydrocarbon molecules at the particle surface, which would avoid the deposition of abundant amorphous carbon. Therefore, the catalysts could preserve active for growth of CNTs. Much work indicated that the nanoparticles would lose catalytic property as their surface was encapsulated with amorphous carbon layers [3.9]. However, high percentage of H_2 would show hampered growth of nanotubes due to the obstruction of absorption of carbon sources at catalyst surfaces.

Fig. 3.2 showed the field emission characteristics of samples as a function of different H_2 flow rates. Accordingly, the sample prepared with H_2/N_2 ratio of 10/990 showed a good field emission performance, achieving the emission current density of

16.2 mA/cm^2 at the electric field of 6V/μm. The detailed data were listed in Table 3.1. The corresponding Raman spectra analysis performed to the samples were illustrated in Fig. 3.3. According to the Raman spectra displayed, two main peaks at approximately 1350 and 1560 nm^{-1} could be distinguished. The G-band peak at 1560 nm^{-1} indicated highly crystalline grapheme layers, while the D-band peak at 1350 nm^{-1} identified the existence of defective grapheme layers, such as amorphous carbon [3.10]. The ratio of the intensity of the D-band to the G-band provided an index to evaluate the quality of the CNTs [3.11]. The lowest I_D/I_G were observed for CNTs synthesized with the condition of 10 sccm H$_2$ flow, suggesting that this growth condition yielded well gaphitized nanotubes of the highest purity with the fewest defects. The results fully matched the outcome of CNT morphology and I-V characteristics.

3.3.2 Effect of Nitrogen

Fig. 3.4 showed the dependence of CNT morphology on the nitrogen flow rate modified from 0 to 5000 sccm, while the flow rates of H$_2$ and C$_2$H$_4$ were fixed at 10 and 75 sccm, respectively. As the N$_2$ flow rate was increased form 0 to 1000 sccm, the morphology of nanotubes changed from randomly spaghetti-like orientation to vertically forest-like alignment. However, further increased to 5000 sccm, the length of nanotubes became short, thereby a poor morphology. Much research clearly indicated that the inert gases, such as nitrogen and helium, functioned as a carrier gas which could improve the uniform flow of other reaction gases due to their fast flow rates [3.12]. Therefore, as N$_2$ overflowed, the phenomenon of over-dilution of hydrocarbon gases would cause a reduction in carbon supply for reaction.

The results of field emission measurement corresponding to the samples were shown in Fig. 3.5, and the detail emission characteristics were summarized at Table

3.2. The sample treated with 1000 sccm N_2 flow exhibited a good performance; low turn-on field of 2.27 V/μm at the emission current density of 10 μA/cm^2, and a high emission current density of 17.52 mA/cm^2 at the electric field of 6 V/μm. Raman spectrum analysis in Fig. 3.6 clearly indicated that CNTs of good morphology also showed a high quality in crystallinity.

3.3.3 Effect of Ethylene

With the H_2 and N_2 flow rates fixed at 10 and 1000 sccm, respectively, the morphology of samples treated with different C_2H_4 flow rates were displayed in Fig. 3.7. Although there were no remarkable difference in morphology shown in the SEM images, sample with a 125 sccm C_2H_4 flow revealed a lower I_D/I_G ratio according to the Raman spectra in Fig. 3.8. Moreover, Fig. 3.9 showed the similar tendency in the field emission characteristics. A high emission current density of 26.5 mA/cm^2 and a low turn-on field of 1.81 V/μm could be achieved with the corresponding sample. Detail data of emission performance dependent upon the hydrocarbon flow rates were listed in Table 3.3.

C_2H_4, produced in the petrochemical industry by steam cracking, was commonly used as the carbon source for synthesis of nanotubes. Therefore, the flow rates of C_2H_4 had the great impact on the carbon supply at the catalyst surface. An optimal flow was expected for conducting the catalytic process. Over or less was liable to cause a poor crystallinity in graphite sheets during formation stage.

3.3.4 Effect of Temperature and Activation Energy

Figures 3.10 and 3.11 showed cross-sectional SEM images of samples deposited at plural temperatures for the multilayer catalyst (20Co/30Ti/100Al) and the single layer one (20Co), respectively. The corresponding tilt-view image of each sample was

shown in the inset. The length of nanotubes increased with temperature and the cross-sectional morphology changed from random spaghetti-like orientation to vertical forest-like alignment. It was generally known that as the temperature increases, the activity of catalysts and reactivity of carbon precursors became higher, and thus the growth rates could be greatly enhanced. Therefore, more active nucleation sites could be formed at higher temperatures, resulting in higher densities of CNTs. A high nanotube nucleation density combined with fast growth rates would contribute to the vertical alignment of CNTs due to a steric effect (crowding effect): the confinement by neighboring nanotubes led to a preferred growth direction perpendicular to the substrates [3.2]. It was worth noting that CNTs could not be grown at the low temperatures of 500 and 550℃ for the samples of single layer catalyst. Despite some curly or wavy nanotubes grown at different temperatures, a reasonable estimation of the average length and corresponding growth rates can be obtained from the cross-sectional images, and the average growth rate of CNTs as a function of temperature was plotted in Fig. 3.12. The data fit well to a linear interpolation, providing an activation energy of 0.89 eV for the multilayer catalyst, which was obviously lower than that of 1.54 eV for the single layer catalyst. According to the results of other studies [3.13-3.14], the activation energy of 1.54 eV for the single layer catalyst in this work was close to the diffusion energy of carbon for thermal deposition (~1.2-1.8 eV). This indicates that the multilayer catalyst could effectively enhance the growth of nanotubes by virtue of the reduction of the diffusion energy of carbon. It was generally agreed that the diffusion of carbon was the rate-determining step in the synthesis of CNTs at low temperatures [3.14]. Thus the lower the carbon diffusion energy, the higher the nanotube growth rate at low temperatures.

3.4 Growth Mechanism

As discussed in chapter 2, in contrast with the conventional single layer catalyst, the multilayer catalyst could form uniform and small sized nanoparticles by the use of supporting layer and interlayer in combination. Based on the growth model of CNTs, carbon atoms should diffuse along the concentration gradient via the surface and/or bulk of the metal particles and precipitate at the preferable nucleation sites to form the graphitic sheets. For large particles, the diffusion path via the bulk of particles was dominant because of the large proportion of the bulk volume to the surface area. Therefore, carbon atoms predominantly diffused via the bulk of particles to precipitation sites and formed graphitic sheets. It was clear that the thermal energy supplied by the thermal CVD system was not high enough for carbon diffusion in bulk of metal particles at low temperatures because of the high diffusion energy for carbon in bulk metal. Therefore, CNTs could not be synthesized at low temperatures with large catalytic particles. In contrast, as the particle size decreased, the nanoparticles with higher surface-to-volume ratios had larger surface area, thereby resulting in a comparable proportion of the bulk volume and that of the surface area. This indicated that the carbon diffusion path via the surface was as favored as that via the bulk so that the activation energy for small nanoparticles was significantly reduced compared with that for large ones. Moreover, it had been well modeled that the melting point of a nanoparticle was a function of its size, which resulting in a decreasing tendency of the melting point with decreasing volume [3.15]. Therefore, the melting temperature of Co nanoparticles would decrease with the reduction of particle diameter. Accordingly, carbon atoms diffusing in these quasi-liquid particles experienced a lower diffusion energy, i.e., a higher diffusion rate. As the carbon atoms

were steadily and continuously supplied to the nanoparticle, the graphitic sheets were formed at the precipitation sites and the length of CNTs increased.

3.5 Summary

Using multilayer catalyst (20Co/30Ti/100Al) for CNT growth at 500℃, the optimal flow rates of reaction gases composing of C_2H_4, H_2, and N_2 were determined to be 125, 10, and 1000 sccm, respectively. Nanotubes synthesized with this growth condition revealed a good field emission performance of the emission current density of 26.5 mA/cm^2 at an electric field of 6 V/μm, and it also showed a low I_D/I_G ratio in Raman Spectrum analysis, indicating a good quality in crystallinity. The temperature-dependent growth rate in the Arrhenius plot for the multilayer catalyst revealed an activation energy of 0.89 eV, which was lower than that required for the conventional catalyst in thermal decomposition (1.54 eV). The fact that CNTs could be deposited at low temperatures with multilayer catalyst was ascribe to the combination of well-distributed small catalytic nanoparticles due to the Al supporting layer and the higher activity due to the Ti co-catalyst layer.

Chapter 4

Fabrication and Characterization of Carbon Nanotube Field Emission Devices with a Self-Focusing Gate Structure

Field emission devices with a novel self-focusing gate structure using carbon nanotubes (CNTs) as emitters had been fabricated. Without additional focusing electrodes, the self-focusing gate structure employed a pair of gate electrodes parallel with the vicinity of emitters, which resulted in an asymmetric emission area as compared with the conventional gate structure. Therefore, electrons emitted from the emitters gave rise to an overlapping region on the anode plate so that a reduction of spot size had been achieved. According to the simulation results and luminescent images, this self-focusing gate structure had a well controllability on the trajectory of electrons, and therefore showed a smaller luminescent spot size than the conventional one. The novel gate structure which utilized a simple fabrication process had the advantages of low-cost manufacturing and large-area scalability, and therefore was promising for the application in field emission displays (FEDs).
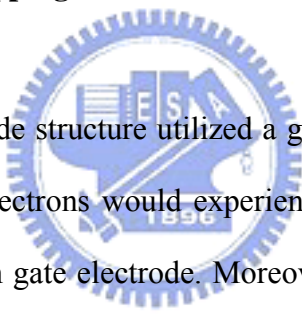
4.1 Introduction

A field emission display (FED), consisting of a baseplate which contains an array of addressable gated field emitters whose electrons are projected towards a phosphor plate in proximity, is a potential technology for flat-panel displays in terms of the

merits including higher brightness, large viewing angles, lower power consumption, and a larger range of operating temperatures. FED can be operated in two configurations: diode-type and triode-type. In contrast to the diode-type which needs a higher voltage driver circuitry, triode-type configuration seems to be a promising candidate because of their better driving ability in low-voltage operation [4.1-4.3]. Several triode-type device structures have been proposed, including normal gate, under gate, and side gate structures, and the normal gate structure reveals to be more promising in terms of low operation voltages as well as device performance [4.4-4.8]. Additionally, for the application of FEDs, a high anode-voltage is essential for the improvement in high efficiency of phosphor, high brightness, and color purity. The high anode voltage requires a large vacuum gap between the cathode and anode plates so as to avoid the problem of arcing. Accordingly, the large vacuum gap gives rise to an issue of electron-beam spreading which would cause cross-talks between adjacent pixels and would deteriorate the resolution of displays. Therefore, much effort has been extended in controlling the trajectory of electrons, thus eliminating the cross-talk noise. Several focusing structures of FEDs have been announced to overcome the issue of electron-beam spreading, such as planar-electrode type [4.9], double-gate type [4.10], and waffle-electrode type [4.11]. Modeling results have shown that the best focusing is obtained with the double gate structure, followed by the in-plane structure, and then by the waffle structure [4.12]. Nevertheless, these structures have some drawbacks, such as the complexity in the manufacturing process and the reduction in emission current owing to the focusing electrodes. Recently, a novel mesh gate structure was proposed to reduce the beam divergence by optimizing the occupation area and number of gate holes [4.13]. The mesh gate structure, however, would have the drawback of large power consumption because of the low efficiency for electrons passing through and arriving at phosphor plates.

In this chapter, CNT-based field emission devices with a self-focusing gate structure were proposed. The fabrication process was compatible with normal triode-type structure, and was simpler due to the fact that it did not require additional focusing electrodes. The results of the simulation and luminescent images revealed a good controllability in electron trajectory with this self-focusing structure, and the spot size was effectively decreased on the anode plate. Therefore, the novel focusing structure combined with simple processes was promising for the feasibility in high-definition panels.

4.2 Concept of Beam Overlapping

Since a conventional triode structure utilized a gate electrode in close proximity to the emitters, the emitted electrons would experience a variation in field potential due to the distance away from gate electrode. Moreover, higher lateral electric fields constructed around emitters degraded the performance in beam convergence. In order to overcome this issue, a fourth electrode, generally biased negatively with respect to gate electrode, was used to modify the potential contour and prevent electrons from traveling in large divergent angles. In order to simplify the manufacturing process, and meanwhile effectively projected a small dimension of electron beam on anode plates, it was desirable to introduce a new concept of device operation. Since the divergence of electron was inevitable in emitters close to gate electrode, a new concept of beam overlapping was proposed for the destination of small beam spot size. The new idea was demonstrated in literature published by Y. Ishizuka *et al*. [4.14], who constructed a crescent-shaped twin patters within a pixel by a pair of emitters located symmetrically with respect to a signal line; the schematic diagrams of the

concept of beam overlapping were shown in Fig. 4.1. In this chapter, a field emission device combining with CNT emitters was investigated for realizing the new concept of twin beam focusing.

4.3 Experimental Procedures

4.3.1 Simulation

The simulations were carried out with a commercial software (SIMION-3D) using the finite element method to investigate the beam spreading of emission electrons. The parameters of device structure and bias condition were described in the following text. The thickness of insulator and gate electrode are 1 μm and 0.2 μm, respectively, and the height of CNTs is set to be 0.8 μm. The distance between gate electrode and CNTs was assigned with 200 nm in length, and the spacer height between cathode and anode plates was set to be 550 μm, The voltages of the cathode and anode plates were applied with 0 V and 1 kV, respectively, while the gate voltage was biased at 80 V. The efficient emission area (or length) of CNTs was estimated to be in the range of 25 μm away from the edge of gate electrodes, which seemed to be a reasonable assumption due to the turn-on field of CNTs (3~4 V/μm) in this work. Meanwhile, emission of electrons was assumed on a flat surface of CNT emitters, and the electron beam divergence range and the energy of electrons emitted from CNTs were set to be -90° ～ +90° and 5 eV, respectively, which was a good assumption for well correlating the results of simulations and those of experimental observation in other work [4.15-4.16].

● **Effect of Gate Width**

In the beginning, we considered the case of conventional gate structure. Fig. 4.2

illustrated the schematic diagrams of the top and cross-sectional views of the CNT field emission devices with the conventional triode structure. The cross-sectional views were taken along section X-X'. The feature of this structure was that the area of emitters was surrounded by an extraction gate, which significantly gave rise to a higher electric field in a region close to the gate than in those far from. The emitter area was designed to be a rectangular shape, whose dimension was 50 and 300 μm in width and length, respectively. The trajectories of electrons emitting from conventional triode devices with different gate widths of 30 to 960 μm were illustrated in Fig. 4.3, and the relationships of the beam spot sizes versus extraction gate widths was shown in Fig. 4.4. The results of simulation clearly indicated that the beam spot sizes could be significantly influenced by the gate widths because of the fact that the electrons emitted from emitters would experience different potential contours dependent on the gate widths. Since the wider gate widths induced a larger lateral image force for electrons, the electrons emitted from cathode plates would travel in a larger lateral path, thus resulting in a large beam spot size projected on the anode plates.

● **Effect of Gate Spacing**

Next we would make an effort to investigate the new design of focusing structure. For the sake of severe beam divergence close to the extraction gates, a new concept of beam overlapping was applied to design a self-focusing gate structure, which consisted of a pair of line electrodes parallel to both the area of emitters, resulting in an asymmetric emission periphery of each emission region. The schematic diagrams of top and cross-sectional views were showed in Fig. 4.5. It was intuitively noted that the beam spot sizes were significantly depended on the gate spacing between the two line electrodes based on the concept of beam overlapping. The trajectories of electrons

emitting from self-focusing gate structures with gate spacing of 100 to 350 μm were illustrated in Fig. 4.6, and the dependence of beam size on gate spacing was shown in Fig. 4.7, which manifestly showed that there existed an optimal range of gate spacing for reduction of beam sizes. For large gate spacing, the effect of beam overlapping was poor because of a small overlapped area; on the contrary, the over-focusing phenomena also gave rise to a poor beam size for small gate spacing.

Conclusively, simulation results showed that the self-focusing structure had a spot size with the width of 232 μm in x direction on the anode plate while the gate spacing was 200 μm. Oppositely, the conventional structure had 622 μm in size for large gate width of 1 mm, which was much larger due to the serious beam divergence. Since the self-focusing structure had an asymmetric emission periphery caused by a pair of parallel gate electrodes, the emitted electrons would travel through the spacing between cathode and anode plates, then bombarding to the anode plate and resulting in an overlapped spot. On the other hand, the conventional gate structure without focusing electrodes could not well confine the electron beams due to the divergence of electron trajectories so as to form a large spot on the anode plate, which would result in a serious cross-talk noise between pixels. Accordingly, it was worth mentioning that the proposed simple self-focusing structure could efficiently reduce the spot size on the anode plate, thus overcoming the issue of electron beam divergence.

### 4.3.2 Device Fabrication an Analysis

The fabrication processes of focusing structure similar to previous work [4.2-4.3] were described in detail here, and schematically shown in Fig. 4.8. A (100) n-type silicon wafer coated with Cr electrode was used as the substrate. In Fig. 4.8(a), the SiO$_2$ insulator (1000 nm) was formed on substrate by Plasma Enhanced Chemical

Vapor Deposition (PECVD), on which a second Cr layer (200 nm) deposited by electron beam evaporation was patterned to form the gate electrode. After a 2nd photolithography defining the emitter area, the gate electrode and insulator were etched by wet solution and reactive ion etching (RIE), respectively, as shown in Fig. 4.8(b). Subsequently, a multilayer catalyst (20Co/30Ti/100Al) formed of Al (10 nm), Ti (3 nm), and Co (2 nm) were sequentially deposited by magnetron sputtering (Ion Tech Microvac 450CB) at the pressure of 7.6×10^{-2} Torr at room temperature. Followed by the lift-off process, CNTs were selectively grown in the emitter areas via thermal CVD, as shown in Figs. 4.8(c)-(e). Samples with catalysts loaded into the quartz tube were heated to the designate temperature of 500℃ in a nitrogen flow, and followed by a pretreatment process with hydrogen gas flow of 50 sccm. Then, growth of nanotubes was proceeding for 30 min with reaction gases, ethylene and hydrogen, at flow rates of 125 and 10 sccm, respectively. The morphologies of the samples were characterized by scanning electron microscopy (SEM; Hitachi S-4700I). The fine internal structures of CNTs were determined by high-resolution transmission electron microscopy (HRTEM; JEOL JEM-2000EX), and Raman spectroscopy was used to characterize the crystallinity of nanotubes.

As compared with the conventional device having an emitter area surrounded with extraction gate, the self-focusing gate structure had two asymmetric emission area formed in proximity to a pair of gate electrode. The SEM micrograph of the self-focusing gate structure was shown in Fig. 4.9(a), which illustrated the top view of the device, while Fig. 4.9(b) was the cross-sectional view of the CNT emitters adjacent to the gate electrode according to the area squared in Fig. 4.9(a).

Figure 4.10(a) showed a HRTEM image of nanotubes grown with the multilayer catalyst at 500℃, which revealed a closed tip filled with catalytic metal particles and a multiwalled structure consisting of the wavy graphite sheets aligned parallel to the

tube axis. The inner and outer diameters were about 10 nm and 25 nm, respectively. The correlative Raman spectrum of nanotubes shown in Fig. 4.10(b) displayed two peaks one of which at 1550~1600 cm^{-1} corresponded to the high-frequency E_{2g} first-order mode of graphite structure (G-band) and another one at 1250~1450 cm^{-1} was related to the disorder of the graphite structure (D-band). The carbon nanotubes with a higher intensity of D-band with respect to G-band indicated the intense disorder of graphite structure existing in tube walls. It was well known that the crystallinity of nanotubes synthesized at low temperatures was poorer than those grown at higher temperatures due to the formation of vacancies, grain boundaries or other defects, and furthermore the deposition of amorphous carbon in outer walls [4.17]. It was noted that the fine structure of nanotubes shown in Fig. 4.10(a) consisted of an outer layer of amorphous carbon, which was conjectured to be the factor giving rise to a high intensity of D-band.
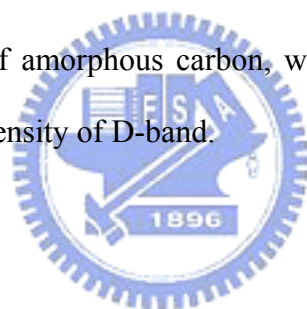
4.3.3 Device Performance

Field emission characteristics of devices were measured with a triode-type configuration in a high-vacuum chamber with the pressure of 5×10^{-6} Torr. A glass substrate coated with indium tin oxide (ITO) and P22 phosphor (ZnS: Cu, Al) was used as the anode plate, and the gap between the cathode and the anode plates was set to be 550 μm. Gate voltages up to 80 V were applied at intervals of 1 V with a source measure unit (Keithley 237) for the verification of field emission characteristics while the cathode and anode were biased at 0 and 1000 V, respectively.

The field emission characteristics of devices with conventional and self-focusing gate structures illustrated as a curve of anode current (I_a) versus extraction gate voltage (V_g) is shown in Fig. 4.11, and the inset represents the corresponding Fowler-Nordheim (F-N) plot. The emission anode currents at the gate voltage of 80 V

for conventional and self-focusing device were of 7.82 and 6.64 mA, respectively. The distances between CNTs and gate electrodes in both the two structures were designed in the same configuration, i.e., nearly 200 nm, which was the simulation parameter assigned in Figs. 4.2 and 4.5. Therefore, the higher emission current in conventional gate structure was conjectured due to its larger extraction gate area as compared with that in self-focusing one. Although the conventional structure had a higher emission current than the self-focusing one, there was no enormous difference between them.

The photo-luminescent images taken via CCD camera were shown in Fig. 4.12. The fact that the photo-luminescent image for the self-focusing gate structure was a bit asymmetrical may come from some reasons, such as the misalignment of the gate electrodes in the y-axis direction with respect to the area of CNT emitters and the non-uniformity of CNTs. Because of the alignment error in photolithography process, an asymmetry of electron beam trajectory in the y-axis would take places and thus resulted in an asymmetric photo-luminescent image. In addition, as the morphology of CNTs in the emission region has non-uniformity issue, the electrons emitted from CNTs governed by the electric field would have different beam trajectories, and therefore the photo-luminescent images would be not symmetrical. Nevertheless, the spot sizes shown on the anode plate along the x-axis were qualitatively consistent with the simulation results, indicating that the self-focusing structure could alleviate the issue of beam divergence and had good functionality in controlling the electron beams as compared with the conventional structure.

4.4 Summary

The field emission devices with a novel self-focusing gate structure consisting of CNT emitters have been successfully fabricated to show a good controllability in the luminescent spot size as compared with those with conventional structure. The results of simulations and luminescent images clearly indicated that the self-focusing gate structure employing a pair of gate electrodes close to the emitters could produce an asymmetric emission area, and the emitted electrons traveling through the spacing between cathode and anode plates would give rise to an overlapping region on the anode plate. Because of the overlapping of electron beams, the luminescent spot sizes could be remarkably reduced to 232 μm in x direction as compared with 622 μm for the conventional gate structure which had a serious issue of beam divergence. As a result, the self-focusing gate structure manufactured with a simple process can produce well-focused electron beams for the application in FEDs.

Chapter 5

Fabrication and Emission Characteristics of Chromium Thin Film Edge Emitters

In this chapter, two simple techniques were proposed for creating sub-micron gaps in edge field emitters. A lateral field emitter was manufactured by thin-film deposition and wet etching processes. The spacing was determined by the lateral etching distance formed during etching stage. In addition, a novel quasi-planar thin-film field emitter was fabricated utilizing the similar idea, and the spacing between the emitter and collector could be well controlled via the thickness of Cr layers, which created sub-micron gap. The device performance could be improved via a forming process which resulted in an increased surface roughness of emitters, thus a higher field enhancement factor.

5.1 Introduction

Recently, there has been a great amount of interest in vacuum microelectronic (VME) devices due to their high tolerance to high temperature and high radiation environment than solid state devices. With the technological breakthroughs in the microfabrication technology and the successful use of field emitters as the source of electrons, VME devices could reap the benefits of both conventional vacuum and solid state devices, and overcome most of the drawbacks associated with the traditional vacuum tubes. In addition, they are particularly used for high speed and

high frequency applications due to their low capacitance features [5.1-5.3]. Two types of microelectronic devices have been proposed: vertical and lateral (planar) type. Vertical type field emission devices have the difficult in incorporation with the collector electrode, and therefore require a series of complicated processing steps to form a cantilevered electrode [5.4]. In the contrary, lateral (planar) field emission devices have attracted considerable attention in vacuum microelectronics due to ease of fabrication, design versatility of electrode geometry, and precise control of spacing between electrodes. Besides, owing to the low operation voltage and simplicity in device structure, lateral field emission devices had attracted much attention for the application in field emission displays (FEDs) [5.5].

Since a small spacing between electrodes is required for the reduction in the operation voltage of lateral field emission devices, thereby a lower power consumption, there have been several methods developed to create the small gaps. A subtenth-micron emitter to anode spacing could be fabricated by using high resolution electron beam lithography (EBL) in combination with a lift-off process [5.6]. Gotoh *et al.* employed a focus ion beam (FIB) technique for the fabrication of lateral-type thin-film edge field emitters [5.7-5.8]. Lee et al. proposed a novel sub-micron gap fabrication method using chemical-mechanical polishing (CMP) to fabricate lateral field emission devices [5.9]. Additionally, the thin film stress generated during high-temperature annealing and cooling could form a nanometer scale silicon gap, which is dependent upon the width of pattern and annealing temperature [5.10]. However, a low throughput is generally limited for the fabrication processes via EBL and FIB techniques. A high-temperature oxidation process is necessary for the CMP and thin film stress techniques, and this also give rise to a high thermal budget. In 2005, Canon and Toshiba demonstrated a 36 inch field emission flat-panel display based on the technology of surface conduction electron emitters [5.11], whose

structure is similar to the lateral field emitters. A nano-scale gap was generated by a forming and activation processes treating on a fine particle film of PdO deposited between two Pt electrodes. The panel showed an amazing graphic image in high quality just like CRTs. However, the manufacturing method is not compatible with thin film deposition process, and thus the productivity is at issue.

In this chapter, the objective of the work was to fabricate a field emission diode which could operate at a low voltage and have a well-controlled sub-micron spacing between the emitter and collector without using complicated manufacturing processes and instruments. Moreover, a low temperature process was also necessary for the destination of being compatible with glass substrates. Two types of lateral field emitters slightly different in fabrication processes were proposed to investigate the field emission characteristics.

5.2 Planar Edge Field Emitter

5.2.1 Sample Fabrication and Analysis

The process flows for manufacturing the planar field emitters were illustrated in Fig. 5.1, which mainly involved the wet-etching and lift-off techniques. Fist, a N-type silicon wafer on which a oxide layer was deposited by PECVD was used as the substrate. A chromium thin film with the thickness of 100 nm was formed on the substrate via electron beam evaporation; followed by a photolithography technique, a wet-etching method was conducted to control the lateral etching distance via the Cr etching solution (CR7T). Then, a second Cr thin film was deposited and lift-off to form a collector electrode.

The morphologies of the samples were characterized by scanning electron microscopy

(SEM; Hitachi S-4700I) and by atomic force microscopy (AFM; Veeco Dimension 5000). The spacing between emitter and collector electrodes could be controlled by the duration of wet-etching, and the corresponding SEM images of submicron gaps were displayed in Fig. 5.2. A SEM micrograph in low magnification shown in Fig. 5.3 revealed the diode device whose emission area was defined to be 200 μm in length by photolithography.

5.2.2 Field Emission Characteristics

The field emission characteristics of planar emitters were characterized in the diode configuration, which was schematically illustrated in Fig. 5.4. Measurement was performed in a high vacuum chamber with a base pressure of 5×10^{-6} Torr; the emitter electrode was biased at ground voltage and collector electrode was drove to positive voltage swing for examining the emission current. As shown in Fig. 5.5, the turn-on voltage, representing the operation voltage of collector required for emission current of 100 nA, was significantly dependent on the gap spacing, that is, turn-on voltage of 48, 62, and 126 V for gap spacing of 200, 300, and 500 nm, respectively. Since the small spacing experienced a higher electric field across the electrodes at the same driving voltage, a low turn-on voltage was expected to induce the electrons emitted out from the emitters. On the other hand, as the spacing got larger, a higher turn-on voltage was necessary for achieving the same emission current. It was worth noted that the device constructed in this work showed a comparable characteristics as compared with the other work mentioned above. Instead of utilizing complex and high-temperature techniques, the method combining wet-etching and lift-off provided a potential process for creation of submicron gap in the manufacture of field emission devices.

5.3 Quasi-Planar Edge Field Emitters

5.3.1 Sample Fabrication and Analysis

Another process of thin film edge emitters was also proposed as following. Figure 5.6 showed the schematic diagram of the fabrication procedure of a quasi-planar field emission diode. A first metallic thin film of chromium (Cr, 300 nm) and an insulated silicon oxide layer (500 nm) were sequentially deposited on a N-type silicon substrate by E-beam evaporation and plasma-enhanced chemical vapor deposition (PECVD), respectively (Fig. 5.6(a)). The thickness of Cr thin film was used to define and control the spacing or the gap distance between the emitters and collectors. After photolithography, the silicon oxide layer and the first Cr thin film were isotropically wet-etched so as to form an undercut (Fig. 5.6(b)). The lateral etching distance of the first Cr layer should be larger than that of silicon oxide, thus forming a micro-cavity of Cr layer under the overhang of silicon oxide. Then, a second Cr layer with the thickness of 100 nm was deposited for the formation of emitter and collector (Fig. 5.6(c)). Finally, a forming process was employed for treatment of the second Cr layer (Fig. 5.6(d)). During the forming process, samples loaded into a quartz tube were heated to a temperature of 550℃ and kept for 30 min in a gas mixture of H_2 (100 sccm) and C_2H_4 (50 sccm).

The cross-sectional and top-view SEM images of a quasi-planar field emission diode were shown in Fig. 5.7. In order to precisely control the field emission area, the measured device had an emission edge of 200 μm in length via photolithography patterning (Fig. 5.7(b)). Figs. 5.8(a) and 5.8(b) were the SEM images showing the surface morphologies of Cr thin film before and after the forming process, respectively. It was obviously seen that the forming process would cause a larger

roughness in the surface of Cr layer, thus resulting in better field emission characteristics. The surface morphology images of AFM shown in the insets indicated that the mean roughness of Cr thin films without the forming process was as low as 2.11 nm (R_{rms}= 2.72 nm) compared with those with the forming process (4.5 nm, R_{rms}= 5.70 nm). The increased surface roughness was conjectured due to the formation of chromium carbides in surface by thermal reaction [5.12].

5.3.2 Field Emission Characteristics

Field emission characteristics of devices were measured with a diode-type configuration in a high vacuum chamber with a pressure below 5×10^{-6} Torr., and the schematic diagram of measurement was shown in Fig. 5.9. Driving voltages (V_d) up to 20 V were applied to the collector at intervals of 1 V by a source measure unit (Keithley 237) for the verification of field emission characteristics while the emitter was biased at 0 V.

A plot of the emission current versus driving voltage was shown in Fig. 5.10. The device treated with forming process showed better field emission characteristics than that without forming process. As mentioned above, the surface morphologies treated by forming process presented a larger roughness than those un-treated. Additionally, it was suggested that a improved field emission property results from the increasing film roughness by the modification of the surface morphology [5.13-5.14]. An emission surface having rougher morphologies possessed a higher field enhancement factor and more emission sites than flat one, thereby showing a better field emission performance. The turn-on voltage (V_{to}) at the emission current of 100 nA for the device with forming process was estimated to be 12 V, and an emission current of 8 μA could be achieve as the driving voltage applied to 20 V, which was as good as previous works [5.15-5.16]. The corresponding Fowler-Nordeim (F-N) plot of

the formed device shown in Fig. 5.10(b) represented a straight line of a negative slope at the high electric field region, implying that the current was due to field emission tunneling. However, the plot was oblique and deviated from the linearity at low electric field. Although the nonlinearity of F-N plot was still at issue, it may be attributed to surface states or geometrical effects as similar to the carbon materials [5.17-5.19]. It was also conjectured by other work that the nonlinearity in the F-N plot may be induced by the transition from thermionic to field emission [5.20].

The spacing between emitter and collector could be adjusted by the thickness of the first and second Cr layers. Owning to the second layer in this study was fixed at a thickness of 100 nm, the traveling distance of the emission electrons would be controlled by the thickness of the first Cr layer. Fig. 5.11 showed the variation of turn-on voltages with respect to the thickness of the first Cr layers, i.e. the gap distance between emitter and collector. As the gap distance decreases, the turn-on voltage decreased.
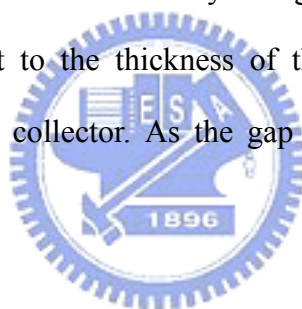
5.4 Summary

Planar thin film edge emitters were fabricated by simple techniques using thin film deposition and wet-etching processes. By controlling the duration of etching time, the distances between emitters and collectors were well defined in submicron ranges. Device performance showed a low turn on voltage of 48 V at emission current of 100 nA as the emitter-collector spacing was 200 nm. In addition, a novel structure of quasi-planar field emission diode formed of Cr thin film was also proposed. The distances between emitters and collectors were controlled by changes in thickness of 2nd Cr layers. Devices treated with a forming process at the temperature of 550℃ had rougher surface morphologies than those un-treated due to the formation of carbides, which could significantly improve the field emission property. With the 1st Cr layer of

300 nm, the turn-on voltage for quasi-planar devices was reduced from 22 to 12 V owing to the incorporation of forming process. The quasi-planar field emission diode with the first Cr layer of 200, 300, and 400 nm showed a low turn-on voltage of 9, 12, and 17 V, respectively, at the current level of 100 nA. Moreover, the spacing between the emitter and collector could be adjustable via the thickness of the first and second Cr layers, which is a simple process for scalability in the field emission devices.

Chapter 6

Summary and Conclusions

For the application of flat panel displays, large-area and cost-effective manufacture processes are essential for the profits of manufacturers. Glasses, naturally containing silica as a main component, could provide sufficient mechanical strength for fabrication processes, and seems to be a good candidate for supporting substrates. However, the softening point of glasses is about 580℃, which limits the fabrication processes that should be carefully designed so as to eliminate the issues of bending or cracking. Moreover, in order to eliminate the cross-talk noises between different pixels and to simply the manufacturing of triode devices based on CNT emitters, a new structure of device configuration was desired. In this dissertation, therefore, low-temperature fabrication processes of CNTs and thin film edge field emission devices were investigated due to their potential in application of flat panel displays; meanwhile, a new field emission triode device with self-focusing gate structure was proposed for simplicity in fabrication and feasibility in scalability.

First, CNTs were synthesized at 550℃ using multilayer catalysts composed of a tri-layer structure via the atmospheric-pressure thermal CVD system. The fact that CNTs could be deposited at low temperatures with the multilayer catalysts was ascribed to the aspect of nano-effect caused by the supporting layer and interlayers. The surface morphologies of catalysts pretreated in H_2 ambient showed a tendency in reduction of particle sizes as the Al supporting layer of optimal thickness (10 nm) was employed. Interlayers which held similar surface energy as that of catalytic metal (Co) could improve the dispersion of nanoparticles as well. From the viewpoint of CNT

62

growth, a supersaturated carbon nearby the surface of catalytic nanoparticles would give rise to an effective growth of nanotubes since an enhanced precipitation of carbon promoted the formation of graphite sheets. Therefore, interlayers whose formation heat of carbides was positive could cause a local overcooled region at the surface of catalytic particles during their transformation into carbide phases. The overcooled region would induce a super-saturation of carbon concentration at local area, and further enhance the precipitation of carbon atoms. It was noted that Ti and Cr both showed the potential candidates for interlayers because of the good morphologies and field emission characteristics of CNTs and that he thickness ratio of interlayer over catalytic metal (2 nm Co) was suggested to be 1~2 both for Cr and Ti. CNTs grown at 550℃ with the multilayer catalysts exhibited a high emission current density of 18.24 and 28.60 mA/cm^2 for the samples employed with interlayers of Cr (30 nm) and Ti (30nm), respectively, as the electric field was applied at 6 V/μm.

Next, in order to improve the morphologies and emission performance of CNTs grown at low temperatures, the flow rates of reaction gases composing of C_2H_4, H_2, and N_2 were changed to investigate and determine the optimal synthesis condition, which were characterized to be 125, 10, and 1000 sccm, respectively. Nanotubes synthesized with optimal growth condition revealed a good field emission performance of an emission current density of 26.50 mA/cm^2 at the electric field of 6.25 V/μm, and it also showed a low I_D/I_G ratio in Raman Spectrum analysis, indicating a good quality in crystallinity. The temperature-dependent growth rate in the Arrhenius plot for the multilayer catalyst revealed an activation energy of 0.89 eV, which is lower than that required for the single-layer catalyst in thermal decomposition (1.54 eV). The fact that CNTs could be deposited at low temperatures with multilayer catalyst was ascribe to the combination of well-distributed small catalytic nanoparticles due to the Al supporting layer and the higher activity due to the

Ti co-catalyst layer. Since the nano-sized catalytic particles had large surface to volume ratios, the diffusion path of carbon atoms prior precipitation at particle surfaces was comparable in proportion to that inside particles. Therefore, the activation energy for CNT growth using multilayer catalysts showed a tendency to be a small value as compared with single-layer catalysts.

Next, a self-focusing gate structure was proposed to obviate the issue of electron beam divergence faced by conventional gate devices. In conventional devices, the beam spot size on the anode plate was strongly dependent on the gate width. As the gate width became wider, the emitted electrons would experience a remarkable electrical potential in lateral direction, which resulted in a phenomenon of beam spreading. A new concept of beam overlapping was proposed to shrink the spot size on the anode plate, which demonstrated a self-focusing gate structure composed of a pair of line gate electrodes. The line gate electrodes each close to an emitter area could produce an asymmetric emission region in contrast to the conventional gate devices which had emitter area surrounded with gate electrodes. Combination with the two asymmetric emission regions, electrons emitted from emitters would travel through the spacing between cathode and anode plates and give rise to an overlapping region on the anode plate. The field emission devices with a novel self-focusing gate structure consisting of CNT emitters have been successfully fabricated to show a good controllability in the luminescent spot size as compared with those with conventional structure. Because of the overlapping of electron beams, the luminescent spot sizes could be remarkably reduced to 232 μm in x direction as compared with 622 μm for the conventional gate structure which had a serious issue of beam divergence. As a result, the self-focusing gate structure manufactured with a simple process can produce well-focused electron beams for the application in FEDs.

Finally, two fabrication methods were proposed for thin film edge emission

devices. First, planar thin film edge emitters were fabricated by simple techniques using thin film deposition and wet-etching processes. By controlling the duration of etching, the distances between emitters and collectors were well defined in submicron ranges. Device performance showed a low turn-on voltage of 48 V at an emission current of 100 nA as the emitter-collector spacing was 200 nm. In addition, a novel structure of quasi-planar field emission diode formed of Cr thin film was also demonstrated based on the thin film process. The distances between emitters and collectors were controlled via changes in thickness of 1st and 2nd Cr layers. Devices treated with a forming process at the temperature of 550℃ had rougher surface morphologies than those un-treated due to the formation of carbides, which could significantly improve the field emission property. With the 1st Cr layer of 300 nm, the turn-on voltage for quasi-planar devices was reduced from 22 to 12 V owing to the incorporation of forming process. The quasi-planar field emission diode with the first Cr layer of 200, 300, and 400 nm showed a low turn-on voltage of 9, 12, and 17 V, respectively, at the current level of 100 nA. Moreover, the spacing between the emitter and collector could be adjustable via the thickness of the first and second Cr layers, which is a simple process for scalability in the field emission devices.

Chapter 7

Future Prospects

For further research, some important topics about the low-temperature-synthesized field emission devices are proposed.

For CNTs grown with multilayer catalysts:

- The demonstration of the large-area synthesis is essential for future application.
- The combination of resistors or thin film transistors is capable of further improving the current stability.
- The achievement of the uniform morphology of CNTs is desired for reliable emission characteristics.
- The employment of surface coating on the CNTs would be a simple method for increasing the emission site density.
- The fabrication of triode devices with low operation voltages should be further developed to realize the commercial feasibility.

For the self-focusing gate devices:

- An improved emission efficiency by device structure should be further investigated.
- An improved uniformity by miniaturized device layout should be further characterized.

For the thin film edge emitters:

- Novel materials should be employed to achieve better device performance.

- Post-treatment method for improving emission characteristics can be further studied.

- An improved efficiency in electron emitted form cathode to anode is important for application of displays.

References

Chapter 1

[1.1]   R. H. Fowler and L. W. Nordheim, "Electron Emission in Intense Field," *Proc. R. Soc. London Ser. A*, Vol. 119A, pp. 173-175, 1928.

[1.2]   C. A. Spindt, "A Thin-Film Field-Emission Cathode," *J. Appl. Phys.,* Vol. 39, pp. 3504-3505, 1968.

[1.3]   J. Bardeen and W. H. Brattain, "The Transistor, A Semi-Conductor Triode," *Phys. Rev.*, Vol. 74, pp. 230-231, 1948.

[1.4]   R. N. Noyce, "Semiconductor Device-and-Lead Structure, " *US Patent* 2,981,877, 1959.

[1.5]   J. S. Kilby, "Invention of the Integrated Citcuit," *IEEE Trans. Electron. Dev.*, Vol. ED-23, No. 7, pp. 684-654, 1976.

[1.6]   S. M. Sze, "Physics of Semiconductor Devices," 2nd ed., John-Wiley & Sons publisher, New York, 648, 1991.

[1.7]   R. H. Fowler and L. W. Nordhiem, "Electron Emission in Intense Field," *Proc. R. Soc. London Ser. A*, Vol. 119A, pp. 173-175, 1928.

[1.8]   K. L. Jensen, "Electron Emission Theory and its Application: Fowler-Nordhiem Equation and Beyond," *J. Vac. Sci. Technol. B*, Vol. 21, 1528-1544, 2003.

[1.9]   R. E. Burgess, H. Kroemer, and J. M. Honston, "Corrected Value of Fowler-Nordhiem Field Emission Function v(y) and s(y)," *Phys. Rev.*, Vol. 90, p.515, 1953.

[1.10]   S. M. Sze, "Physics of Semiconductor Devices," 2nd ed., John-Wiley & Sons punlisher, New York, 648, 1991.

[1.11] P. Vaudaine and R. Myer, "Microtips Fluorescent Display," *International Electron Devices Meeting*, pp. 197-200, 1991.

[1.12] C. Curtin, "The Field Emission Display: A New Flat Panel Technology," *Proceedings of the International Display Research Conference, SID,* pp. 12-15, 1991.

[1.13] C. A. Spindt, C. E. Holland, I. Brodie, J. B. Mooney, and E. R. Westerburg, "Field-emitter Array to Vacuum Fluorescent Display," *IEEE Trans. Electron. Dev.*, Vol. 36, No. 1, pp. 225-228, 1989.

[1.14] D. A. Cathey. Jr., "Field Emission Displays," *International Symposium on VLSI Technology Systems, and Applications, Proceedings of Technical Papers, Taiwan*, pp. 131-136, 1995.

[1.15]   "Pixel Tech to produce color FEDs" *Nikkei Electronics ASIA*, p. 42, Nov., 1995.

[1.16] H. G. Kosmahl, "A Wide-bandwith High-gain Small Size Distributed Amplifier with Field Emission Triodes (FETRODE's) for the 10 to 300 GHz Frequency Range," *IEEE trans. Electron. Dev.*, Vol. 36, No. 11, pp. 2728-2737, Nov. 1989.

[1.17] P. M. Lally, E. A. Nettesheim, Y. Goren, C. A. Spindt, and A. Rosengreen, "A 10 GHz Tuned Amplifier Based on the SRI Thin Film Field-Emission Cathode," *ternational Electron Devices Meeting*, p.522, 1998.

[1.18] C. A. Spindt, C. E. Holland, A. Rosengreen, and I. Brodie, "Field-emitter-array Development for High Frequency Operation," *J. Vac. Sci. Technol. B*, Vol. 11, pp. 468-473, 1993.

[1.19] C. A. Spindt, "Microfabricated Field-emission and Field-ionization Sources," *Surface Sci.*, Vol. 266, pp. 145-154, 1992.

[1.20] T. H. P. Chang, D. P. Kern, M. A. McCord, and L. P. Muray, "A Scanning

Tunneling Microscope Controlled Field Emission Micro Probe System," *J. Vac. Sci. Tech. B*, No. 9, pp. 438-443, 1991.

[1.21] H. H. Busta, J. E. Pogemiller, and B. J. Zimmerman, "The Field-Emtter Triode as a Displacement/Pressure Sensor," *J. Micromech. Microeng.*, Vol. 3, pp. 49-56, 1933.

[1.22] H. C. Lee and R. S. Huang. "A Novel Field Emission Array Pressure Sensor," *IEEE Transducers-International Solid-State Sensors and Actuators*, Vol. 126, pp. 241-244, 1991.

[1.23] R. Meyer, A. Ghis, P. Rambaud, and F. Muller, "Microtips Fluorescent Display," *in Workshop Digest, Japan Display*, p. 513, 1986.

[1.24] R. Meyer, "6" diagonal microtips fluorescent display for TV applications," *Euro display* 90, p. 189, 1993.

[1.25] H. S. Yoo, W. Y. Sung, S. J. Yoon, Y. H. Kim, and S. K. Joo, "Novel Triode-Type Field Emission Arrays and Appropriate Driving Method for Flat Lamp Using Carbon Nanofibers Grown by Plasma Enhanced Chemical Vapor Deposition," *Jpn. J. Appl. Phys.*, Vol. 46, pp. 4381-4385, 2007.

[1.26] D. A. Buck and K. R. Shoulders, "An Approach to Microminiature Printed Systems," *Eastern Joint Computer Conference*, pp. 55-59, 1959.

[1.27] K. R. Shoulders, "Microelectronics Using Electron Beam Activated Machining Technologies," *Advances in Computers*, Vol. 2, pp. 135-293, 1961.

[1.28] M. E. Crost, K. Shoulders, and M. E. Zinn, "Thin Electron Tube with Electron Emitters at the Intersection of Crossed Conductors," *US Patent* 3,500, 102, 1970.

[1.29] C. A. Spindt and K. R. Shoulders, "Research in Micro-size Field-Emission Tubes," *IEEE Conference on Tube Techniques*, pp. 143-147, 1966.

[1.30] W. Zhu, "Vacuum Microelectronics," John-Wiley & Sons publisher, New York, 2001.

[1.31] K. Betsui, "Fabrication and Characteristics of Si Field Emitter Arrays," *Tech. Dig. 4th Int. Vacuum Microelectronics Conf.*, Naghama, Japan, p.26-29, 1991.

[1.32] H. F. Gray, "Silicon Field Emitter Array Technology," *Proc. 29th Int. Field Emission Symp.*, Stockholm, Sweden, p. 111, 1982.

[1.33] G. J. Campisi, H. F. Gray, and R. F. Greene, "A Vacuum Field Effect Transistor Using Silicon Field Emitter Arrays," *IEDM Technical Digest*, pp. 776-779, 1986.

[1.34] P. B. Marcus and T. T. Sheng, "The Oxidation of Shaped Silicon Surface," *J. Electrochem. Soc.*, Vol. 129, pp.1278-1282, 1982.

[1.35] C. A. Mead, "Operation of Tunnel-Emission Devices," *J. Appl. Phys.*, Vol. 32, pp.646-652, 1961.

[1.36] Y. Kumagai, K. Kawarada, and Y. Shibata, "Energy Distribution of Electrons Tunneling through a Metal-Insulator-Metal Sandwich Structure," *Jpn, J. Appl. Phys.*, Vol. 6, pp.280-296, 1966.

[1.37] J. G. Simmons, "Generalized Formula for the Electric Tunnel Effect between Similar Electrodes Separated by a Thin Insulating Film," *J. Appl. Phys.*, Vol. 34, pp.1793-1803, 1963.

[1.38] K. Ohta, J. Nishida, and T. Hayashi, "Electron Emission Pattern of Thin-Film Tunnel Cathode," *Jpn. J. Appl. Phys.*, Vol. 7, pp. 784-784, 1968.

[1.39] T. Kusunoki, M. Suzuki, S. Sasaki, T. Yaguchi, and T. Adia, "Fluctuation-Free Electron Emission from Non-Formed Metal-Insulator-Metal (MIM) Cathodes Fabricated by Low Current Anodic Oxidation," *Jpn. J. Appl. Phys.*, Vol. 32, pp.L1695-L1697, 1993.

[1.40] H. Adachi, "Emission Characteristics of Metal–insulator–metal Tunnel

Cathodes," *J. Vac. Sci. Technol. B*, Vol. 14, pp. 2093-2095, 1996.

[1.41] T. Komoda, X. Sheng, and N. Koshida, *Mater Res Soc Symp Proc,* vol. 509, p. 187, 1998.

[1.42] T. Komoda, X. Sheng, and N. Koshida, "Mechanism of efficient and stable surface-emitting cold cathode based on porous polycrystalline silicon films," *J. Vac Sci. Technol. B*, Vol. 17, pp. 1076-1079, 1999.

[1.43] T. Komoda, Y. Honda, T. Hatai, Y. Watabe, T. Ichihara, K. Aizawa, Y. Kondo, and N. Koshida, "Efficient Quasi-Ballistic Cold Cathode Based on Porous Polysilicon Thin Film for Possible Application to Flat Panel Display," *IDW '99, Tech Digest,* pp. 939-942, 1999.

[1.44] T. Ichihara, Y. Honda, K. Aizawa, T. Komoda, and N. Koshida, "Development of ballistic electron cold cathode by a low-temperature processing of polycrystalline silicon films," *J Crys Growth,* Vol. 237–239, pp. 1915-1919, 2002.

[1.45] T. Ichihara, Y. Honda, T. Baba, Y. Takegawa, Y. Watabe, T. Hatai, K. Aizawa, T. Komoda, V. Vezin, and N. Koshida, "Improved Electron Emission Characteristics of BSD (Ballistic Electron Surface-Emitting Display) on a Glass Substrate Fabricated with Low Temperature Process," *IDW '02, Tech Digest*, pp. 1033-1036, 2002.

[1.46] R. C. Miller and A. Savage, "Motion of 180° Domain Walls in Metal Electroded Barium Titanate Crystals as a Function of Electric Field and Sample Thickness," *J. Appl. Phys.*, Vol. 31, pp. 662-669, 1960.

[1.47] A. Koller and M. Beranek, "Einige neue Erkenntnisse über die Degradation von Titanaten im Zusammenhang mit der Exoemission," *Czech, J. Phys.*, Vol. 9, pp. 402-403, 1959.

[1.48] G. Rosenman, D. Shur, Y. E. Krasik, and A. Dunaevsky, "Electron Emission

from Ferroelectrics," *J. Appl. Phys.*, Vol. 88, pp. 6109-6161, 2000.

[1.49]   W. Zhu, "Vacuum Microelectronics," John-Wiley & Sons publisher, New York, 2001.

[1.50]   E. Yamaguchi, K. Sakai, I. Nomura, T. Ono, M. Yamanobe, N. Abe, T. Hara, K. Hatanaka, Y. Osada, H. Yamamoto, and T. Nakagiri, "A 10-in. Surface-Conduction Electron-Emitter Display," *J. SID*, Vol. 5, pp. 345-348, 1997.

[1.51]   J. A. Oro and D. D. Ball, "Lateral field-emission devices with subtenth-micron emitter to anode spacing," *J. Vac. Sci. Technol. B*, Vol. 11, pp. 464-467, 1993.

[1.52]   Y. Gotoh, T. Ohtake, N. Fujita, K. Inoue, H. Tsuji, and J. Ishikawa, "Fabrication of lateral-type thin-film edge field emitters by focused ion beam technique," *J. Vac. Sci. Technol. B*, Vol. 13, pp. 465-468, 1995.

[1.53]   C. S. Lee and C. H. Han, "A novel sub-micron gap fabrication technology using chemical–mechanical polishing (CMP): application to lateral field emission device (FED)," *Sens. Actuators A*, Vol. 97-98, pp. 739-743, 2002.

[1.54]   F. J. Himpsel, J. A. Knapp, J. A. van Vechten, and D. E. Eastman, "Quantum photoyield of diamond(111)—A stable negative-affinity emitter," *Phys. Rev. B*, Vol. 20, pp. 624-627 ,1979.

[1.55]   S. Lee, B. K. Ju, Y. H. Lee, D. Jeon, and M. H. Oh, "Fabrication and field emission study of gated diamondlike-carbon-coated silicon tips," *J. Vac. Sci. Technol. B*, Vol. 15, p.425, 1997.

[1.56]   K. L. Park, J. H. Moon, S. J. Chung, J. Jang, M. H. Oh, and W. I. Milne, "Deposition of N-type Diamond-like Carbon by Using the Layer-by-layer Technique and its Electron Emission Properties," *Appl. Phys. Lett.*, Vol. 70, pp. 1381-1383, 1997.

[1.57] F. Y. Chuang, C. Y. Sun, T. T. Chen, and I. N. Lin, "Local Electron Field Emission Characteristics of Pulsed Laser Deposited Diamond-like Carbon Films," *Appl. Phys. Lett.*, Vol. 69, pp. 3504-3506, 1996

[1.58] J. Robertson, "Recombination and Photoluminescence Mechanism in Hydrogenated Amorphous Carbon," *Phys. Rev. B*, Vol. 53, pp.16302-16305, 1996.

[1.59] J. Rinstein, J. Schafer, and L. Ley, "Effective Correlation Energies for Defects in a-C:H from a Comparison of Photelectron Yield and Electron Spin Resonance Experiments," *Diam. Relat. Mater.*, Vol. 4, pp. 508-516, 1995.

[1.60] S. Iijima, "Helical Microtubules of Graphitic Carbon," *Nature*, Vol. 354, pp. 56-58, 1991.

[1.61] W. A. de Heer, A. Chateline, D. Ugrate, "A Carbon Nanotube Field-emission Electron Source," *Science*, Vol. 270, pp. 1179-1180, 1995.

[1.62] K. A. Dean and B. R. Chalamala, "Current Saturation Mechanisms in Carbon Nanotube Field Emitters," *Appl. Phys. Lett.*, Vol. 76, pp. 375-377, 2000.

[1.63] W. Zhu, C. Bower, O. Zhou, G. Kochanski, and S. Jin, "Large Current Density from Carbon Nanotube Field Emitters," *Appl. Phys. Lett.*, Vol. 75, pp. 873-875, 1999.

[1.64] H. Zeng, L. Zhu, G. Hao, and R. Sheng, "Synthesis of various forms of carbon nanotubes by AC arc discharge," *Carbon*, Vol. 36, pp. 259-261, 1998.

[1.65] M. Yudasaka, T. Komatsu, T. Ichihashi, and S. Iijima, "Single-wall carbon nanotube formation by laser ablation using double-targets of carbon and metal," *Chem. Phys. Lett.*, Vol. 278, pp. 102-106, 1997.

[1.66] M. Su, B. Zheng, and J. Liu, "A scalable CVD method for the synthesis of single-walled carbon nanotubes with high catalyst productivity," *Chem. Phys. Lett.*, Vol. 322, pp. 321-326, 2000.

Chapter 2

[2.1]   S. Iijima, "Helical Microtubules of Graphitic Carbon," *Nature*, Vol. 354, pp. 56-58, 1991.

[2.2]   W. A. de Heer, A. Châtelain, and D. Ugarte, "A Carbon Nanotube Field-Emission Electron Source," *Science*, Vol. 270, pp. 1179-1180, 1995.

[2.3]   S. Fan, M. G. Chapline, N. R. Franklin, T. W. Tombler, A. M. Cassell, and H. Dai, "Self-Oriented Regular Arrays of Carbon Nanotubes and Their Field Emission Properties," *Science*, Vol. 283, p. 512, 1999.

[2.4]   P. G. Collins and A. Zettl, "A simple and robust electron beam source from carbon nanotubes," *Appl. Phys. Lett.*, Vol. 69, pp. 1969-1971, 1996.

[2.5]   Q. H. Wang, T. D. Corrigan, J. Y. Dai, R. P. H. Chang, and A. R. Krauss, "Field emission from nanotube bundle emitters at low fields," *Appl. Phys. Lett.*, Vol. 70, pp. 3308-3310, 1997.

[2.6]   W. Zhu, C. Bower, O. Zhou, G. Kochanski, and S. Jin, "Very Large Current Density from Carbon Nanotube Field Emitters," *IEDM Technical Digest*, pp. 705-708, 1999.

[2.7]   W. B. Choi, D. S. Chung, J. H. Kang, H. Y. Kim, Y. W. Jin, I. T. Han, Y. H. Lee, J. E. Jung, N. S. Lee, G. S. Park, and J. M. Kim, "Fully sealed, high-brightness carbon-nanotube field-emission display," *Appl. Phys. Lett.*, Vol. 75, pp. 3129-3131, 1999.

[2.8]   J. Yotani, S. Uemura, T. Nagasako, H. Kurachi, H. Yamada, T. Ezaki, T. Maesoba, T. Nakao, M. Ito, Y. Saito, and M. Yumura, "CNT-FED for Character Displays," *SID Int. Symp. Dig. Tech. Pap.,* Vol. 35, pp. 828-831, 2004.

[2.9]   K. A. Dean, B. F. Coll, E. Howard, S. V. Johnson, M. R. Johnson, H. Li, D. C. Jordan, L. Hilt Tisinger, M. Hupp, S. G. Thomas, E. Weisbrod, S. M. Smith, S. R. Young, J. Baker, D. Weston, W. J. Dauksher, Y. Wei, and J. E. Jaskie, "Color Field Emission Display for Large Area HDTV," *SID Int. Symp. Dig. Tech. Pap.,* Vol. 36, pp. 1936-1939, 2005.

[2.10]   R. L. Fink, L. H. Thuesen, V. Ginsberg, D. S. Mao, Y. J. Li, and Z. Yaniv, "Twenty-Five Inch Diagonal Carbon Nanotube Field Emission Display," *SID Int. Symp. Dig. Tech. Pap.,* Vol. 37, pp. 1748-1751, 2006.

[2.11]   W. B. Choi, D. S. Chung, J. H. Kang, H. Y. Kim, Y. W. Jin, I. T. Han, Y. H. Lee, J. E. Jung, N. S. Lee, G. S. Park, and J. M. Kim, "Fully sealed, high-brightness carbon-nanotube field-emission display," *Appl. Phys. Lett.*, Vol. 75, pp. 3129-3131, 1999.

[2.12]   W. B. Choi, Y. W. Jin, H. Y. Kim, S. J. Lee, M. J. Yun, J. H. Kang, Y. S. Choi, N. S. Park, N. S. Lee, and J. M. Kim, "Electrophoresis deposition of carbon nanotubes for triode-type field emission display," *Appl. Phys. Lett.*, Vol. 78, pp. 1547-1549, 2001.

[2.13]   S. I. Honda, K. Y. Lee, K. Aoki, T. Hirao, K. Oura, and M. Katayama, "Low-Temperature Synthesis of Aligned Carbon Nanofibers on Glass Substrates by Inductively Coupled Plasma Chemical Vapor Deposition," *Jpn. J. Appl. Phys.*, Vol. 45, pp. 5326-5328, 2006.

[2.14]   Y. S. Woo, I. T. Han, Y. J. Park, H. J. Kim, J. E. Jung, N. S. Lee, D. Y. Jeon, and J. M. Kim, "Effect of Ion Bombardment on Microstructures of Carbon Nanotubes Grown by Electron Cyclotron Resonance Chemical Vapor Deposition at Low Temperatures," *Jpn. J. Appl. Phys.*, Vol. 42, pp. 1410-1413, 2003.

[2.15]   Z. F. Ren, Z. P. Huang, J. W. Xu, J. H. Wang, P. Bush, M. P. Siegal, and P.

N. Provencio, "Synthesis of Large Arrays of Well-Aligned Carbon Nanotubes on Glass," *Science*, Vol. 282, pp. 1105-1107, 1998.

[2.16] Y. J. Park, I. T. Han, H. J. Kim, Y. S. Woo, N. S. Lee, Y. W. Jin, J. E. Jung, J. H. Choi, D. S. Jung, C. Y. Park, and J. M. Kim, "Effect of Catalytic Layer Thickness on Growth and Field Emission Characteristics of Carbon Nanotubes Synthesized at Low Temperatures Using Thermal Chemical Vapor Deposition," *Jpn. J. Appl. Phys.*, Vol. 41, pp. 4679-4685, 2002.

[2.17] I. T. Han, H. J. Kim, Y. J. Park, Y. W. Jin, J. E. Jung, J. M. Kim, B. K. Kim, N. S. Lee, and S. K. Kim, "Synthesis of Highly Crystalline Multiwalled Carbon Nanotubes by Thermal Chemical Vapor Deposition Using Buffer Gases," *Jpn. J. Appl. Phys.*, Vol. 46, pp. 3631-3635, 2004.

[2.18] S. Hofmann, G. Csa´nyi, A. C. Ferrari, M. C. Payne, and J. Robertson, "Surface Diffusion: The Low Activation Energy Path for Nanotube Growth," *Phys. Rev. Lett.*, Vol. 95, p. 036101, 2005.

[2.19] S. Hofmann, C. Ducati, J. Robertson and, B. Kleinsorge, "Low-temperature growth of carbon nanotubes by plasma-enhanced chemical vapor deposition," *Appl. Phys. Lett.*, Vol. 83, pp. 135-137, 2003.

[2.20] R. T. L. Baker and M. A. Barber: in *Chemistry and Physics of Carbon*, ed. P. L. Walker and P. A. Thrower (Dekker, New York, 1978), Vol. 14, p. 83.

[2.21] C. J. Lee, J. Park, S. Han, and J. Ihm, "Growth and field emission of carbon nanotubes on sodalime glass at 550°C using thermal chemical vapor deposition," *Chem. Phys. Lett.*, Vol. 337, pp. 398-403, 2001.

[2.22] C. J. Lee, T. J. Lee, and J. Park, "Carbon nanofibers grown on sodalime glass at 500°C using thermal chemical vapor deposition," *Chem. Phys. Lett.*, Vol. 340, pp. 413-418, 2001.

[2.23] G. Takeda, L. Pan, S. Akita, and Y. Nakayama, "Vertically Aligned Carbon

Nanotubes Grown at Low Temperatures for Use in Displays," *Jpn. J. Appl. Phys.*, Vol. 44, pp. 5642-5645, 2005.

[2.24] Y. Ishikawa and H. Jinbo, "Synthesis of Multiwalled Carbon Nanotubes at Temperatures below 300℃ by Hot-Filament Assisted Chemical Vapor Deposition," *Jpn. J. Appl. Phys.*, Vol. 44, pp. L394-L397, 2005.

[2.25] K. Kamada, T. Ikuno, S. Takahashi, T. Oyama, T. Yamamoto, M. Kamizono, S. Ohkura, S. Honda, M. Katayama, T. Hirao, and K. Oura, "Surface morphology and field emission characteristics of carbon nanofiber films grown by chemical vapor deposition on alloy catalyst," *Appl. Surf. Sci.*, Vol. 212-213, pp. 383-387, 2003.

[2.26] A. A. Puretzky, D. B. Geohegan, S. Jesse, I. N. Ivanov, and G. Rres, "In situ measurements and modeling of carbon nanotube array growth kinetics during chemical vapor deposition," *Appl. Phys. A*, Vol. 81, pp. 223-240, 2003.

[2.27] L. Jodin, A. C. Dupuis, E. Rouviere, and P. Reiss, "Influence of the Catalyst Type on the Growth of Carbon Nanotubes via Methane Chemical Vapor Deposition," *J. Phys. Chem. B*, Vol. 110, pp. 7328-7333, 2006.

[2.28] L. Delzeit, B. Chen, A. Cassell, R. Stevens, C. Nguyen, and M. Meyyappan, "Multilayered metal catalysts for controlling the density of single-walled carbon nanotube growth," *Chem. Phys. Lett.*, Vol. 348, pp. 368-374, 2001.

[2.29] H. Cui, G. Eres, J. Y. Howe, A. Puretkzy, M. Varela, D. B. Geohegan, and D. H. Lowndes, "Growth behavior of carbon nanotubes on multilayered metal catalyst film in chemical vapor deposition," *Chem. Phys. Lett.*, Vol. 374, pp. 222-228, 2003.

[2.30] G. A. J. Amaratunga and S. R. P. Silva, "Nitrogen containing hydrogenated amorphous carbon for thin-film field emission cathodes," *Appl. Phys. Lett.*, Vol. 68, pp. 2529-2531, 1996.

[2.31] K. Y. Lee, S. Honda, M. Katayama, T. Miyake, K. Himuro, K. Oura, J. G. Lee, H. Mori, and T. Hirao, "Vertically aligned growth of carbon nanotubes with long length and high density," *J. Vac. Sci. Technol. B*, Vol. 23, pp. 1450-1453, 2005.

[2.32] S. Satio, A. Kawabata, D. Kondo, M. Nihei, and Y. Awano, "Carbon nanotube growth from titanium–cobalt bimetallic particles as a catalyst," *Chem. Phys. Lett.*, Vol. 402, pp. 149-154, 2005.

[2.33] G. Radhakrishnan, P. M. Adams, and D. M. Speckman, "Low temperature pulsed laser deposition of titanium carbide on bearing steels," *Thin Solid Films*, Vol. 358, pp. 131-138, 2000.

[2.34] Y. Y. Chang, S. J. Yang, and D. Y. Wang, "Structural and mechanical properties of Cr–C–O thin films synthesized by a cathodic-arc deposition process," *Surface & Coatings Technology*, Vol. 202, pp. 941-945, 2007.

Chapter 3

[3.1] C. Ducati, I. Alexandrou, M. Chhowalla, J. Robertson, and G. A. J. Amaratunga, "The role of the catalytic particle in the growth of carbon nanotubes by plasma enhanced chemical vapor deposition," *J. Appl. Phys.*, Vol. 95, pp. 6387-6391, 2004.

[3.2] S. Fan, M. G. Chapline, N. R. Franklin, T. W. Tombler, A. M. Cassell, and H. Dai, "Self-Oriented Regular Arrays of Carbon Nanotubes and Their Field Emission Properties," *Science*, Vol. 283, p. 512, 1999.

[3.3] C. P. Deck and K. Vecchio, "Prediction of carbon nanotube growth success by the analysis of carbon–catalyst binary phase diagrams," *Carbon*, Vol. 44, pp. 267-275, 2006.

[3.4]   Y. M. Shyu, F. C. N. Hong, "The effects of pre-treatment and catalyst composition on growth of carbon nanofibers at low temperature," *Diamond Relat. Mater.*, Vol. 10, pp. 1241-1245, 2001.

[3.5]   Y. J. Park, I. T. Han, H. J. Kim, Y. S. Woo, N. S. Lee, Y. W. Jin, J. E. Jung, J. H. Choi, D. S. Jung, C. Y. Park, and J. M. Kim, "Effect of Catalytic Layer Thickness on Growth and Field Emission Characteristics of Carbon Nanotubes Synthesized at Low Temperatures Using Thermal Chemical Vapor Deposition," *Jpn. J. Appl. Phys.*, Vol. 41, pp. 4679-4685, 2002.

[3.6]   M. P. Siegal, D. L. Overmyer, and F. H. Kaatz, "Controlling the site density of multiwall carbon nanotubes via growth conditions," *Appl. Phys. Lett.*, Vol. 84, pp. 5156-5158, 2004.

[3.7]   I. T. Han, H. J. Kim, Y. J. Park, Y. W. Jin, J. E. Jung, J. M. Kim, B. K. Kim, N. S. Lee, and S. K. Kim, "Synthesis of Highly Crystalline Multiwalled Carbon Nanotubes by Thermal Chemical Vapor Deposition Using Buffer Gases," *Jpn. J. Appl. Phys.*, Vol. 43, pp. 3631-3635, 2004.

[3.8]   G. Y. Xiong, Y. Suda, D. Z. Wang, J. Y. Huang, and Z. F. Ren, "Effect of temperature, pressure, and gas ratio of methane to hydrogen on the synthesis of double-walled carbon nanotubes by chemical vapour deposition," *Nanotechnology*, Vol. 16, pp. 532-535, 2005.

[3.9]   K. Kuwana, H. Endo, K. Saito, D. Qian, R. Andrews, and E. A. Grulke, "Catalyst deactivation in CVD synthesis of carbon nanotubes," *Carbon*, Vol. 43, pp. 253-260, 2005.

[3.10] M. Sveningsson, R. E. Morjan, O.A. Nerushev, Y. Sato, J. Bäckström, E.E.B. Campbell, F. Rohmund, "Raman spectroscopy and field-emission properties of CVD-grown carbon-nanotube films," *Appl. Phys. A*, Vol. 73, pp. 409-418, 2001.

[3.11]   C. Lan, P. B. Amama, T. S. Fisher, and R. G. Reifenberger, "Correlating electrical resistance to growth conditions for multiwalled carbon nanotubes," *Appl. Phys. Lett.*, Vol. 91, p. 093105, 2007.

[3.12]   G. F. Malgas, C. J. Arendse, N. P. Cele, and F. R. Cummings, "Effect of mixture ratios and nitrogen carrier gas flow rates on the morphology of carbon nanotube structures grown by CVD," *J Mater. Sci.*, Vol. 43, pp. 1020-1025, 2008.

[3.13]   S. Hofmann, C. Ducati, J. Robertson, and B. Kleinsorge, "Low-temperature growth of carbon nanotubes by plasma-enhanced chemical vapor deposition," *Appl. Phys. Lett.*, Vol. 83, pp. 135-137, 2003.

[3.14]   R. T. L. Baker and M. A. Barber: in *Chemistry and Physics of Carbon*, ed. P. L. Walker and P. A. Thrower (Dekker, New York, 1978), Vol. 14, p. 83.

[3.15]   K. K. Nanda, S. N. Sahu, and S. N. Behera, "Liquid-drop model for the size-dependent melting of low-dimensional systems," *Phys. Rev. A*, Vol. 66, p. 013208, 2002.

Chapter 4

[4.1]   Q. H. Wang, M. Yan, and R. P. H. Chang, "Flat panel display prototype using gated carbon nanotube field emitters," *Appl. Phys. Lett.*, Vol. 78, pp. 1294-1296, 2001.

[4.2]   K. J. Chen, W. K. Hong, C. P. Lin, K. H. Chen, L. C. Chen, and H. C. Cheng, "Low Turn-On Voltage Field Emission Triodes With Selective Growth of Carbon Nanotubes," *IEEE Electron Device Lett.*, Vol. 22, pp. 516-518, 2001.

[4.3]   H. C. Cheng, K. J. Chen, W. K. Hong, F. G. Tantair, C. P. Lin, K. H. Chen, and L. C. Chen, "Fabrication and Characterization of Low Turn-On Voltage

Carbon Nanotube Field Emission Triodes," *Electronchem. Solid-State Lett.*, Vol. 4, pp. H15-H17, 2001.

[4.4]   Y. S. Choi, J. H. Park, W. B. Choi, C. J. Lee, S. H. Jo, C. G. Lee, J. H. You, J. E. Jung, N. S. Lee, and J. M. Kim, "An under-gate triode structure field emission display with carbon nanotube emitters," *Diamond Relat. Mater.*, Vol. 10, pp. 1705-1708, 2001.

[4.5]   J. E. Jung, Y. W. Jin, J. H. Choi, Y. J. Park, T. Y. Ko, D. S. Chung, J. W. Kim, J.E. Jang, S. N. Cha, W. K. Yi, S. H. Cho, M. J. Yoon, C. G. Lee, J. H. You, N. S. Lee, J. B. Yoo, and J. M. Kim, "Fabrication of triode-type field emission displays with high-density carbon-nanotube emitter arrays," *Physica B*, Vol. 323, pp. 71-77, 2002.

[4.6]   Y. S. Choi, J. H. Kang, H. Y. Kim, B. G. Lee, C. G. Lee, S. K. Kang, Y. W. Jin, J. W. Kim, J. E. Jung, and J. M. Kim, "A simple structure and fabrication of carbon-nanotube field emission display," *Appl. Surf. Sci.*, Vol. 221, pp. 370-374, 2004.

[4.7]   D. Y. Kim, J. B. Yoo, I. T. Han, H. J. Kim, H. J. Kim, J. E. Jung, Y. W. Jin, J. M. Kim, and K. H. Chin, "The density control of carbon nanotubes using spin-coated nanoparticle and its application to the electron emitter with triode structure," *Diamond Relat. Mater.*, Vol. 14, pp. 2084-2088, 2005.

[4.8]   Y. C. Choi, K. S. Jeong, I. T. Han, H. J. Kim, Y. W. Jin, J. M. Kim, B. G. Lee, J. H. Park, and D. H. Choe, "Double-gated field emitter array with carbon nanotubes grown by chemical vapor deposition," *Appl. Phys. Lett.*, Vol. 88, p. 263504, 2006.

[4.9]   C. M. Tang, T. A. Swyden, and A. C. Ting, "Planar lenses for field-emitter arrays," *J. Vac. Sci. Technol. B*, Vol. 13, pp. 571-575, 1995.

[4.10] L. Dvorson and A. I. Akinwande, "Double-gated Spindt emitters with stacked

focusing electrode," *J. Vac. Sci. Technol. B*, Vol. 20, pp. 53-59, 2002.

[4.11]   C. Xie, Y. Wei, and B. G. Smith, "A Novel Approach for Focusing Electron Beams Using Low-Cost Ceramic Grid," *IEEE Trans. Electron Devices*, Vol. 49, pp. 324-328, 2002.

[4.12]   Wei Zhu, "Vacuum Microelectronics," John-Wiley & Sons publisher, New York, 2001.

[4.13]   N. Tsukahara, H. Nakano, H. Murakami, M. Hirakawa, T. Kojima, K. Kageyama, and T. Sasaki, "A 4.8 inch GNF-FED with A Mesh Gate Structure," *SID Int. Symp. Dig. Tech. Pap.,* Vol. 37, pp. 660-662, 2006.

[4.14]   Y. Ishizuka, T. Oyaizu, T. Oguchi, H. Hoshi, and E. Yamaguchi, "High-brightness, High-resolution, High-contrast, and Wide-gamut Features of Surface-conduction Electron-emitter Displays," *IDW '05, Tech Digest*, pp. 1655-1658, 2005.

[4.15]   J. H. Choi, A. R. Zoulkarneev, Y. W. Jin, Y. J. Park, D. S. Chung, B. K. Song, I. T. Han, H. W. Lee, S. H. Park, H. S. Kang, H. J. Kim, J. E. Jung, and J. M. Kim, "Carbon nanotube field emitter arrays having an electron beam focusing structure," *Appl. Phys. Lett.*, Vol. 84, pp. 1022-1024, 2004.

[4.16]   J. H. Choi, A. R. Zoulkarneev, Y. J. Park, D. S, Chung, B. K. Song, H. S. Kang, C. W. Baik, I. T. Han, H. J. Kim, M. J. Shin, H. J. Kim, T. S. Oh, Y. W. Jin, J. M. Kim, and N. Lee, "Optimization of Electron Beam Focusing for Gated Carbon Nanotube Field Emitter Arrays," *IEEE Trans. Electron Devices*, Vol. 52, pp. 2584-2590, 2005.

[4.17]   M. S. Dresselhaus and P. C. Eklund, "Phonons in carbon nanotubes," *Adv. Phys.*, Vol. 52, pp. 705-814, 2000.

Chapter 5

[5.1] H. F. Gray, G. J. Campisi, and R. F. Greene, "A Vacuum Field Effect Transistor Using Silicon Field Emitter Arrays," *IEDM Technical Digest*, pp. 776-779, 1986.

[5.2] I. Brodie and C. A. Spindt, "Vacuum microelectronics," Adv. Electron. *Electron Phys.*, Vol. 83, pp. 1-106, 1992.

[5.3] H. H. Busta, "Vacuum microelectronics-1992," *J. Micromech. Microeng*, Vol. 2, pp. 43-74, 1992.

[5.4] J. P. Spallas and N. C. MacDonald, "Fabrication and Operation of Silicon Field Emission Cathode Arrays," *IEDM Technical Digest*, pp. 209-212, 1991.

[5.5] T. Maruyama, S. Katoh, and T. Kobayashi, "Design and Experiments on Improved Cathode Configuration for Diamond Planar Field Emission Display Elements**,**" *Jpn. J. Appl. Phys.*, Vol. 42, pp. 274-279, 2003.

[5.6] J. A. Oro and D. D. Ball, "Lateral field-emission devices with subtenth-micron emitter to anode spacing**,**" *J. Vac. Sci. Technol. B*, Vol. 11, pp. 464-467, 1993.

[5.7] Y. Gotoh, K. Inoue, T. Ohtake, H. Ueda, Y. Hishida, H. Tsuji, and J. Ishikawa, "Application of Focused Ion Beam Techniques to the Fabrication of Lateral-Type Thin-Film Edge Field Emitters**,**" *Jpn. J. Appl. Phys.*, Vol. 33, pp. L63-L66, 1994.

[5.8] Y. Gotoh, T. Ohtake, N. Fujita, K. Inoue, H. Tsuji, and J. Ishikawa, "Fabrication of lateral-type thin-film edge field emitters by focused ion beam technique**,**" *J. Vac. Sci. Technol. B*, Vol. 13, pp. 465-468, 1995.

[5.9] C. S. Lee and C. H. Han, "A novel sub-micron gap fabrication technology using chemical–mechanical polishing (CMP): application to lateral field

emission device (FED)**,**” *Sens. Actuators A*, Vol. 97-98, pp. 739-743, 2002.

[5.10]   W. J. Zang, J. H. Lee, J. H. Lee, Y. H. Bae, C. A. Choi, and S. H. Hahm, “Lateral field emission diode with wedge-type tip and nanogap on separation by implantation of oxygen silicon**,**” *J. Vac. Sci. Technol. B*, Vol. 18, pp. 1006-1008, 2000.

[5.11]   T. Oguchi, E. Yamaguchi, K. Sasaki, K. Suzuki, S. Uzawa, and K. Hatanaka, “A 36-inch Surface-conduction Electron-emitter Display (SED),” *SID Int. Symp. Dig. Tech. Pap.*, Vol. 36, pp. 1929-1931, 2005.

[5.12]   K. M. Lee, H. J. Han, S. Choi, K. H. Park, S. G. Oh, S. Lee, and K. H. Koh, “Effects of metal buffer layers on the hot filament chemical vapor deposition of nanostructured carbon films**,**” *J. Vac. Sci. Technol. B*, Vol. 21, pp. 623-626, 2003.

[5.13]   X. W. Liu, S. H. Tsai, L. H. Lee, M. X. Yang, and A. C. M. Yang, “Electron field emission from amorphous carbon nitride synthesized by electron cyclotron resonance plasma**,**” *J. Vac. Sci. Technol. B*, Vol. 18, pp. 1840-1846, 2000.

[5.14]   X. W. Liu, L. H. Chan, W. J. Hsieh, J. H. Lin, and H. C. Shih, “The effect of argon on the electron field emission properties of a-C:N thin films**,**” *Carbon*, Vol. 41, pp. 1143-1148, 2003.

[5.15]   M. S. Lim, C. M. Park, and M. K. Han, “Investigation of field emission characteristics for Si-base materials: Titanium silicide, poly-Si, and single crystal Si**,**” *J. Vac. Sci. Technol. B*, Vol. 17, pp. 635-637, 1999.

[5.16]   W. P. Kang, J. L. Davidson, A. Wisitsora-at, M. Howell, A. Jamaludin, Y. M. Wong, K. L. Soh, and D. V. Kerns, “Fabrication and field emission characteristics of lateral diamond field emitter**,**” *J. Vac. Sci. Technol. B*, Vol. 21, pp. 593-596, 2003.

[5.17]   J. Y. Luo, K. S. Liu, J. S. Lee, I. N. Lin, and H. F. Cheng, "The influence of film-to-substrate characteristics on the electron field emission behavior of the diamond films," *Diamond Relat. Mater.*, Vol. 7, pp. 704-710, 1998.

[5.18]   A. Hart, B. S. Satyanarayana, W. I. Milne, and J. Robertson, "Field emission from tetrahedral amorphous carbon as a function of surface treatment and substrate material," *Appl. Phys. Lett.*, Vol. 74, pp. 1594-1596, 1999.

[5.19]   N. S. Xu, J. Chen, and S. Z. Deng, "Physical origin of nonlinearity in the Fowler–Nordheim plot of field-induced emission from amorphous diamond films: Thermionic emission to field emission," *Appl. Phys. Lett.*, Vol. 76, pp. 2463-2465, 2000.

[5.20]   J. B. Cui, K. B. Teo, J. T. H. Tsai, J. Robertson, and W. I. Milne, "The role of dc current limitations in Fowler–Nordheim electron emission from carbon films," *Appl. Phys. Lett.*, Vol. 77, pp. 1831-1833, 2000.
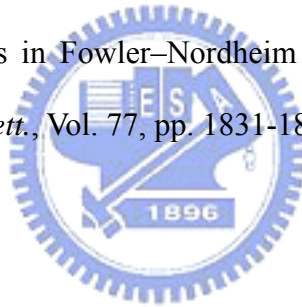
Tables

Table 1.1 Comparison between vacuum microelectronics and solid-state electronics

Items	Solid State Microelectronics	Vacuum Microelectronics
Current Density	$10^4 - 10^5$ (A/cm^2)	similar
Turn-on Voltage	0.1 – 0.7 V	5 – 300 V
Structure	solid/solid interface	solid/vacuum interface
Electron Transport	in solid	in vacuum
Electron Velocity	3×10^7 (cm/sec)	3×10^{10} (cm/sec)
Flicker Noise	due to interface	due to emission
Thermal & Short Noise	comparable	comparable
Electron Energy	< 0.3 eV	a few to 1000 eV
Cut-off Frequency	< 20 GHz (Si) & 100 GHz (GaAs)	< 100 – 1000 GHz
Power	small – medium	medium – large
Radiation Hardness	poor	excellent
Temperature Effect	-30 – 50 °C	< 500 °C
Fabrication & Materials	well established (Si) & fairly well (GaAs)	not well established

Table 1.2 The history of vacuum microelectronics

1950s	Foundations of field emission physics
1958	Buck and Shoulders (SRI) – proposals for fabricating vacuum microelectronics devices
1961	Shoulders (SRI) – proposals for vertical and lateral microtriodes
1968	Spint (SRI) –fabrication and operation of gated Mo-FEAs
1981	Henry Gary (NRL) – lateral vacuum triode using silicon field emitters
1985	Robert Meyer – demonstration of matrix addressable monochrome display with field-emission cathode array
1988	Meyer and Baptist (LETI) – Mo microtips with lateral resistive layer
1993	Pixtech Consortium – demonstration of full color FED
1993	Kumar (MCC) – demonstration of FED with carbon/diamond film
1995	Pixtech/Futaba – demonstration of low voltage color display
1997	Motorola – demonstration of high voltage full color FED
2000	Sony/Candescent – demonstration of full color 5.5" and 13.2" FED

Table 1.3 The comparison of several flat panel displays

	FED	OLED	PDP	LCD	CRT
low cost	?	▲	▲	▲	★
viewing angle	★	★	★	✕	★
life time	?	✕	▲	★	★
response time	★	▲	★	✕	★
power consumption	★	▲	✕	★	✕
resolution	▲	★	▲	★	✕
weight	★	★	★	★	✕
display area	★	▲	★	★	✕

★： good

▲： medium

✕： bad

 ?： unsure

Table 2.1 Field emission characteristics of CNTs synthesized with different catalysts

Catalysts	Turn on Field (V/µm) @ J≈10µA/cm^2	Anode Current (mA/cm^2) @ E≈6 V/µm
20Co	N/A	N/A
20Co/20Cr	N/A	N/A
20Co/100Al	5.2	0.11
20Co/20Cr/20Al	4.1	0.82
200Co/20Cr/50Al	4.3	1.02
20Co/20Cr/100Al	3.8	8.28
20Co/20Cr/200Al	3.1	2.48

Table 2.2 Field emission characteristics of CNTs synthesized with multilayer catalysts consisting of different interlayers

Interlayer	Turn on Field (V/µm) @ J≈10µA/cm^2	Anode Current (mA/cm^2) @ E≈6 V/µm
N/A	4.38	1.95
Cu	4.63	0.60
Mo	4.38	0.98
Pd	4.93	0.48
Pt	4.43	0.98
Ta	4.03	2.35
Ti	4.38	12.80
W	4.78	0.23
Cr	3.72	12.80
Hf	3.90	2.64

Table 2.3 Field emission characteristics of CNTs synthesized with multilayer catalysts (Co/Cr/Al) consisting of different Cr interlayer thickness

Cr interlayer thickness (Å)	Turn on Field (V/μm) @ J≈10μA/cm^2	Anode Current (mA/cm^2) @ E≈6 V/μm
0	4.38	1.95
10	4.25	7.28
20	3.72	12.80
30	3.71	18.24
50	4.59	14.28
100	N/A	N/A

Table 2.4 Field emission characteristics of CNTs synthesized with multilayer catalysts (Co/Ti/Al) consisting of different Ti interlayer thickness

Ti interlayer thickness (Å)	Turn on Field (V/μm) @ J≈10μA/cm^2	Anode Current (mA/cm^2) @ E≈6 V/μm
0	4.38	1.95
10	3.63	6.88
20	4.38	12.80
30	3.50	28.60
50	3.50	19.00
100	3.13	12.56
150	3.56	2.78

Table 2.5 Formation heat of metal carbides

Carbide	Sub lattice	$\triangle$H (eV)
TiC	FCC	1.91
CrC	FCC	-0.01
Cr_3C_2	Compl.	0.442
Cr_7C_3	Compl.	0.555
$Cr_{23}C_6$	Compl.	0.567
FeC	FCC	-0.43
Fe_3C	Compl.	-0.22
CoC	FCC	-0.53
Co_3C	Compl.	-0.2
NiC	FCC	-0.64
Ni_3C	Compl.	-0.3
PdC	FCC	-0.66
PtC	FCC	-0.64
TaC	FCC	1.48
Ta_2C	FCC	2.16
HfC	FCC	2.17
MoC	simple	0.13
Mo_2C	hex	0.48
WC	simple	0.42
W_2C	hex	0.54

Table 3.1 Field emission characteristics of CNTs depending on the H_2/N_2 flow ratios

H_2/N_2 (sccm)	Turn on Field (V/μm) @ J≈10μA/cm²	Anode Current (mA/cm²) @ E≈6 V/μm
0/1000	3.46	4.72
10/990	3.43	16.20
20/980	4.28	1.43
50/950	N/A	N/A

Table 3.2 Field emission characteristics of CNTs depending on the N_2 flow rates

N_2 (sccm)	Turn on Field (V/μm) @ J≈10μA/cm²	Anode Current (mA/cm²) @ E≈6 V/μm
0	3.69	8.28
250	4.48	0.69
500	4.12	3.35
750	2.84	11.92
1000	2.27	17.52
1250	3.71	0.96
1500	3.75	1.48
2000	4.81	0.37
5000	5.78	0.04

Table 3.3 Field emission characteristics of CNTs depending on the C_2H_4 flow rates

C_2H_4 (sccm)	Turn on Field (V/μm) @ J≈10μA/cm²	Anode Current (mA/cm²) @ E≈6.25 V/μm
25	4.46	0.58
50	3.91	6.84
75	2.53	17.44
100	2.01	19.40
125	1.81	26.50
138	3.41	22.10

Figures

(a)

(b)
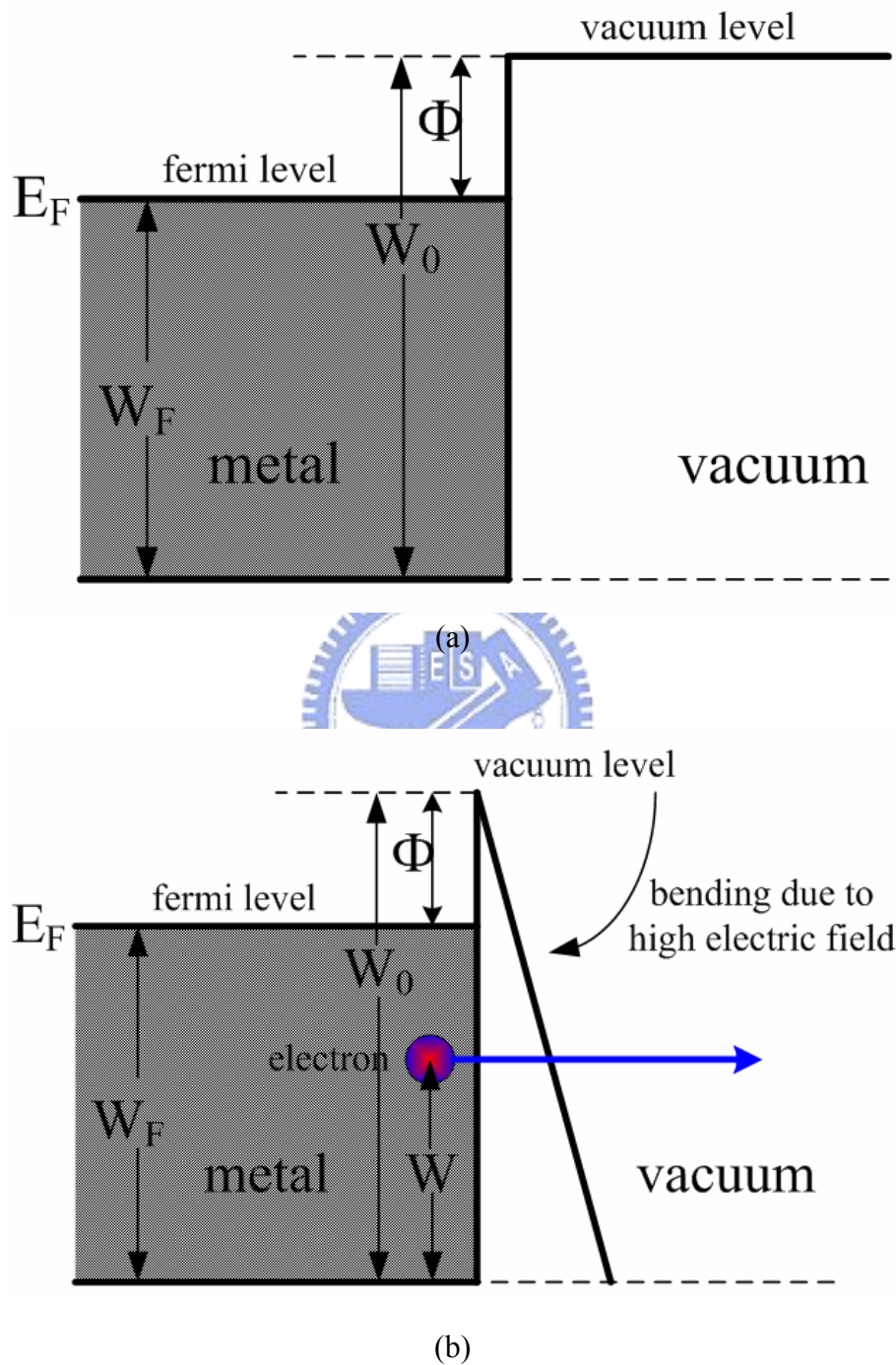
Figure 1.1   The band diagram of the field-emission emitters in the vacuum environment (a) without applied electric field and (b) with applied electric field.

In a CRT, the electron gun locate far from the anode.

In a FED, the emitter array sits only a milimeter away from the anode.

cross-section of a FED

1. dielectric
2. patterned resister layer
3. cathode glass
4. row metal
5. emitter array
6. single emitter cone & gate hole
7. column meteal
8. focusing gride
9. wall
10. phosphor
11. black matrix
12. aluminum layer
13. pixel on
14. faceplate glass
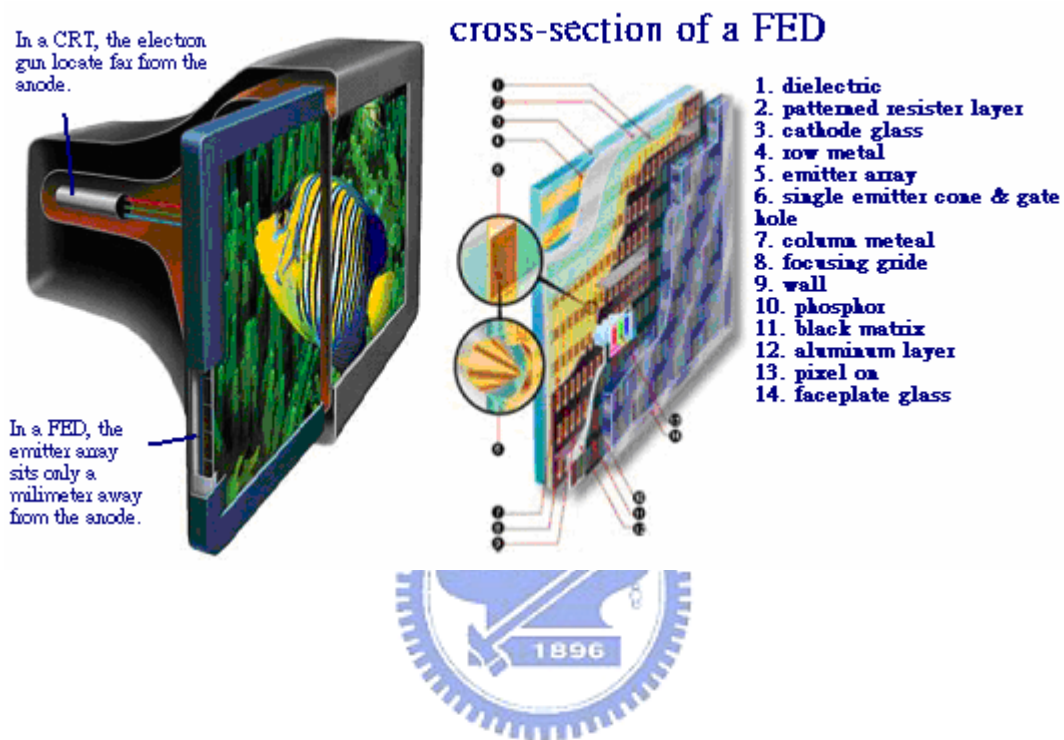
Figure 1.2   A schematic illustration for the structures of (a) a cathode-ray tube and (b) a field-emission display.
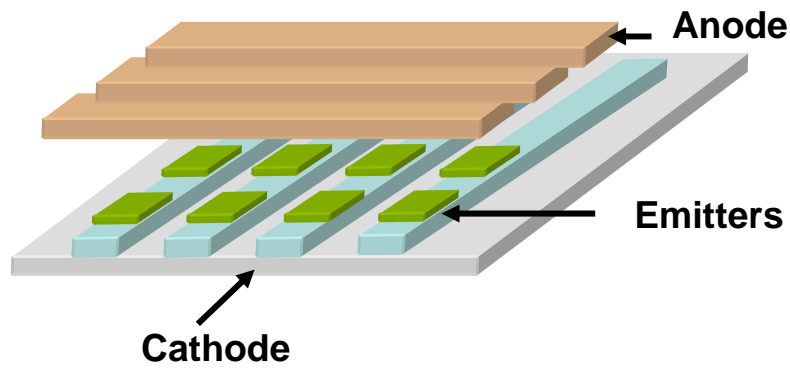
(a)
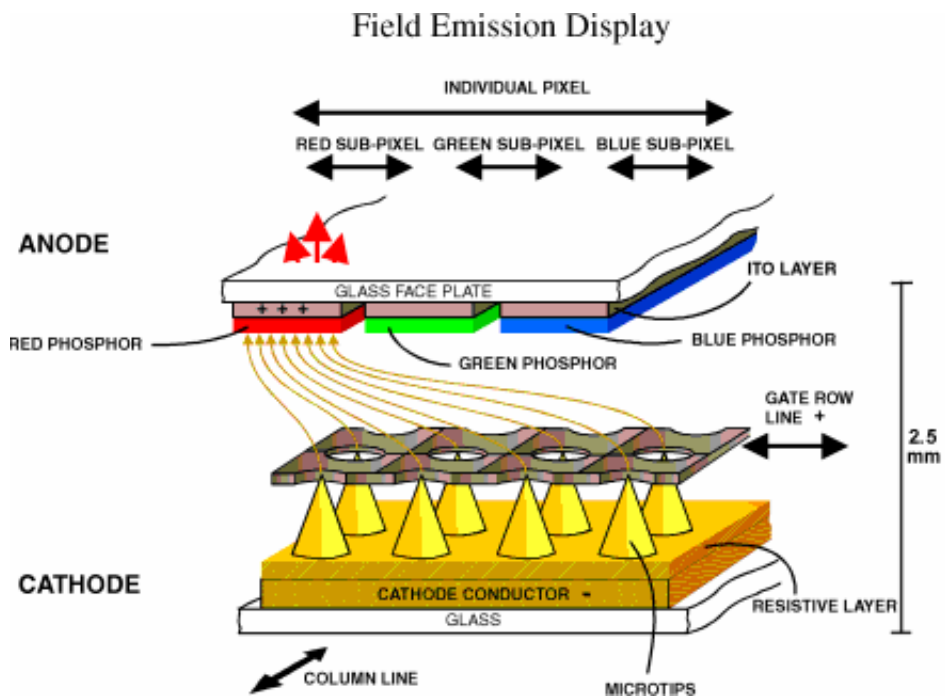
(b)

Figure 1.3   The device structures of (a) diode-type and (b) triode-type in field-emission displays. The main differences between the diode-type and the triode-type device structure are the gate electrode around the emitter which can extract electrons from the cathodes at relative low electric field.
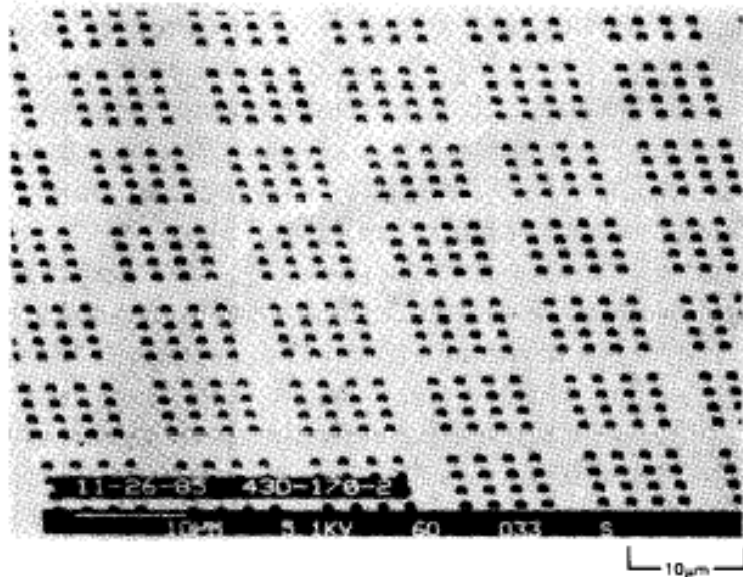
(a)
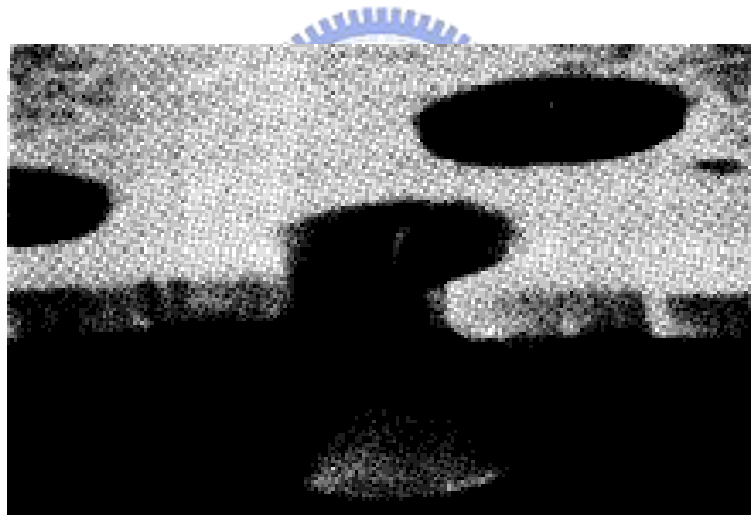
(b)

Figure 1.4   The micrographs taken by SEM for (a) Spindt field emitter arrays and (b) device structure with higher resolution.
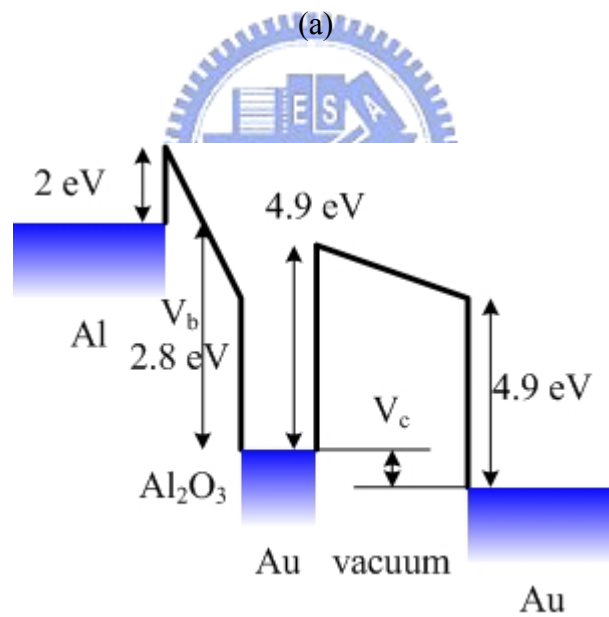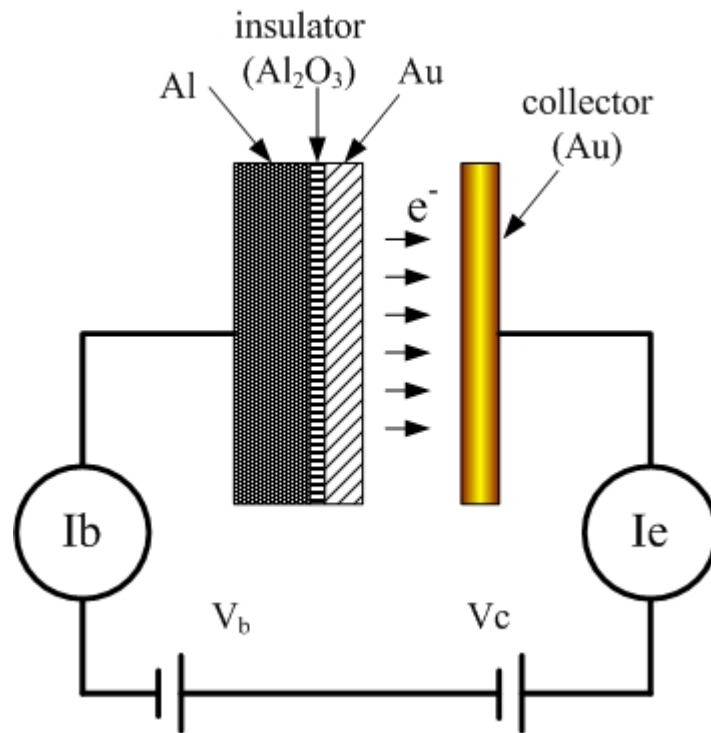
Figure 1.5 The schematic depiction of (a) the MIM device structure and (b) the emission mechanism.
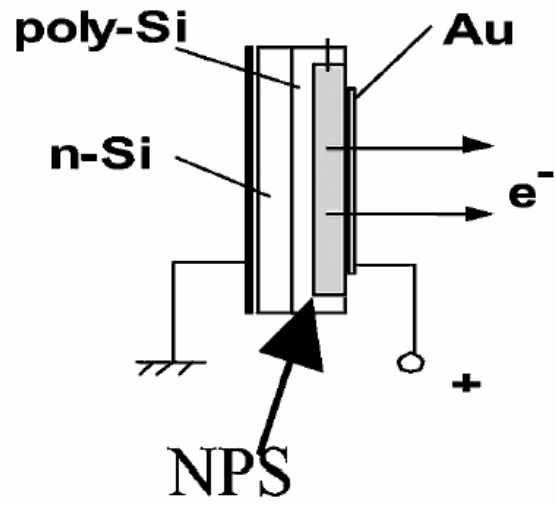
(a)
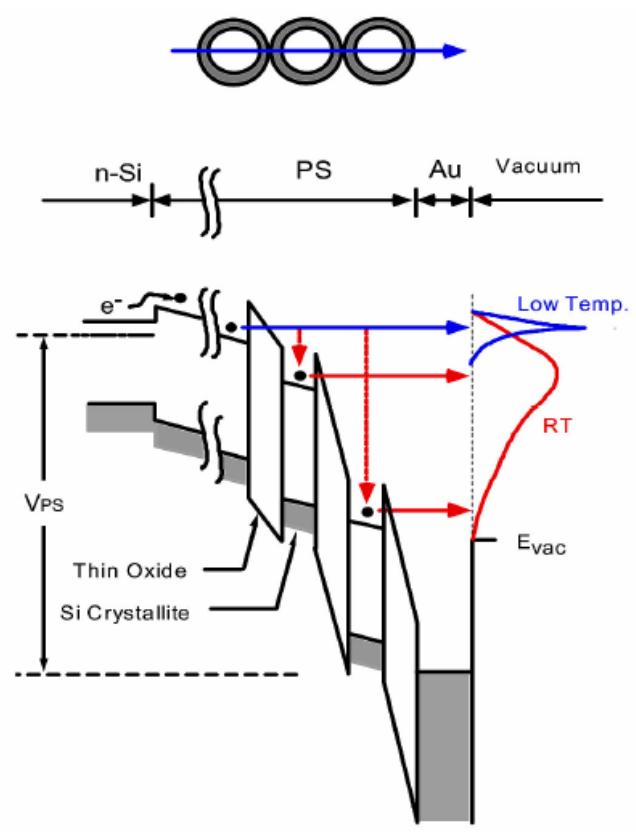
(b)

Figure 1.6   The schematic diagram of (a) the BSD device structure and (b) the electron emission model.
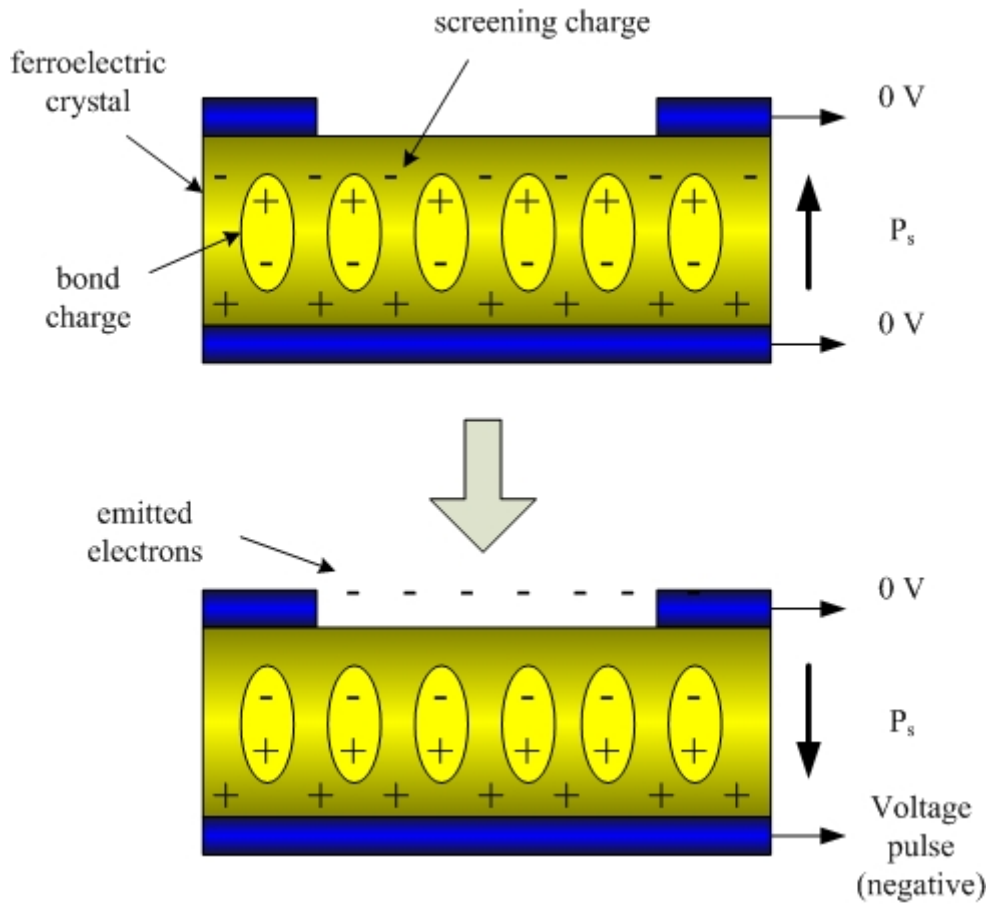
Figure 1.7   The schematic illustration of the ferroelectric emission mechanism. The screening charges are developed to compensate the net charges and a fast reversal of the polarization results a large electric field that ejects the electrons from the negative charged surface.

gap in nano scale (10 nm)

ultrafine PdO film

cathode electrode

gate electrode

V

(a)

multiple scattering

e⁻

e⁻

ultrafine PdO film

V

(b)
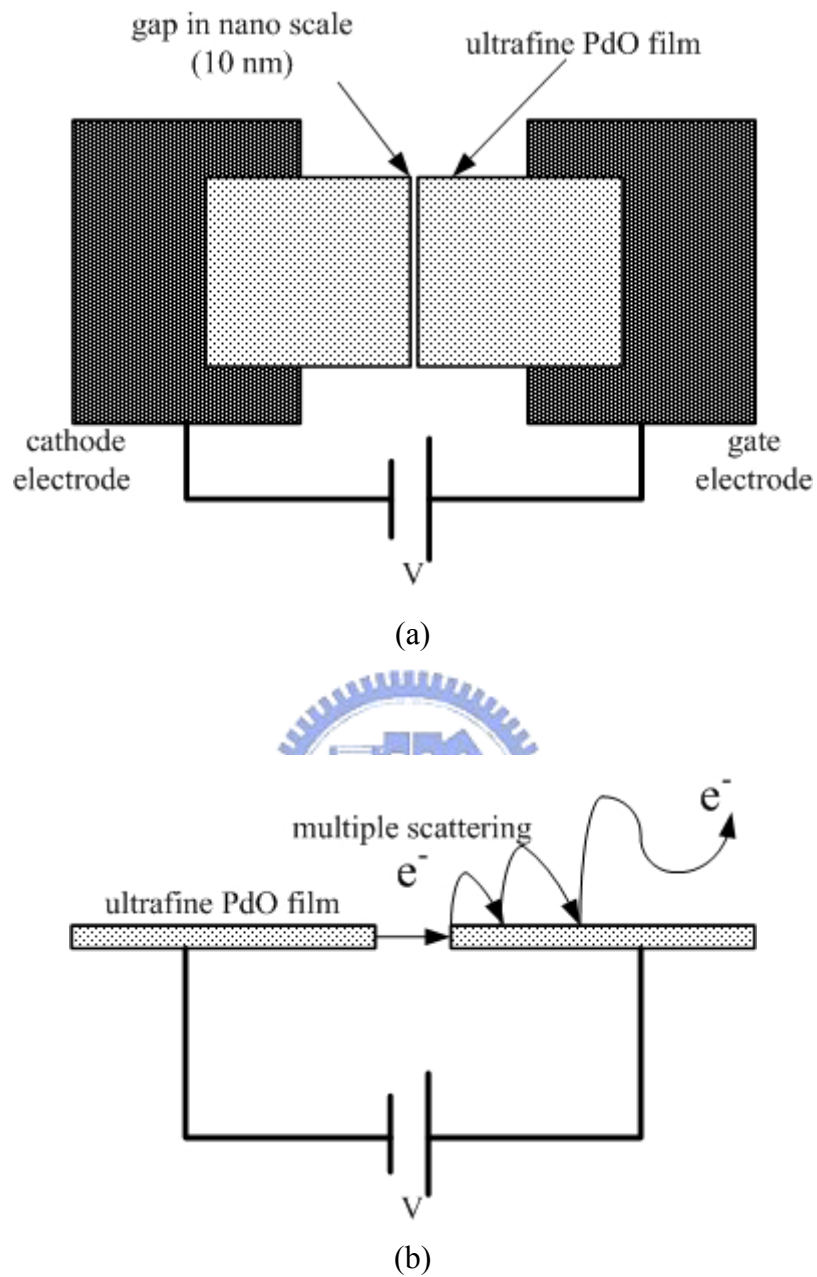
Figure 1.8　The illustration of surface conduction emitters: (a) the device structure from top view with two ultrafine PdO films as cathode and gate electrodes and (b) the mechanism of surface conduction emission.
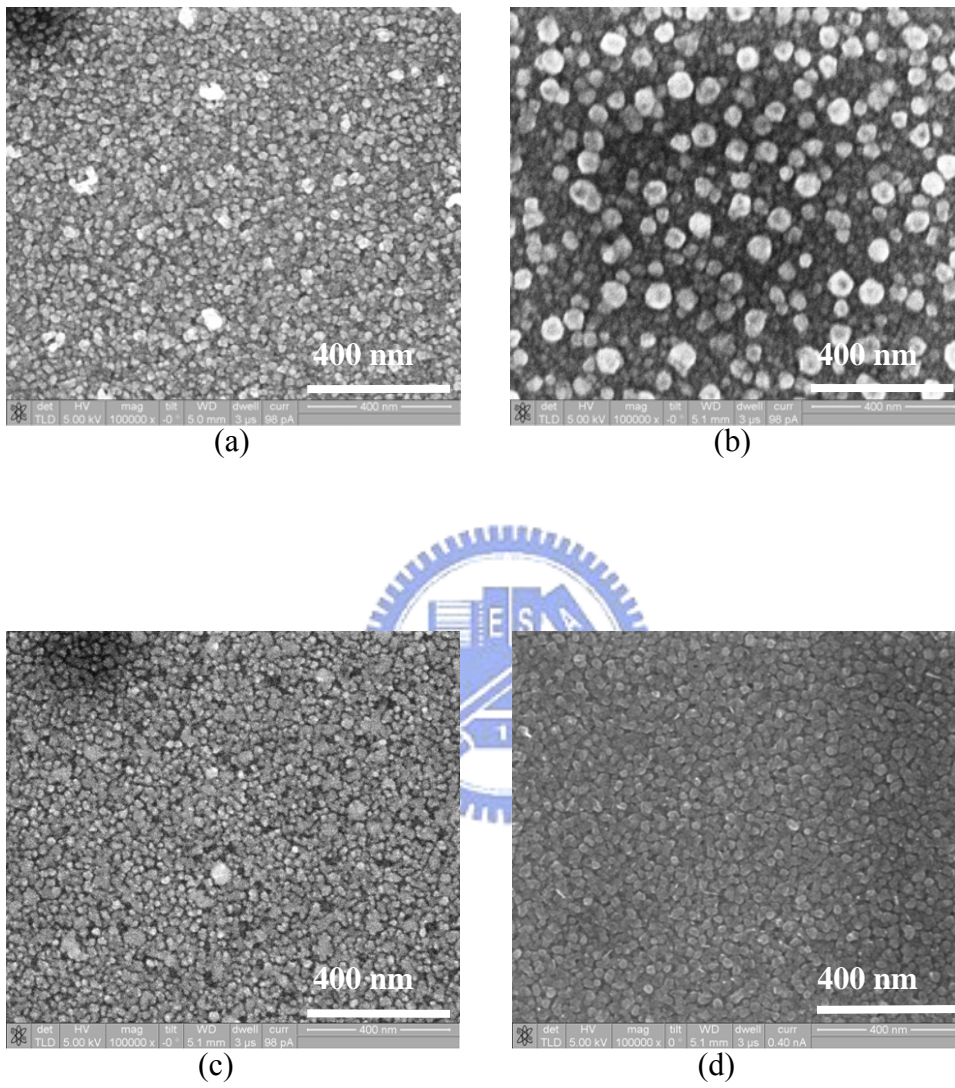
Figure 2.1   High-resolution SEM images of morphology of catalysts after pretreatment: (a) 20Co, (b) 20Co/20Cr, (c) 20Co/100Al, and (d) 20Co/20Cr/100Al.
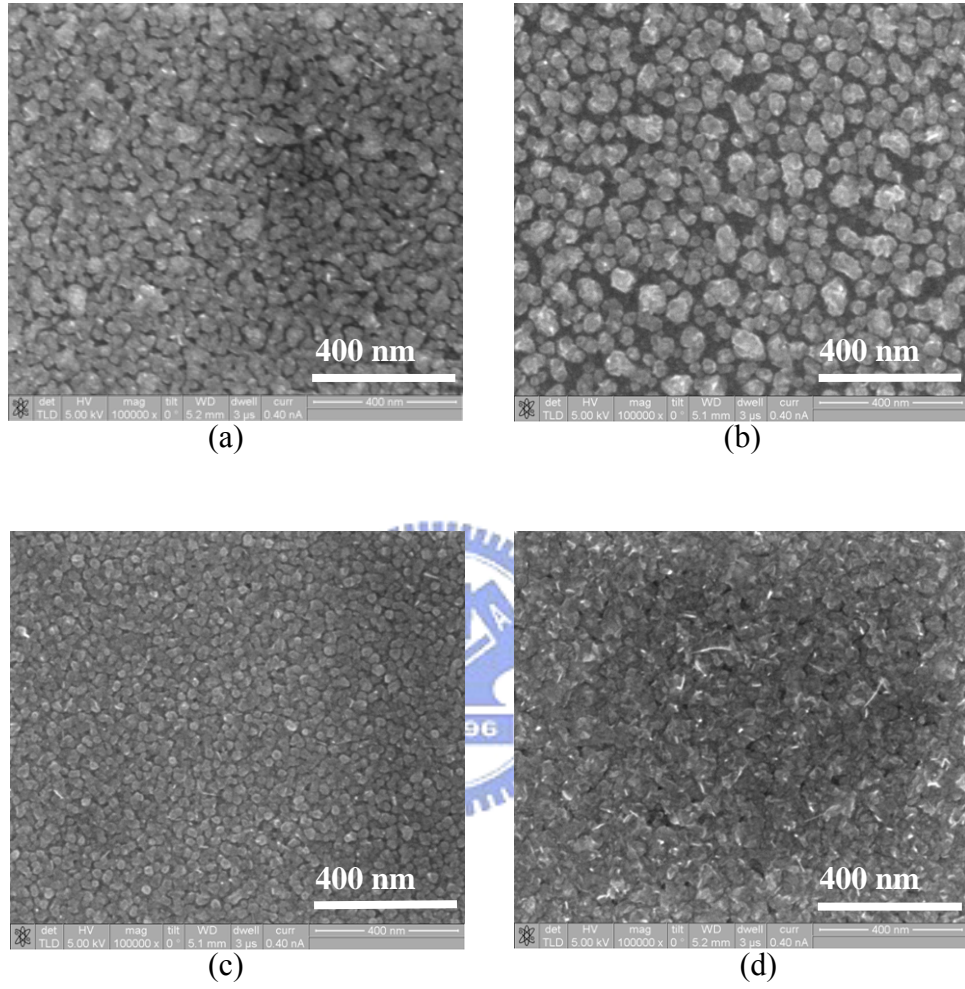
Figure 2.2   High-resolution SEM images of surface morphologies of samples with different Al supporting layer thickness after pretreatment: (a) 2 nm, (b) 5nm, (c) 10 nm, and (d) 20nm.
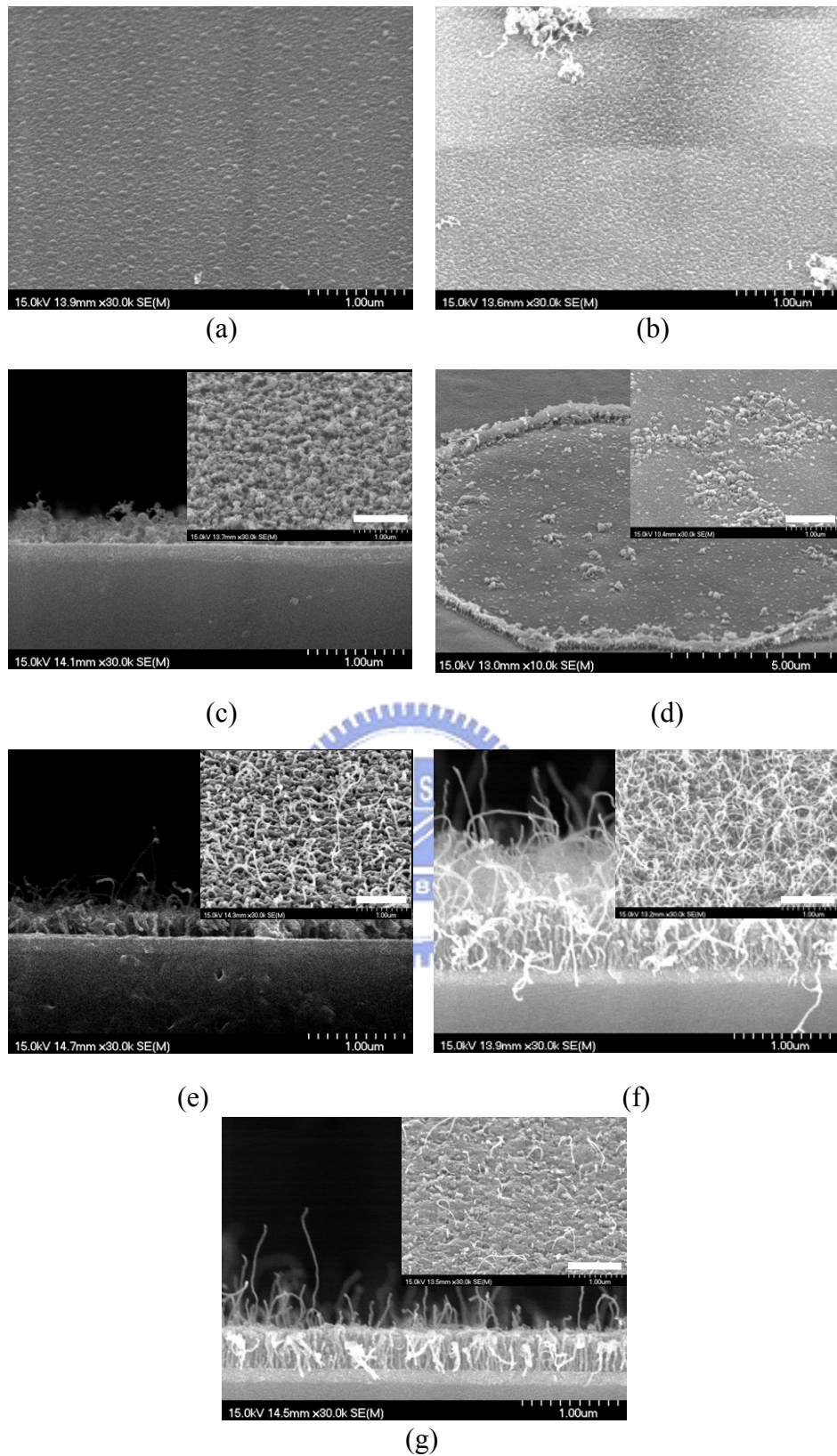
Figure 2.3   SEM images of surface morphologies of samples with different catalysts after CNT synthesis process: (a) 20Co, (b) 20Co/20Cr, (c) 20Co/100Al, (d) 20Co/2oCr/20Al, (e) 20Co/20Cr/50Al, (f) 20Co/20Cr/100Al, and (g) 20Co/20Cr/200Al. (The scale bars in the insets represent 1 μ m)

104

(a)
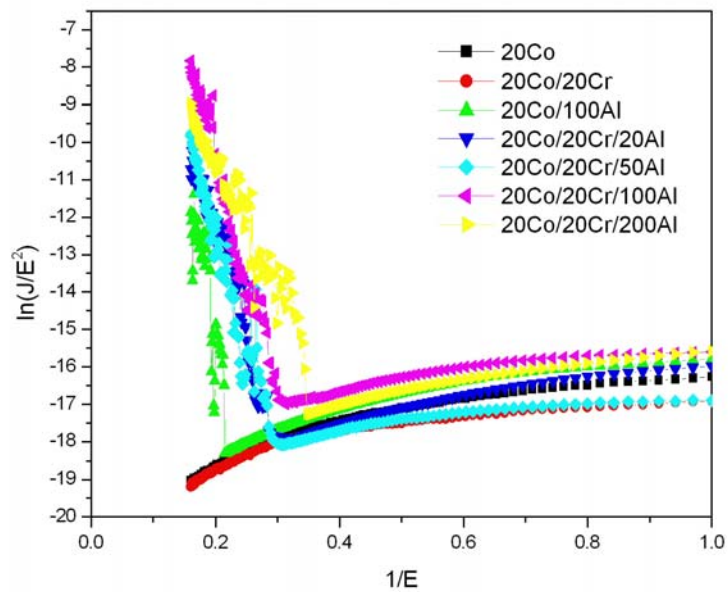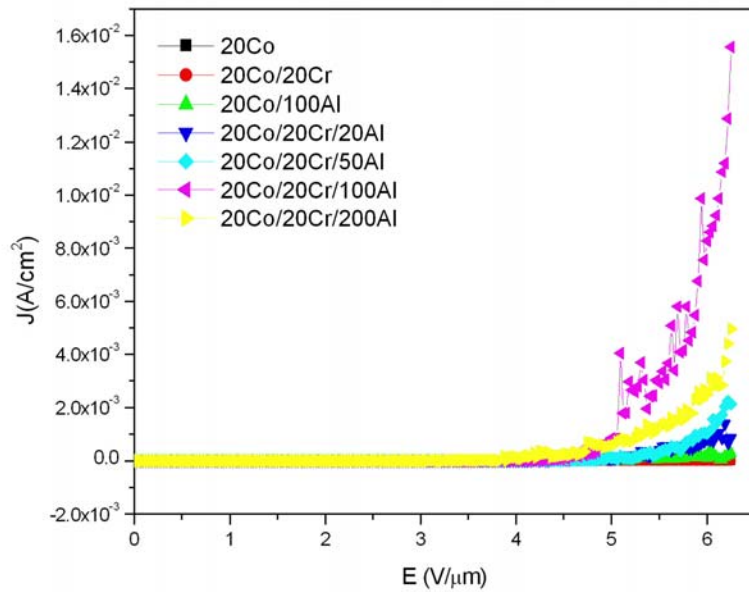
(b)

Figure 2.4 Field emission characteristics of samples with different catalysts after CNT synthesis process: (a) J-E curve and (b) FN plot.
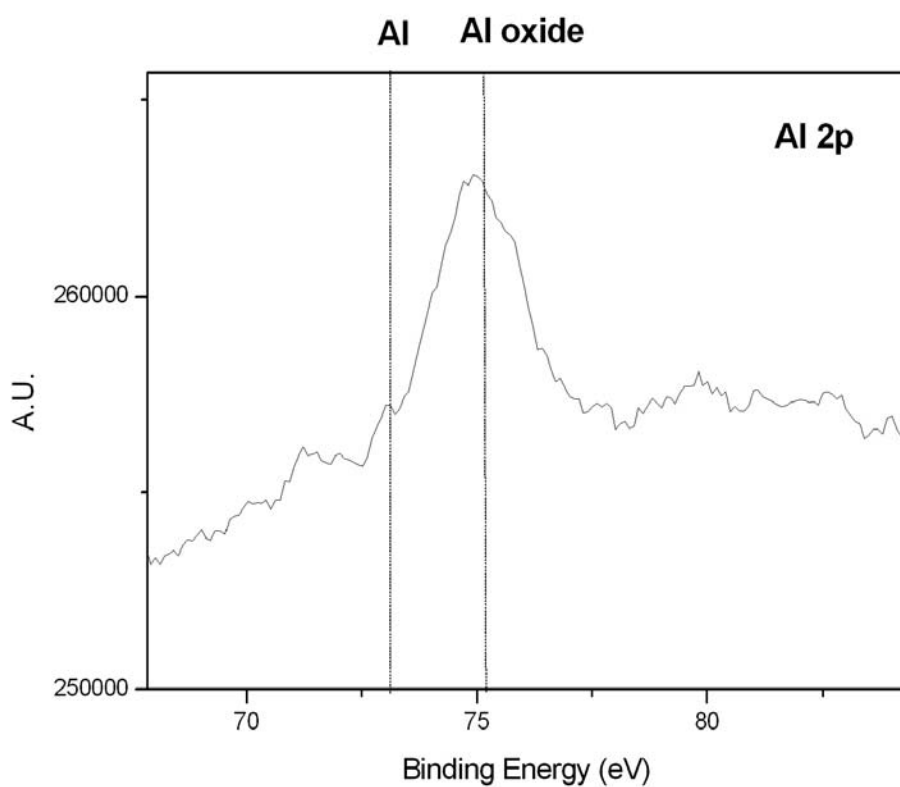
Figure 2.5   XPS analysis of the Al 2p perk for the sample with multilayer catalysts (20Co/20Cr/100Al).
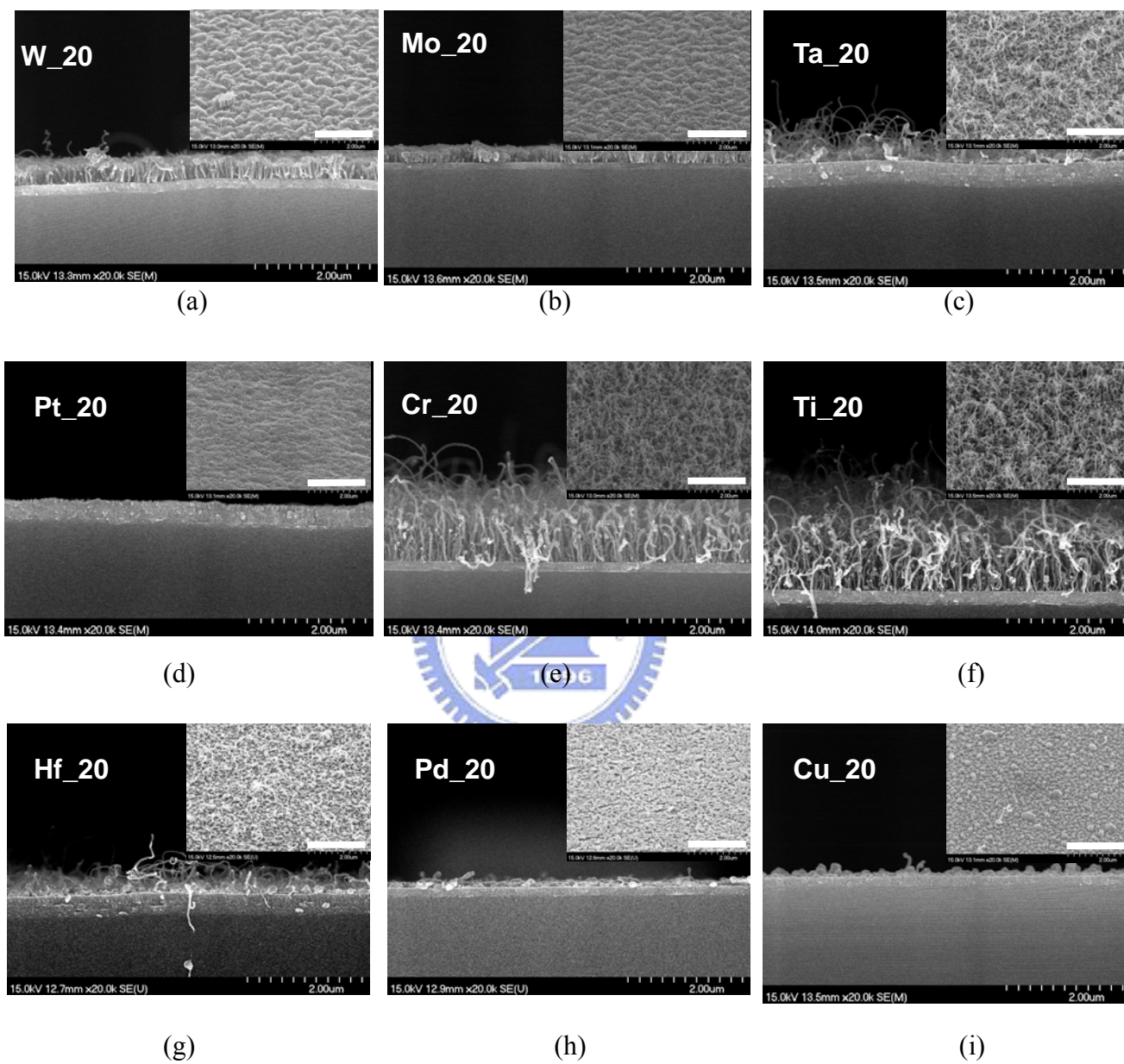
Figure 2.6　SEM images of surface morphologies of samples with multilayer catalysts consisting of different interlayer metals: (a) 2 nm W, (b) 2 nm Mo, (c) 2 nm Ta, (d) 2 nm Pt, (e) 2 nm Cr, (f) 2 nm Ti, (g) 2 nm Hf, (h) 2 nm Pd, and (i) 2 nm Cu. (The scale bars in the insets represent 2 μ m)
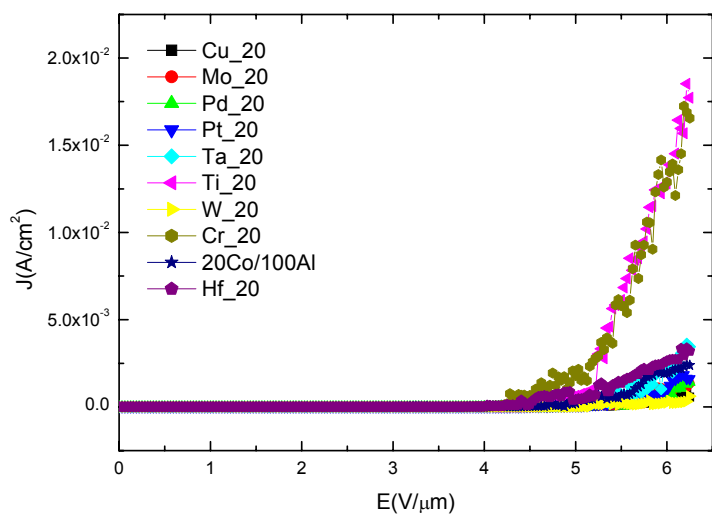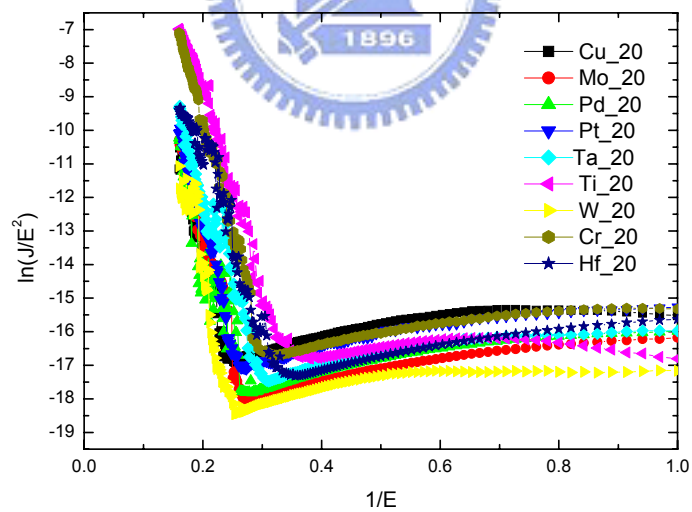
Figure 2.7　Field emission characteristics of samples with multilayer catalysts consisting of different interlayer metals after CNT synthesis process: (a) J-E curve and (b) FN plot.
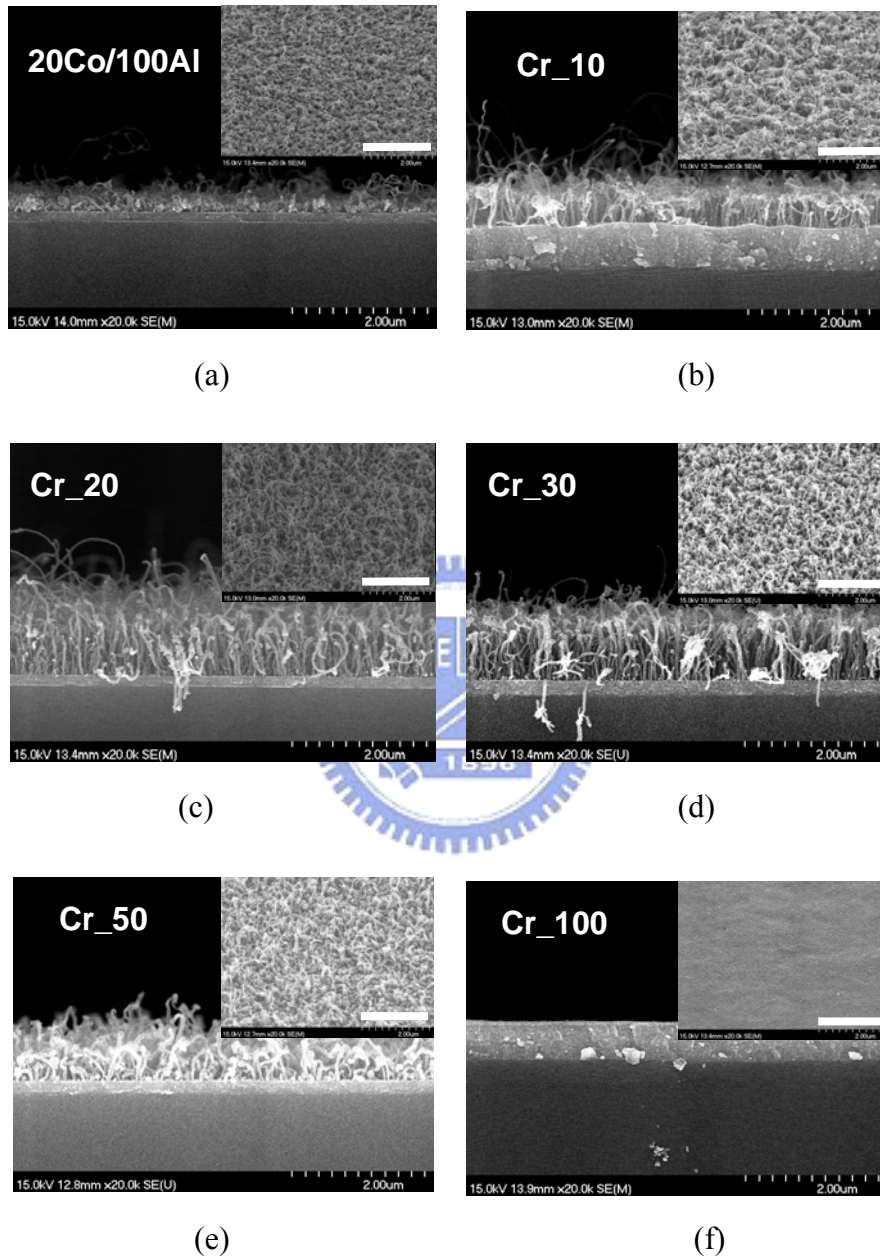
Figure 2.8   SEM images of surface morphologies of samples with multilayer catalysts consisting of different Cr interlayer thickness: (a) 0 nm, (b) 1 nm, (c) 2 nm, (d) 3 nm, (e) 5 nm, and (f) 10 nm. (The scale bars in the insets represent 2 μ m)
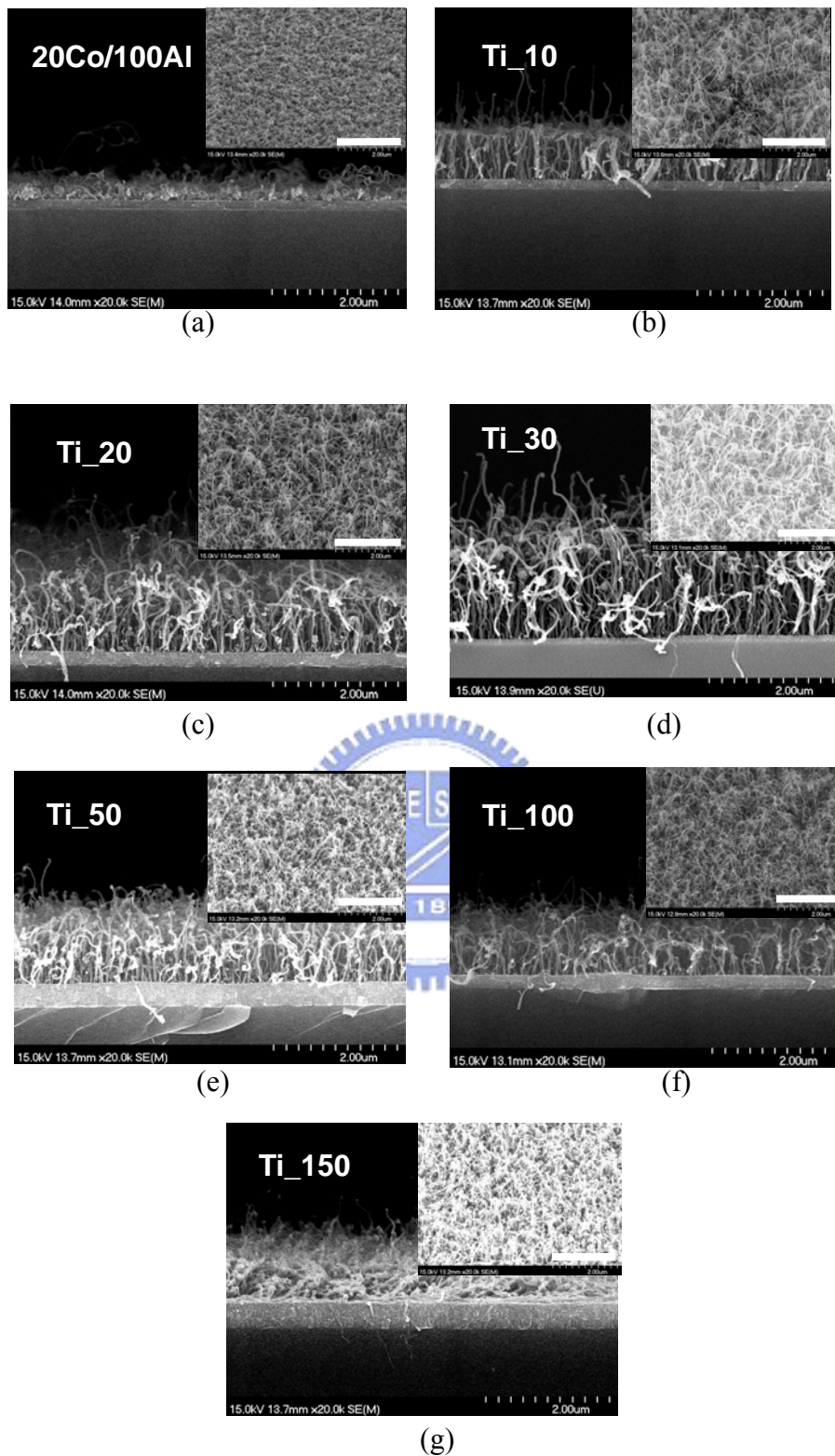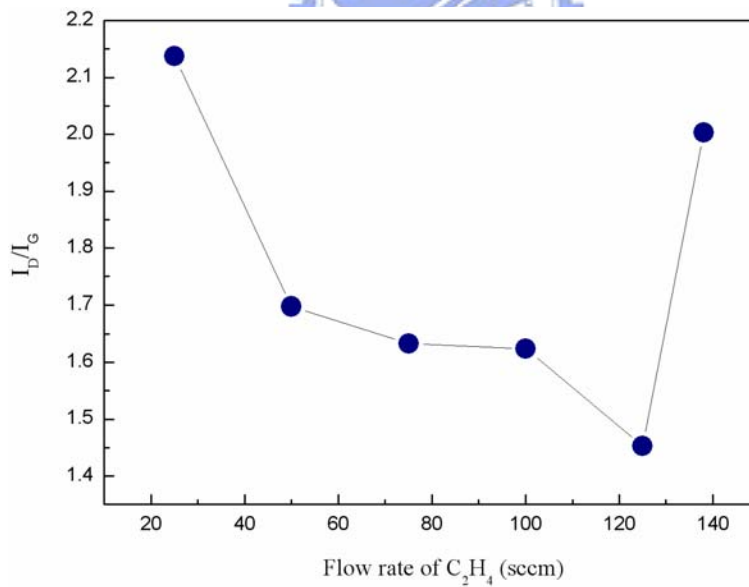
Figure 2.9   SEM images of surface morphologies of samples with multilayer catalysts consisting of different Ti interlayer thickness: (a) 0 nm, (b) 1 nm, (c) 2 nm, (d) 3 nm, (e) 5 nm, (f) 10 nm, and (g) 15 nm. (The scale bars in the insets represent $2\,\mu$m)

(a)
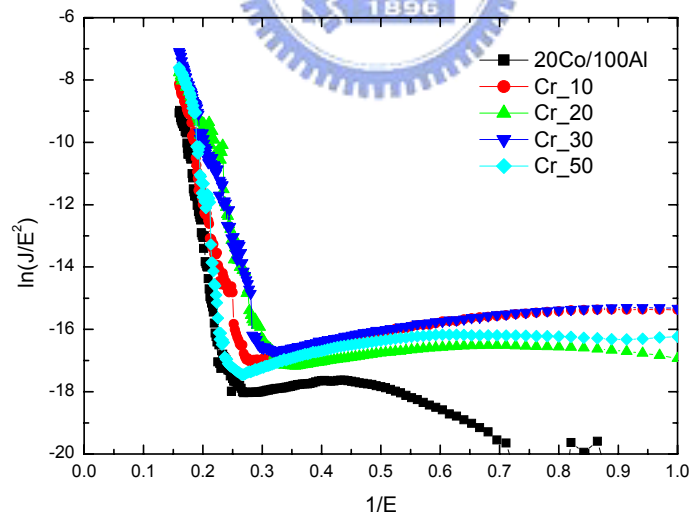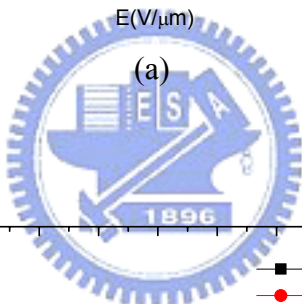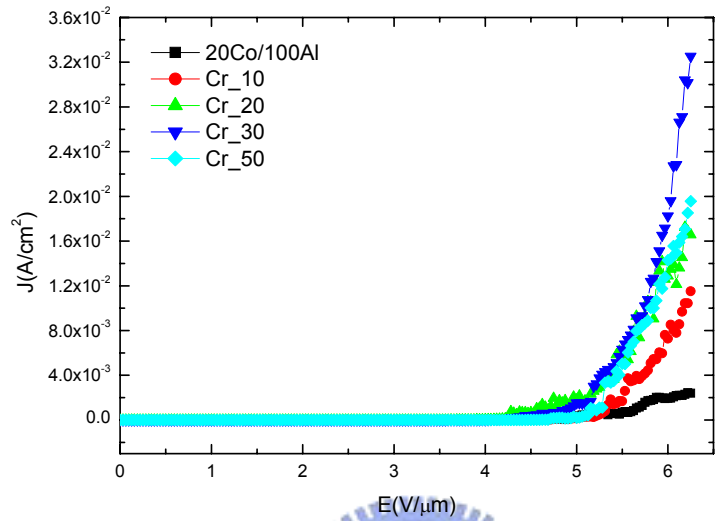
(b)

Figure 2.10   Field emission characteristics of samples with multilayer catalysts consisting of different Cr interlayer thickness after CNT synthesis process: (a) J-E curve and (b) FN plot.
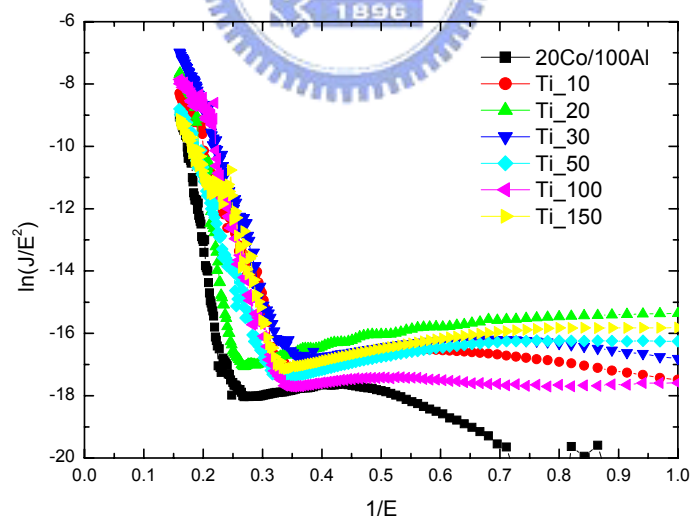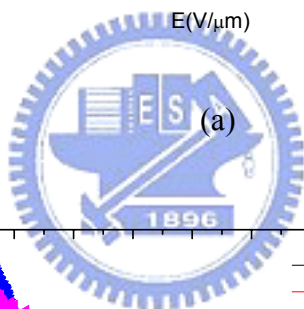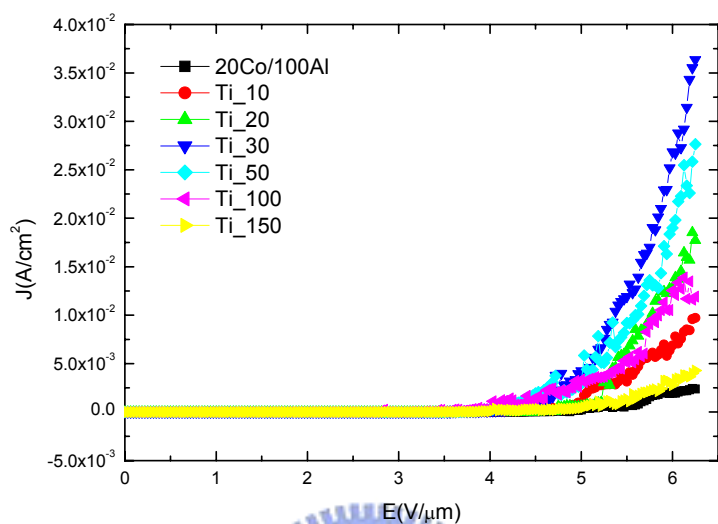
Figure 2.11 Field emission characteristics of samples with multilayer catalysts consisting of different Ti interlayer thickness after CNT synthesis process: (a) J-E curve and (b) FN plot.
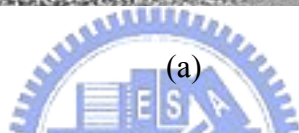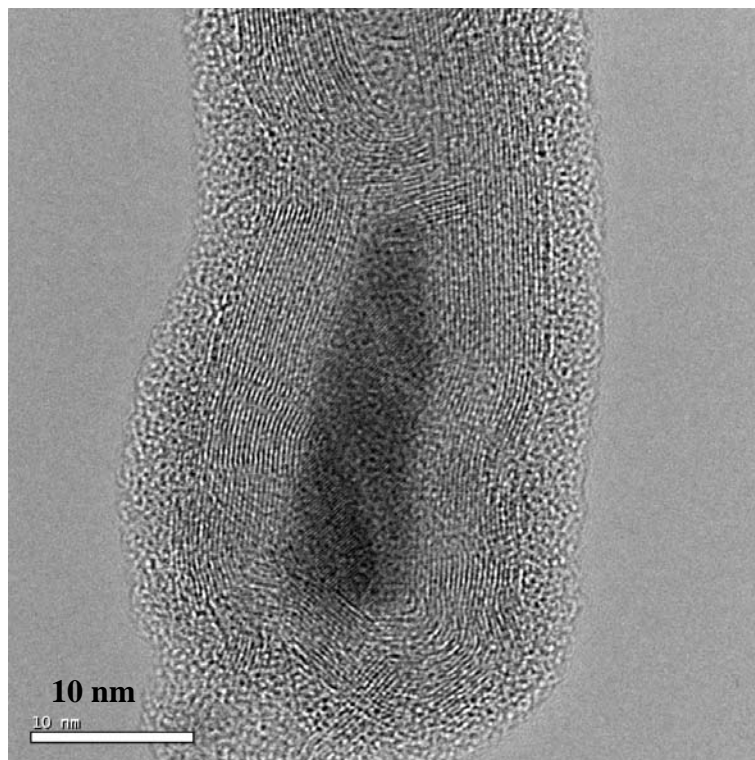
(a)
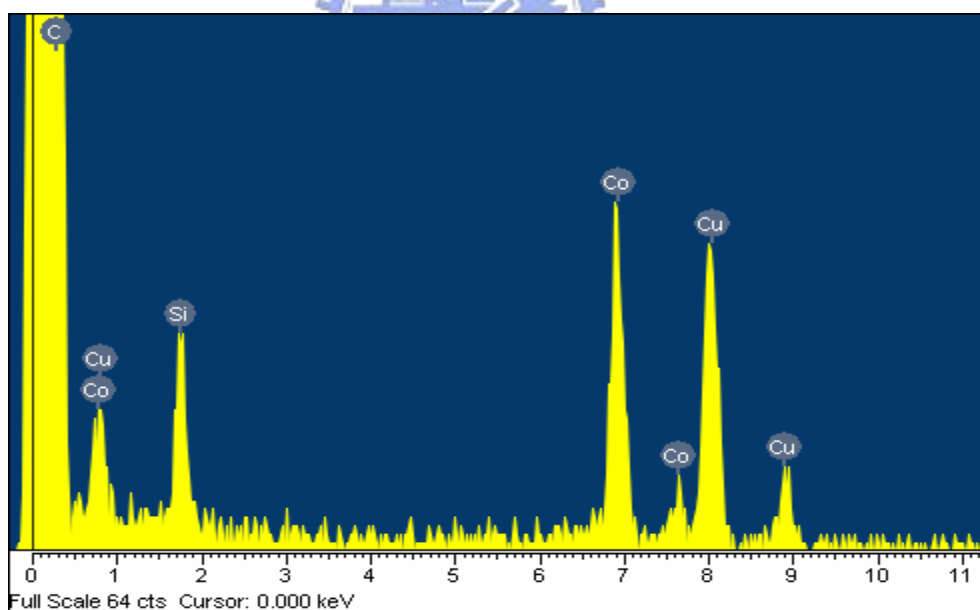
(b)

Figure 2.12   (a) TEM images of CNTs synthesized with multilayer catalysts (20Co/30Ti/100Al) consisting of 3 nm Ti interlayer, and (b) the EDS analysis of catalytic particle shown in (a).

(a)
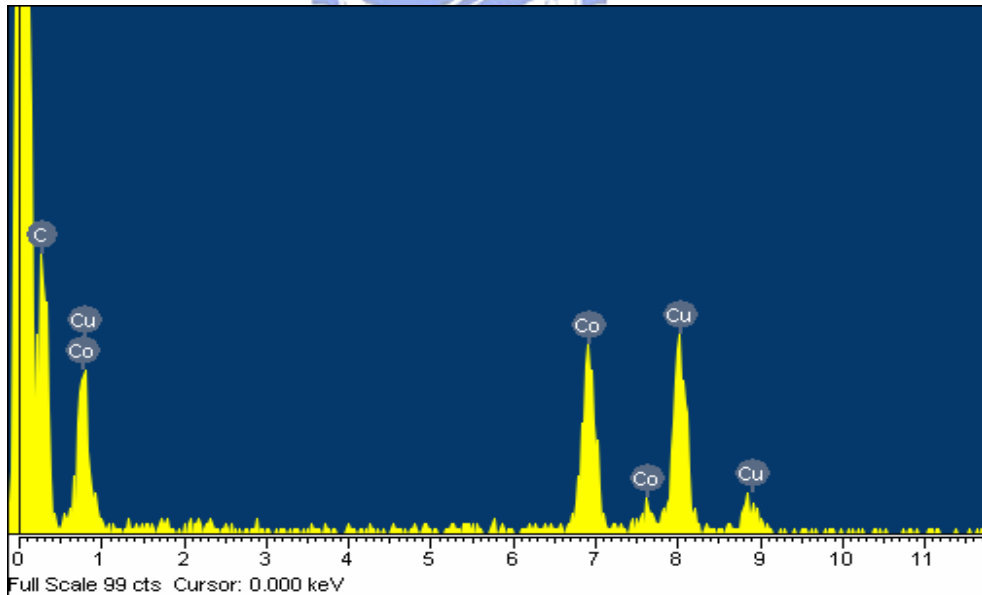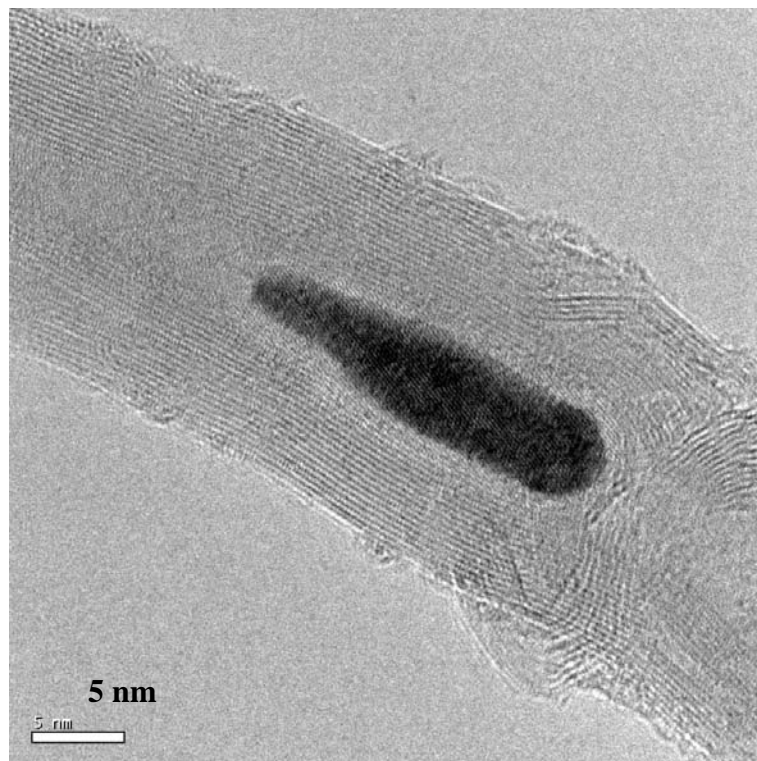
(b)

Figure 2.13   (a) TEM images of CNTs synthesized with multilayer catalysts (20Co/30Cr/100Al) consisting of 3 nm Cr interlayer, and (b) the EDS analysis of catalytic particle shown in (a).
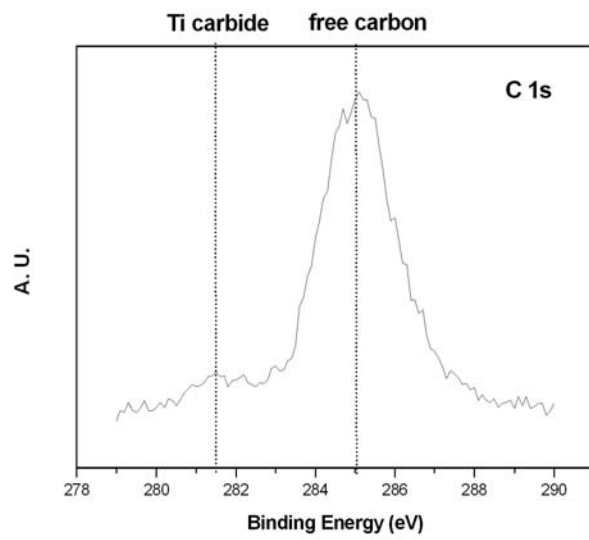
(a)
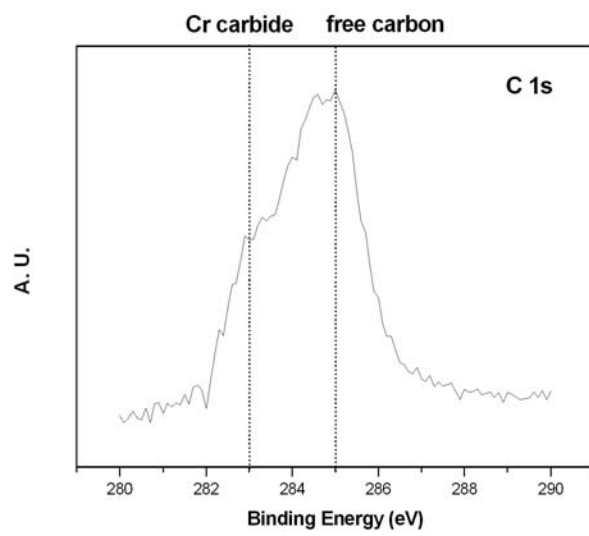
(b)

Figure 2.14   XPS analysis of samples with multilayer catalysts consisting of (a) Ti interlayer and (b) Cr interlayer.
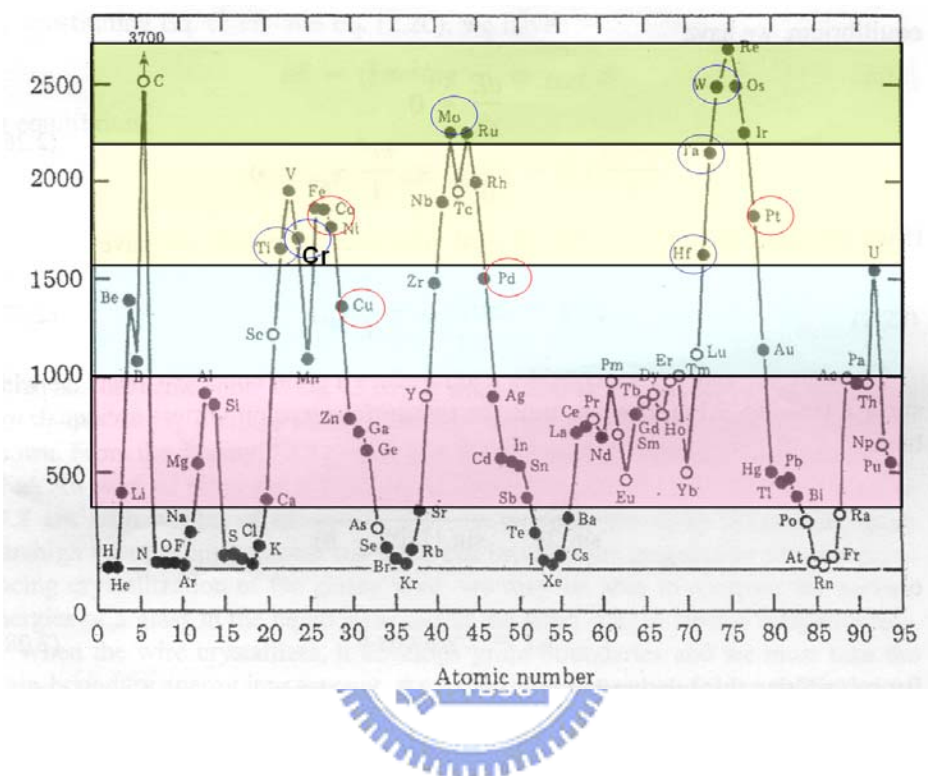
Figure 2.15   Surface energies of elements.

116
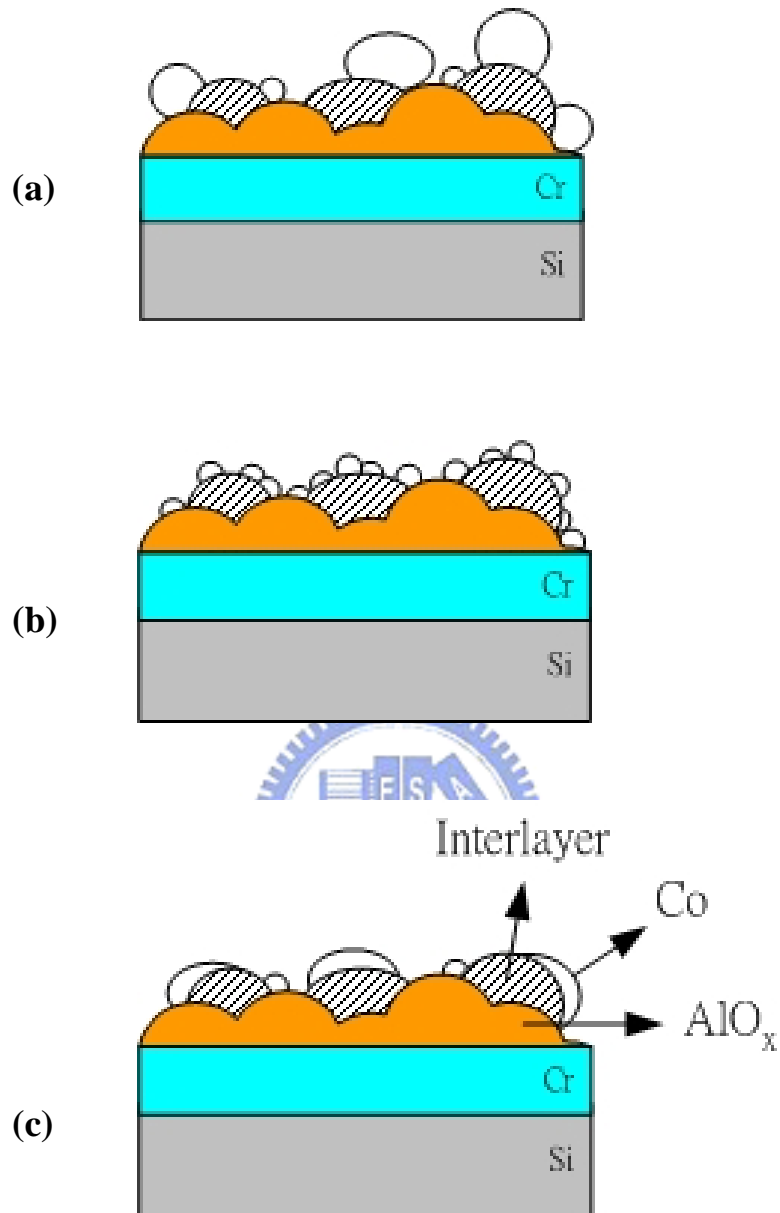
Figure 2.16　Schematic diagrams of morphologies of catalytic nanoparticles formed due to the difference of surface energies between catalytic thin film and interlayer thin films: (a) surface energy of interlayer thin film smaller than that of Co, (b) surface energy of interlayer thin film close to that of Co, and (c) surface energy of interlayer thin film larger than that of Co.
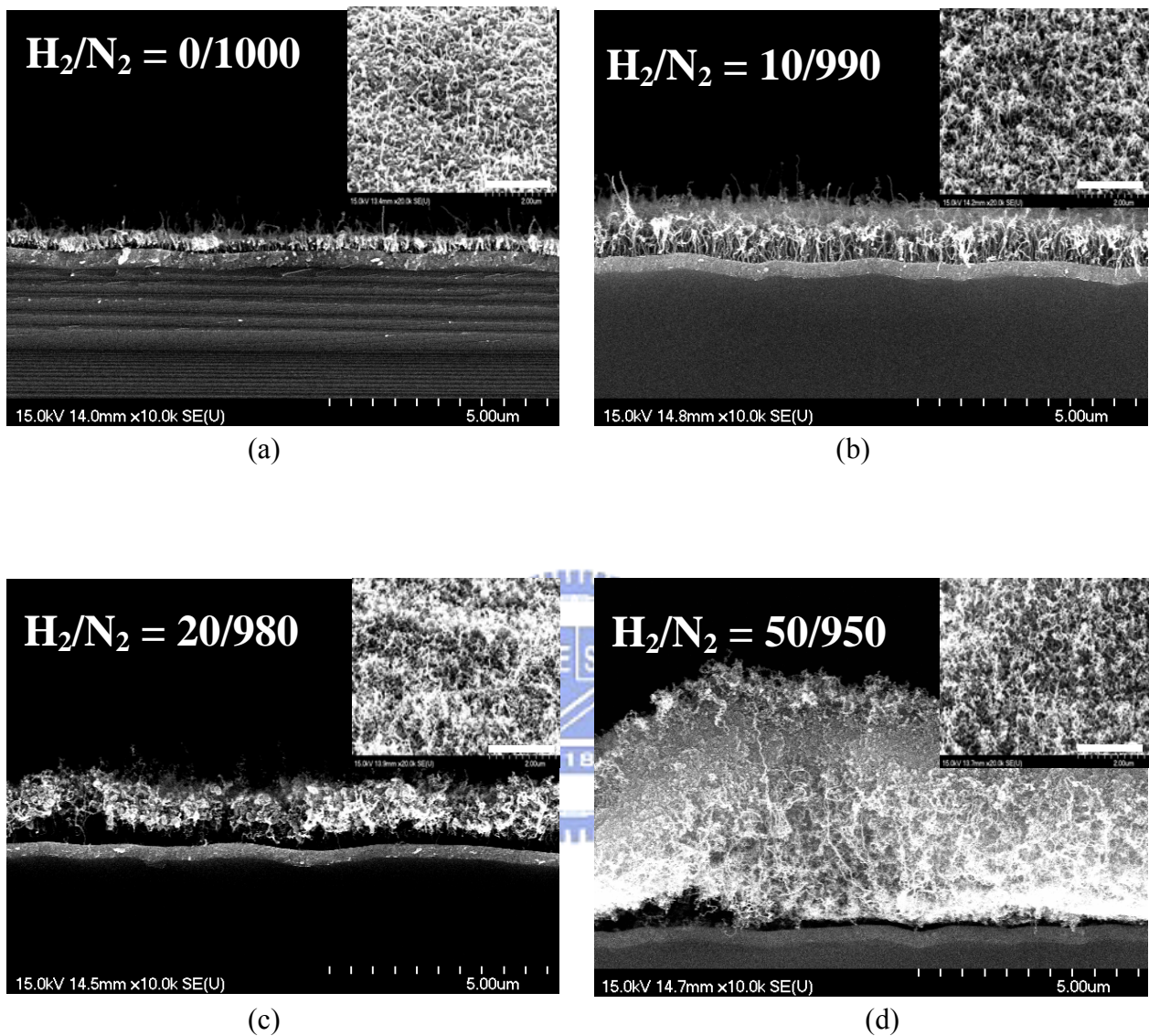
Figure 3.1 SEM images of surface morphologies of samples after CNT synthesis process conducted with different H_2/N_2 flow rate ratios: (a) 0/1000, (b) 10/990, (c) 20/980, and (d) 50/950. (The scale bars in the insets represent 2 μ m)
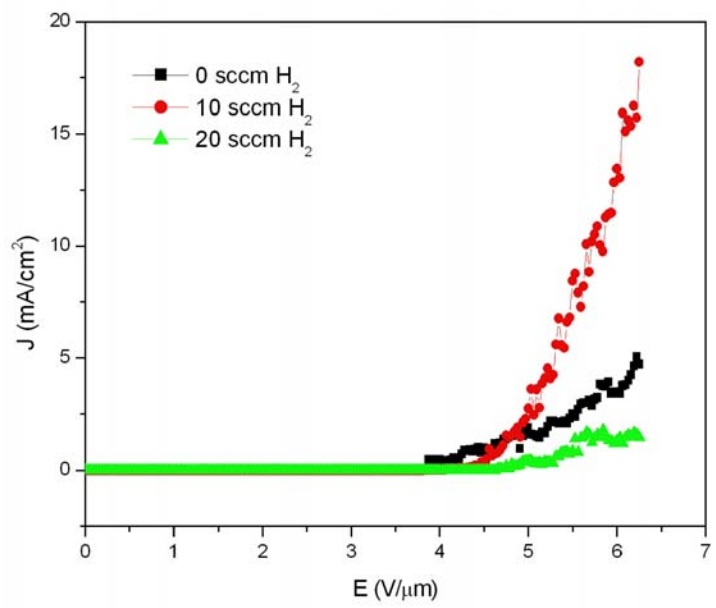
(a)
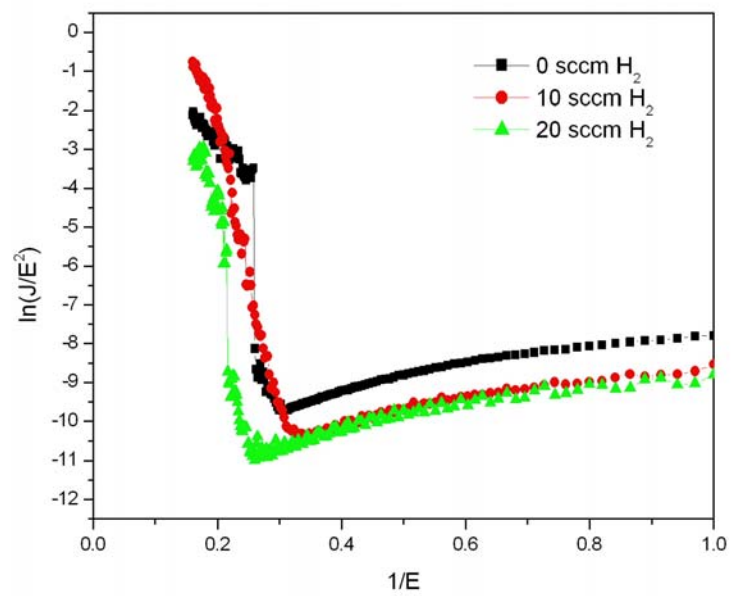
(b)

Figure 3.2   (a) J-E field emission characteristics of CNTs synthesized with different H_2 flow rates and (b) the corresponding FN plot.
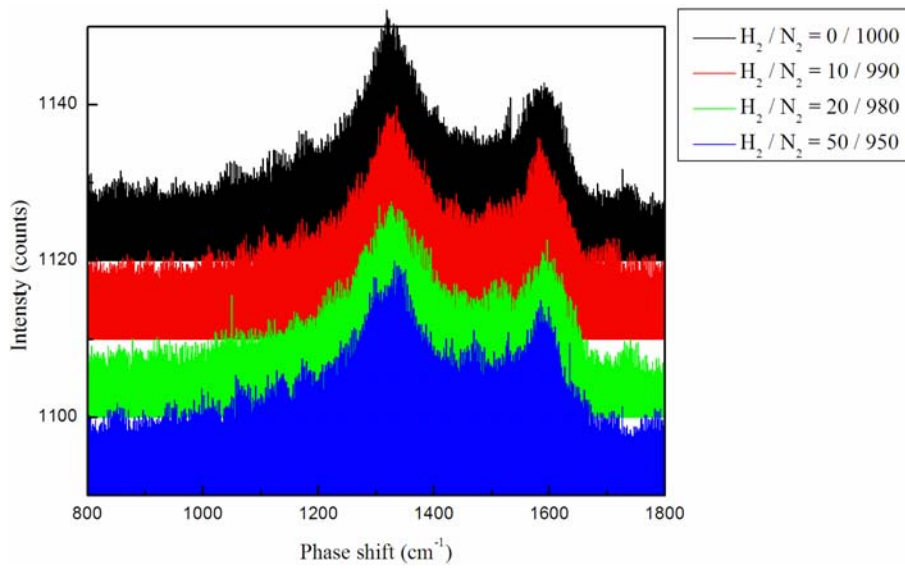
(a)
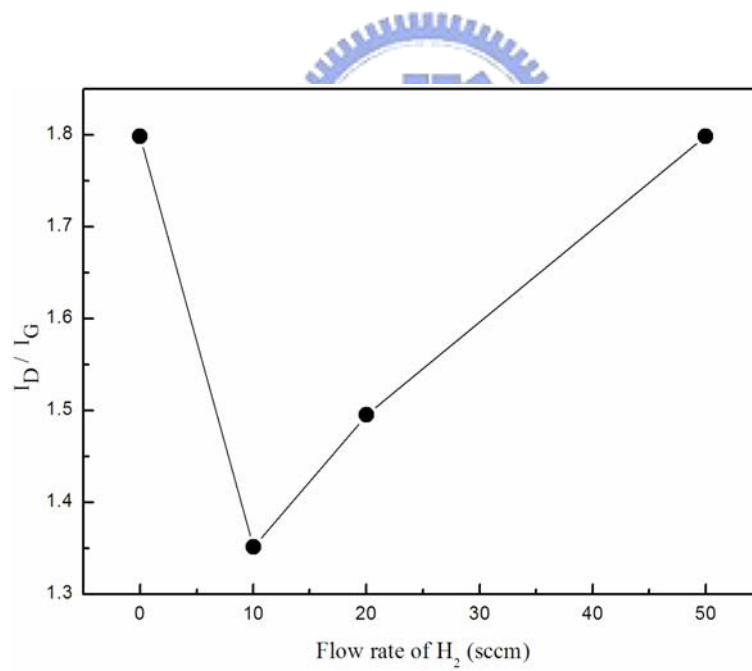
(b)

Figure 3.3 (a) Raman analysis of samples after CNT synthesis process conducted with different H_2/N_2 flow rate ratios and (b) the plot of I_D/I_G intensity vs. H_2 flow rates.
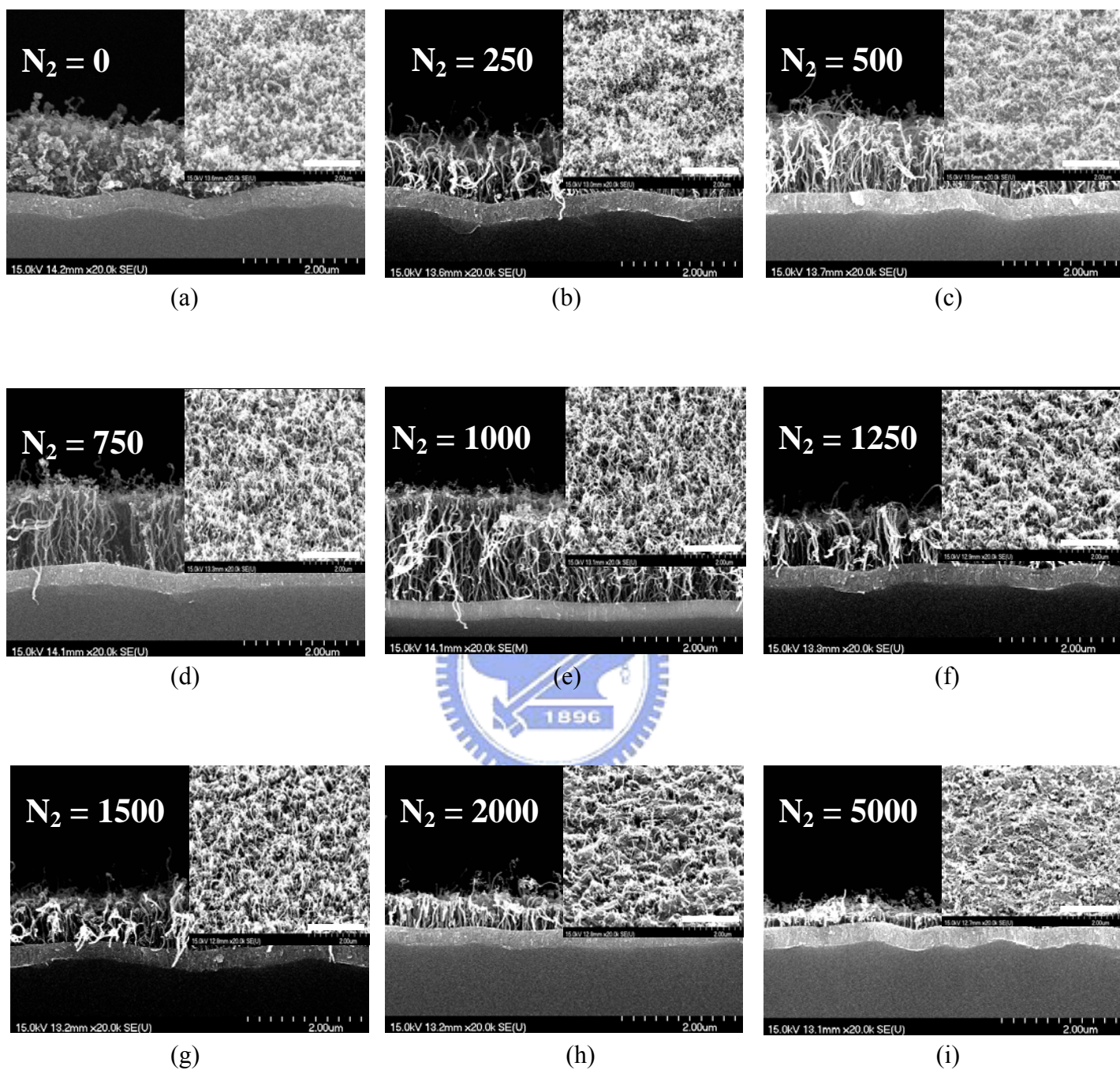
Figure 3.4 SEM images of surface morphologies of samples after CNT synthesis process conducted with different N_2 flow rates: (a) 0, (b) 250, (c) 500, (d) 750, (e) 1000, (f) 1250, (g) 1500, (h) 2000, and (i) 5000 sccm. (The scale bars in the insets represent 2 μ m)
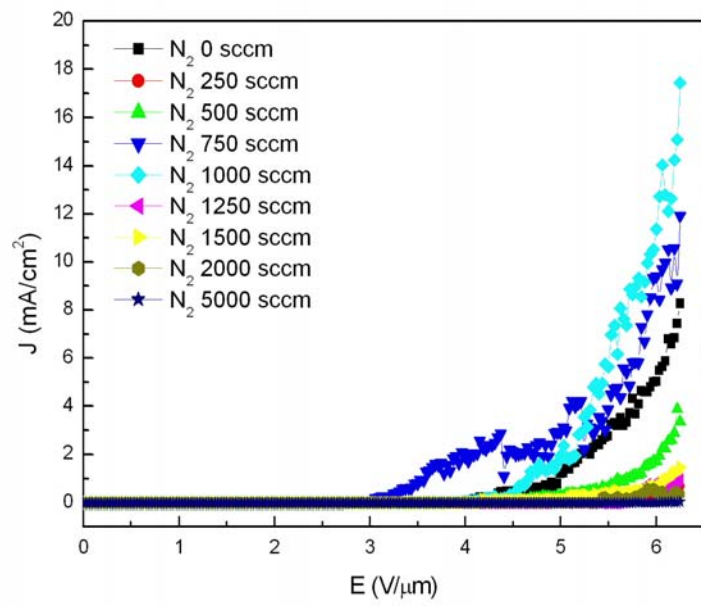
(a)
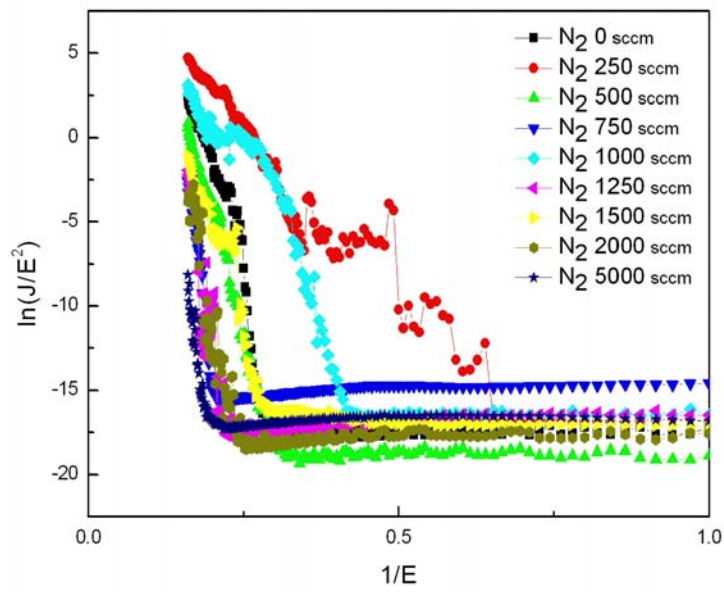
(b)

Figure 3.5   (a) J-E field emission characteristics of CNTs synthesized with different N$_2$ flow rates and (b) the corresponding FN plot.
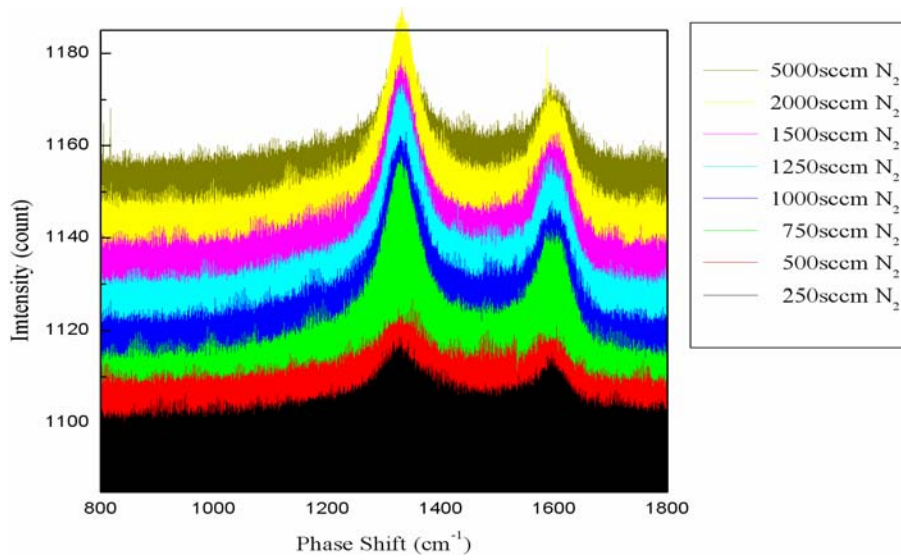
(a)
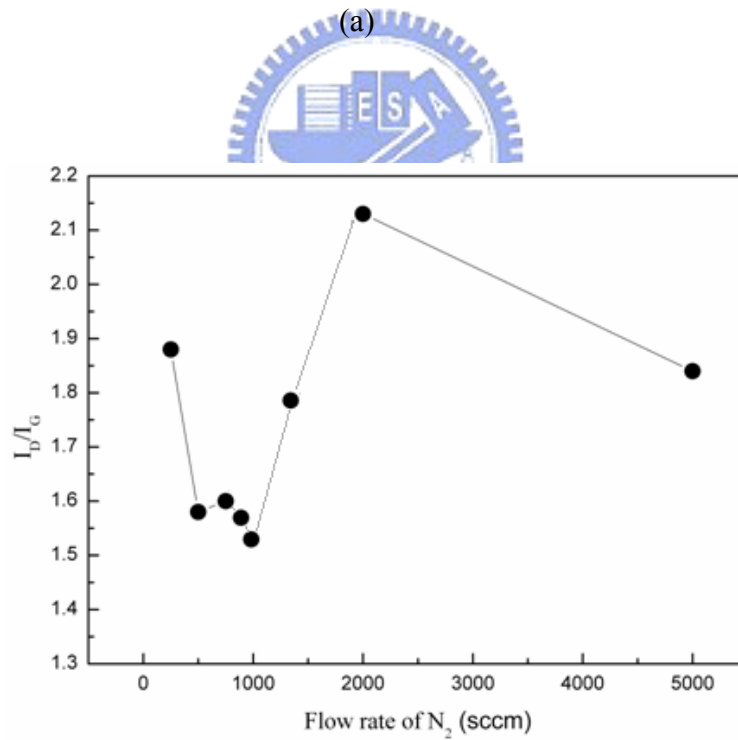
(b)

Figure 3.6 (a) Raman analysis of samples after CNT synthesis process conducted with different N_2 flow rates and (b) the plot of I_D/I_G intensity vs. N_2 flow rates.
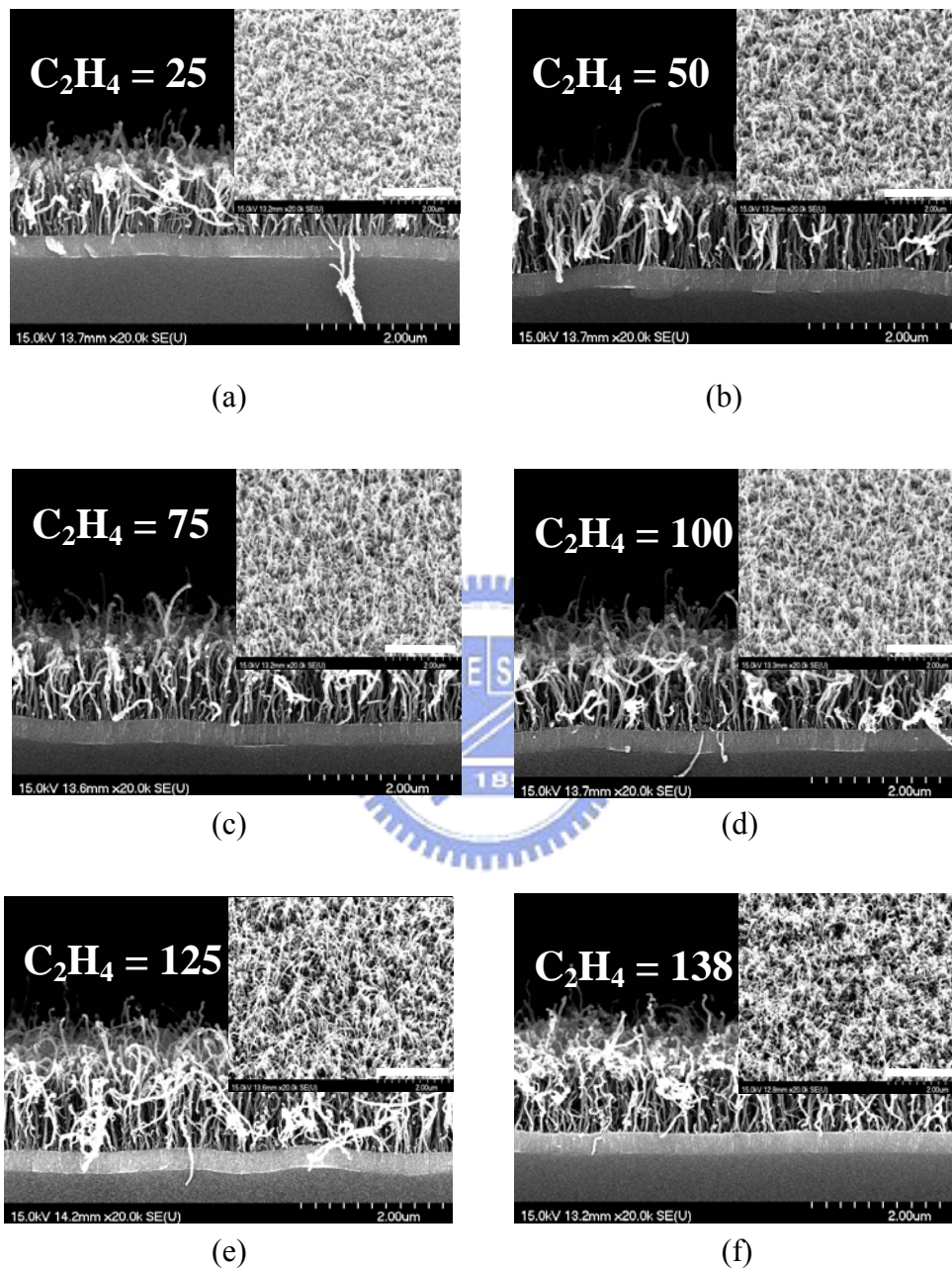
Figure 3.7   SEM images of surface morphologies of samples after CNT synthesis process conducted with different C_2H_4 flow rate ratios: (a) 25, (b) 50, (c) 75, (d) 100, (e) 125, and (f) 138 sccm. (The scale bars in the insets represent $2\,\mu$m)

(a)

(b)
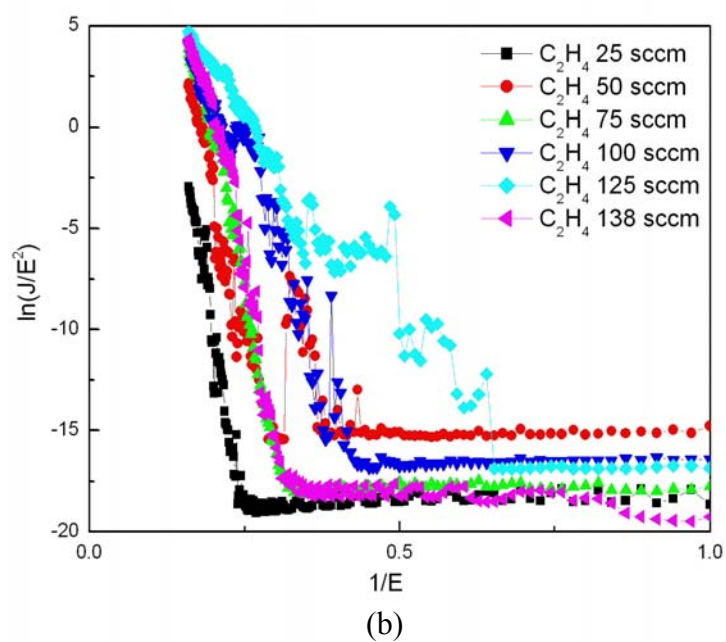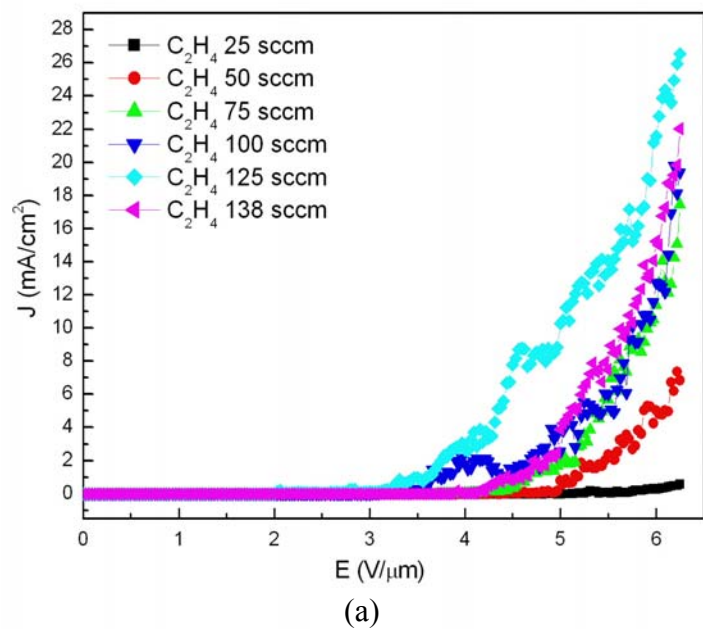
Figure 3.8　(a) J-E field emission characteristics of CNTs synthesized with different C_2H_4 flow rates and (b) the corresponding FN plot.
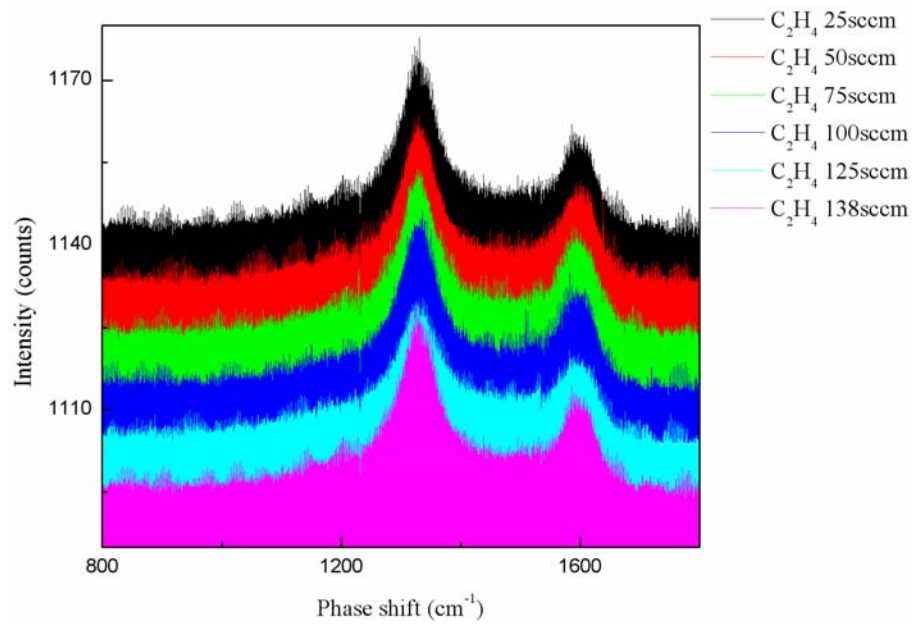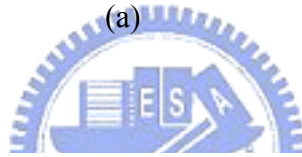
Figure 3.9 (a) Raman analysis of samples after CNT synthesis process conducted with different C_2H_4 flow rates and (b) the plot of I_D/I_G intensity vs. C_2H_4 flow rates.
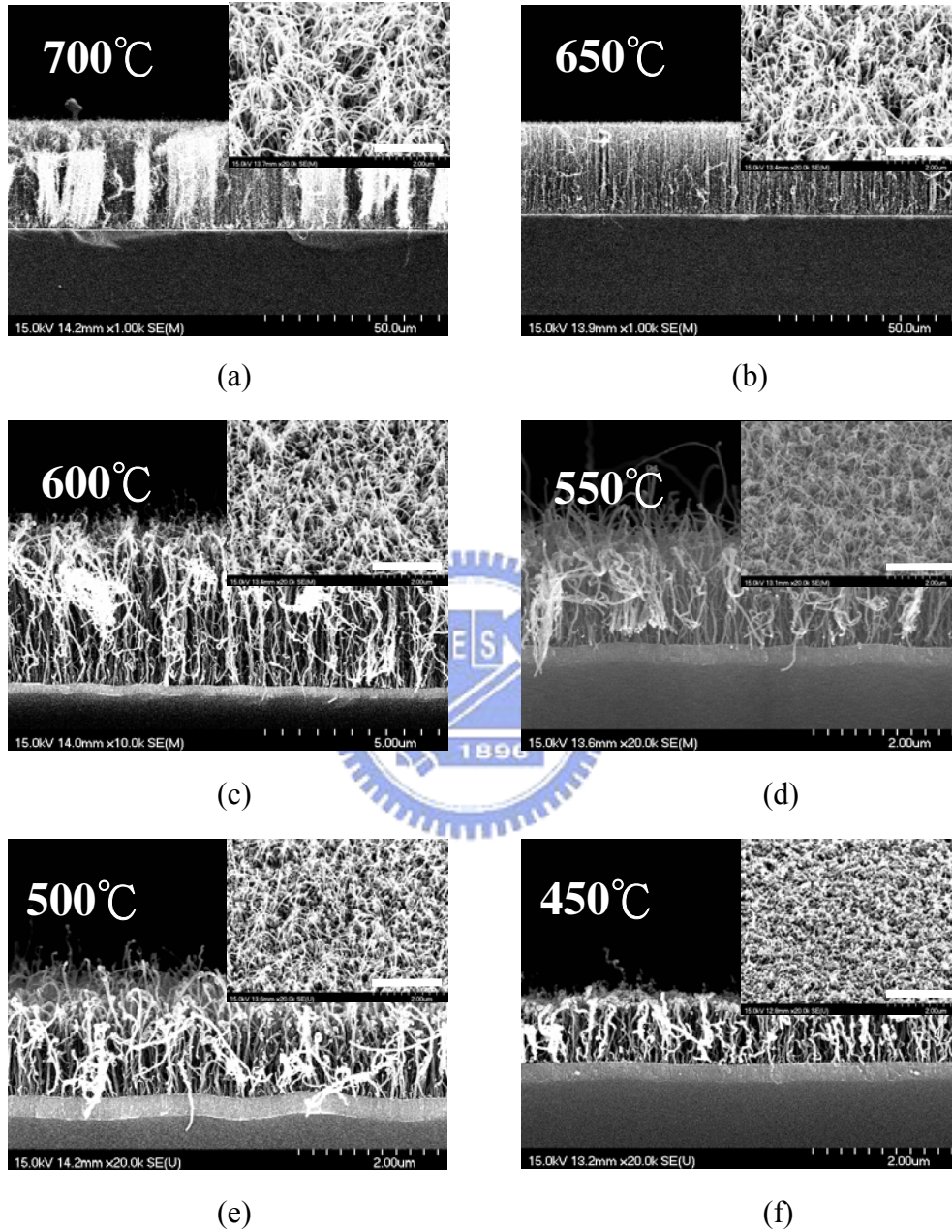
Figure 3.10 SEM images of surface morphologies of samples using multilayer catalysts (20Co/30Ti/100Al) after CNT synthesis process conducted at different temperatures: (a) 700, (b) 650, (c) 600, (d) 550, (e) 500, (f) 450, (g) 400, and (h) 370℃. (The scale bars in the insets represent 2 μ m)

(g)   (h)
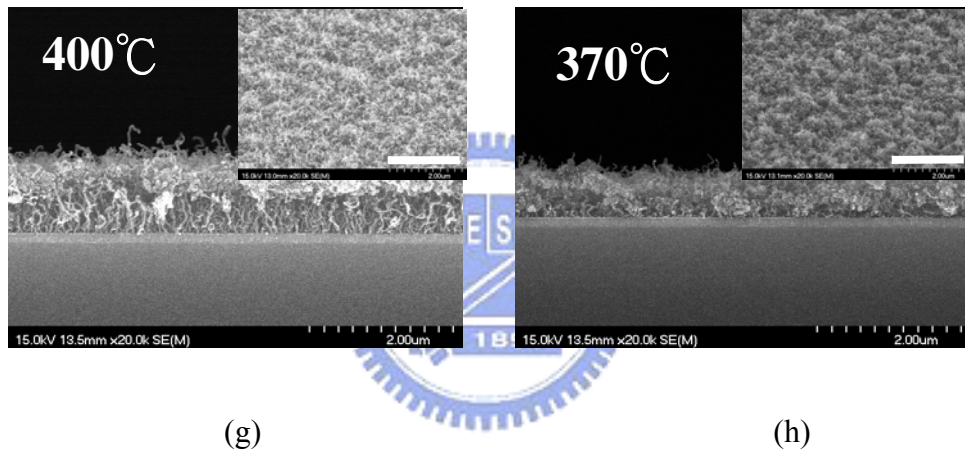
Figure 3.10　SEM images of surface morphologies of samples using multilayer catalysts (20Co/30Ti/100Al) after CNT synthesis process conducted at different temperatures: (a) 700, (b) 650, (c) 600, (d) 550, (e) 500, (f) 450, (g) 400, and (h) 370℃. (The scale bars in the insets represent 2 μ m)
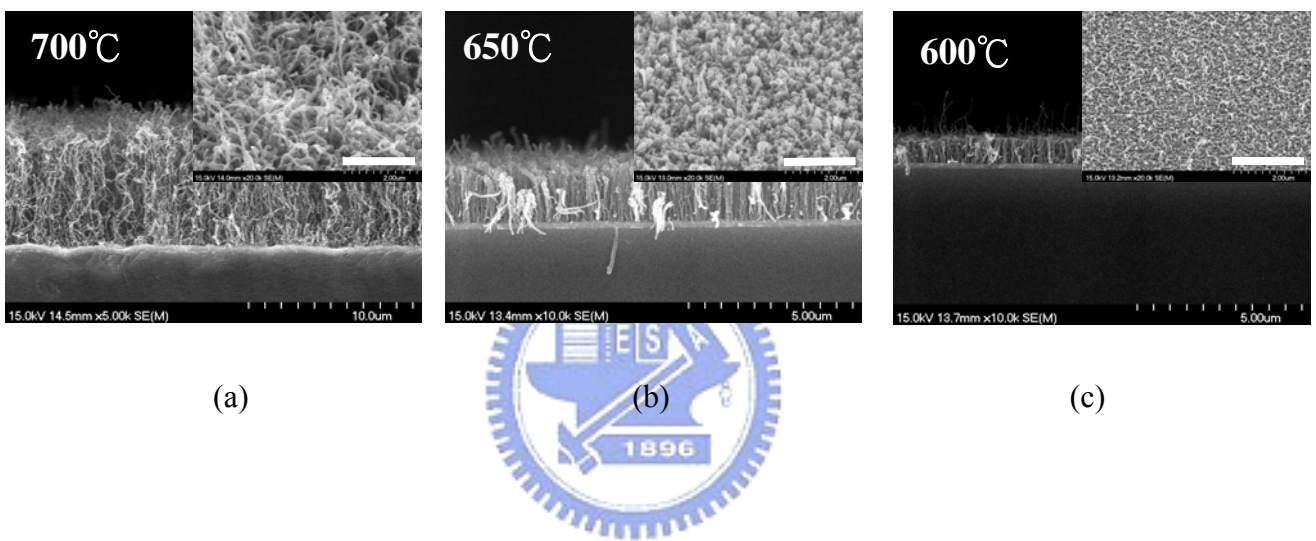
Figure 3.11   SEM images of surface morphologies of samples using single layer catalyst (20Co) after CNT synthesis process conducted at different temperatures: (a) 700, (b) 650, and (c) 600℃. (The scale bars in the insets represent 2 μ m)
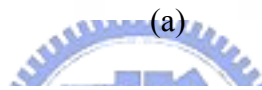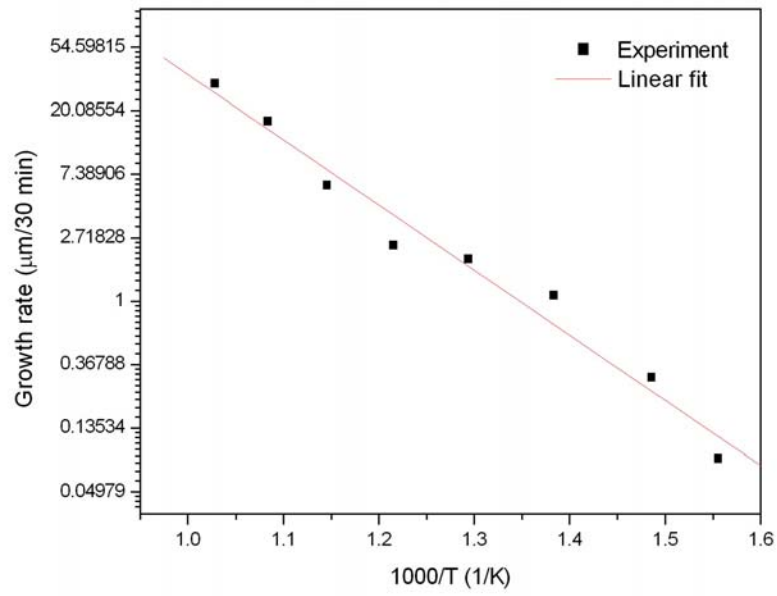
(a)
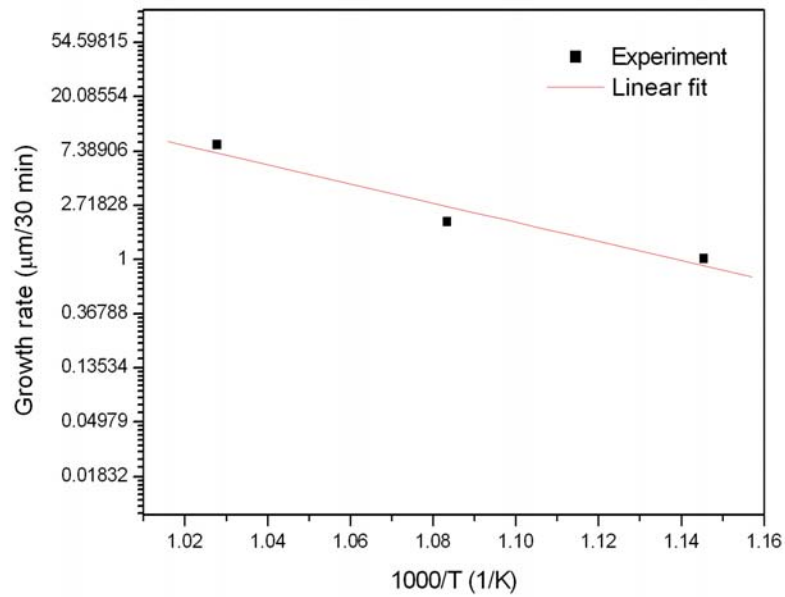
(b)

Figure 3.12   Arrhenius plots for (a) the multilayer catalyst (20Co/30Ti/100Al) and (b) the single layer catalyst (20Co).
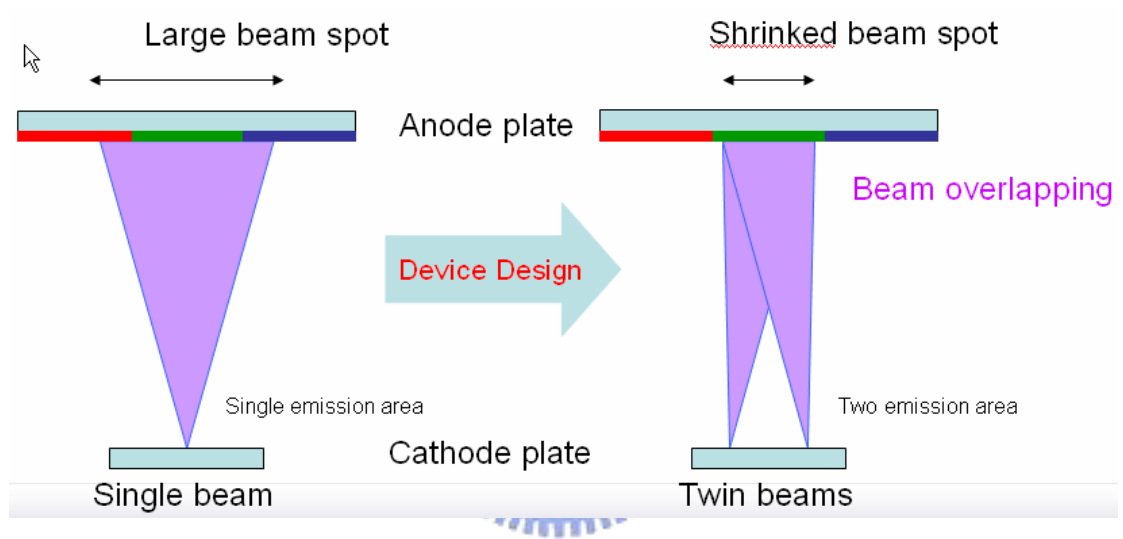
Figure 4.1   Schematic diagrams showing the concept of beam overlapping.
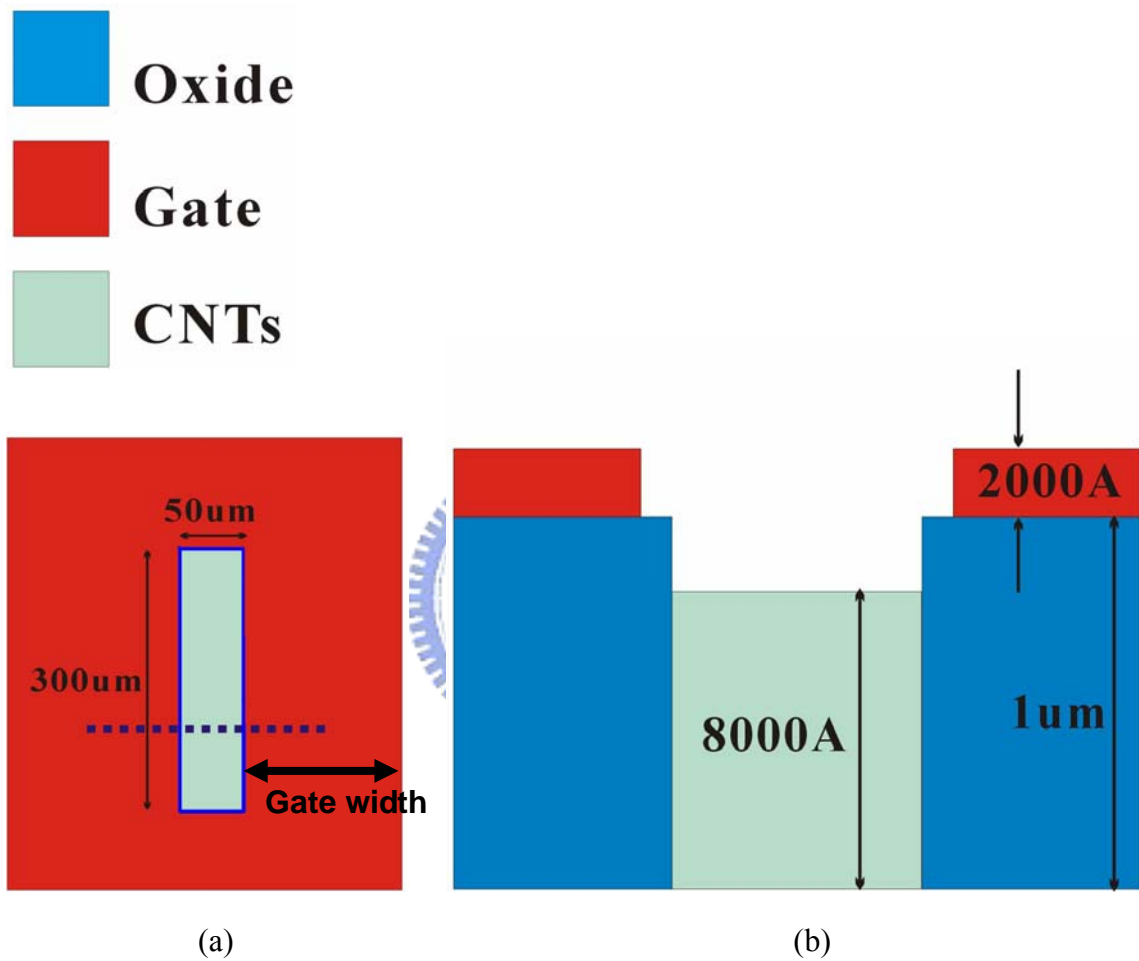
Figure 4.2 Schematic of the conventional gate structure: (a) top image and (b) cross-sectional image.
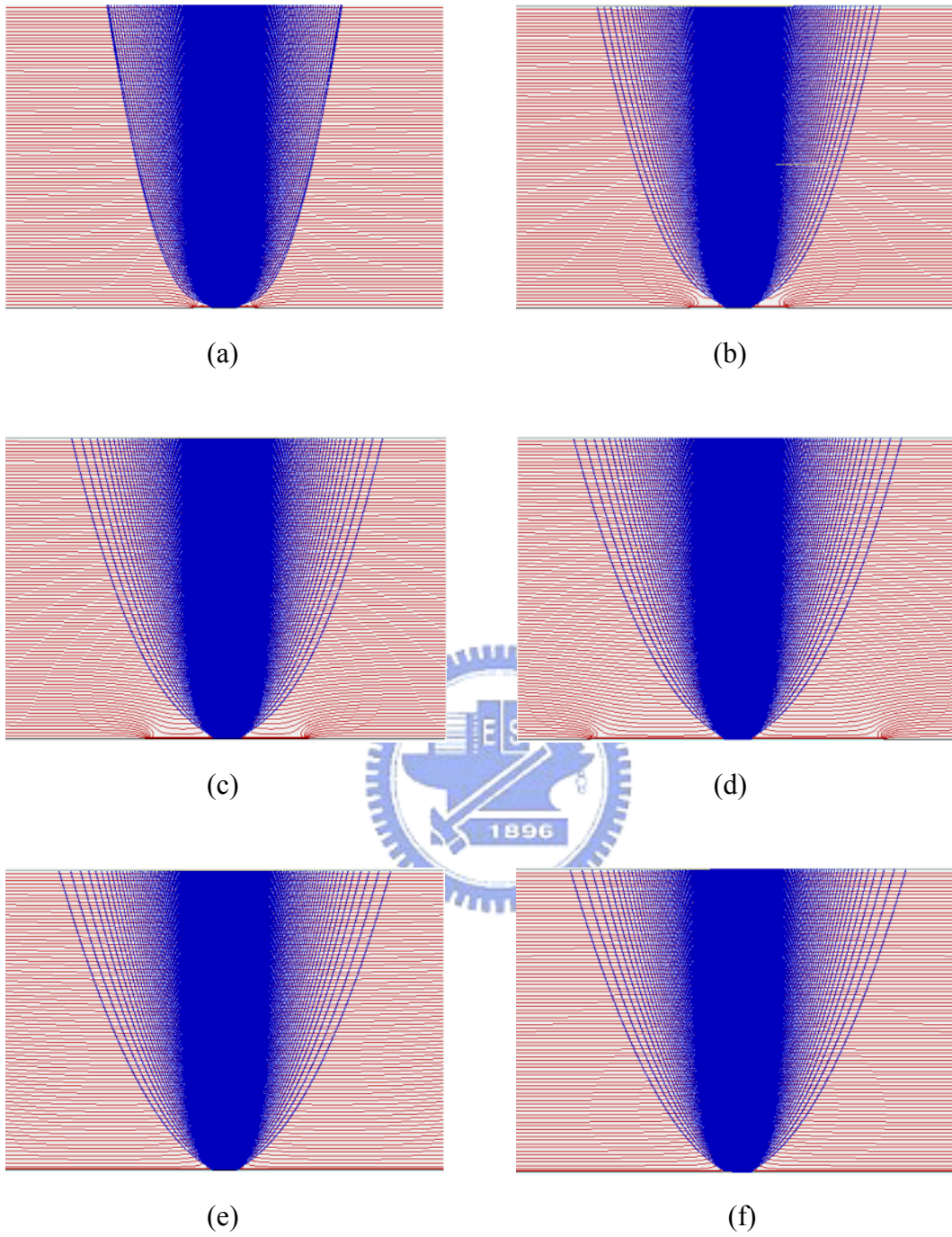
Figure 4.3   The trajectories of electrons emitting from conventional triode devices with different gate widths: (a) 30, (b) 60, (c) 120, (d) 240, (e) 480, and (f) 960 μm.
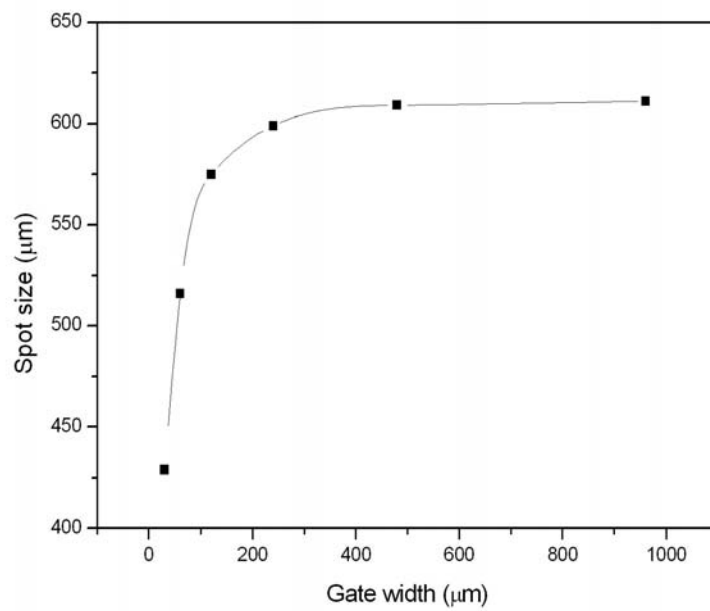
Figure 4.4   Spot sizes as a function of gate width in the conventional gate structure.
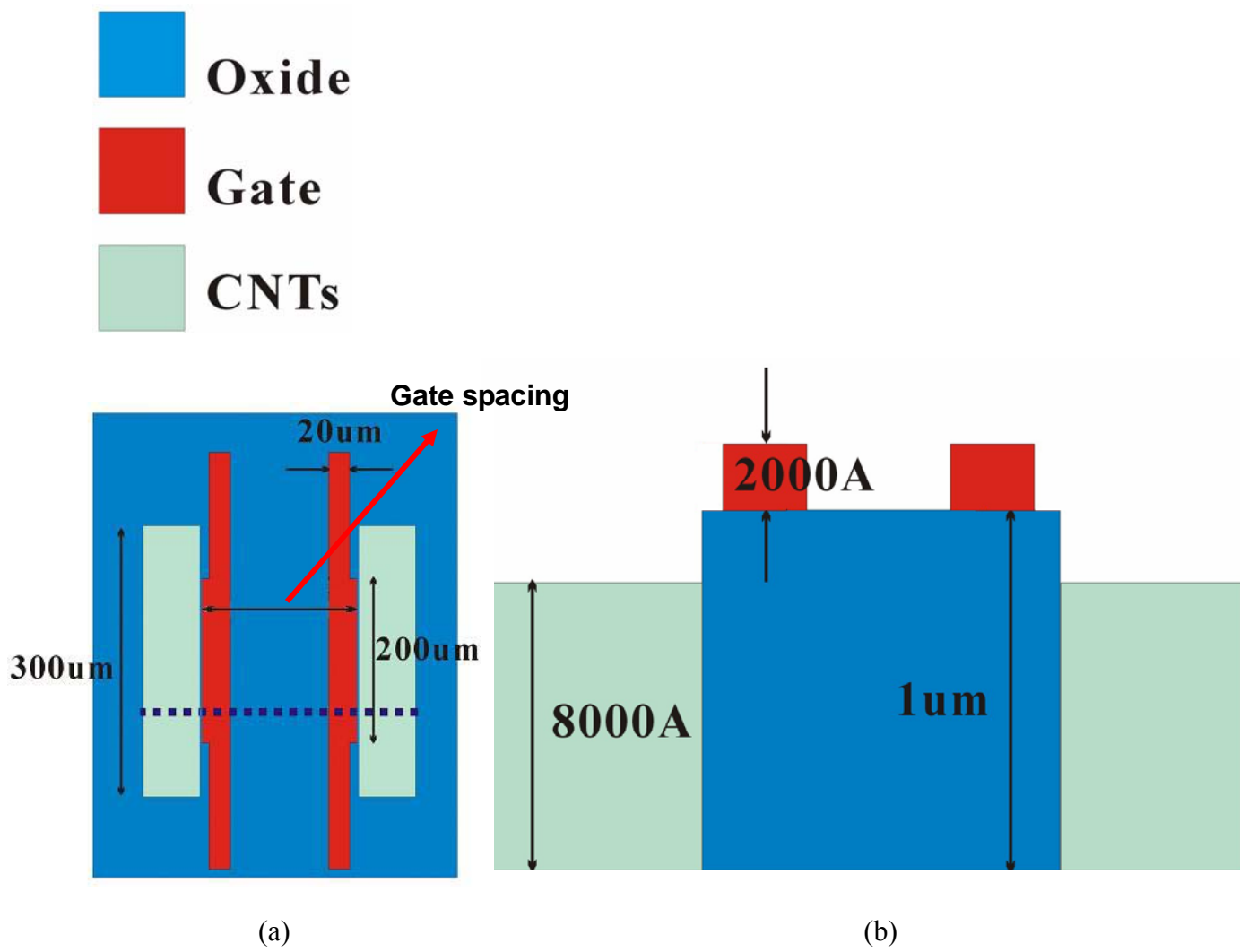
Figure 4.5   Schematic of the focusing gate structure: (a) top image and (b) cross-sectional image.
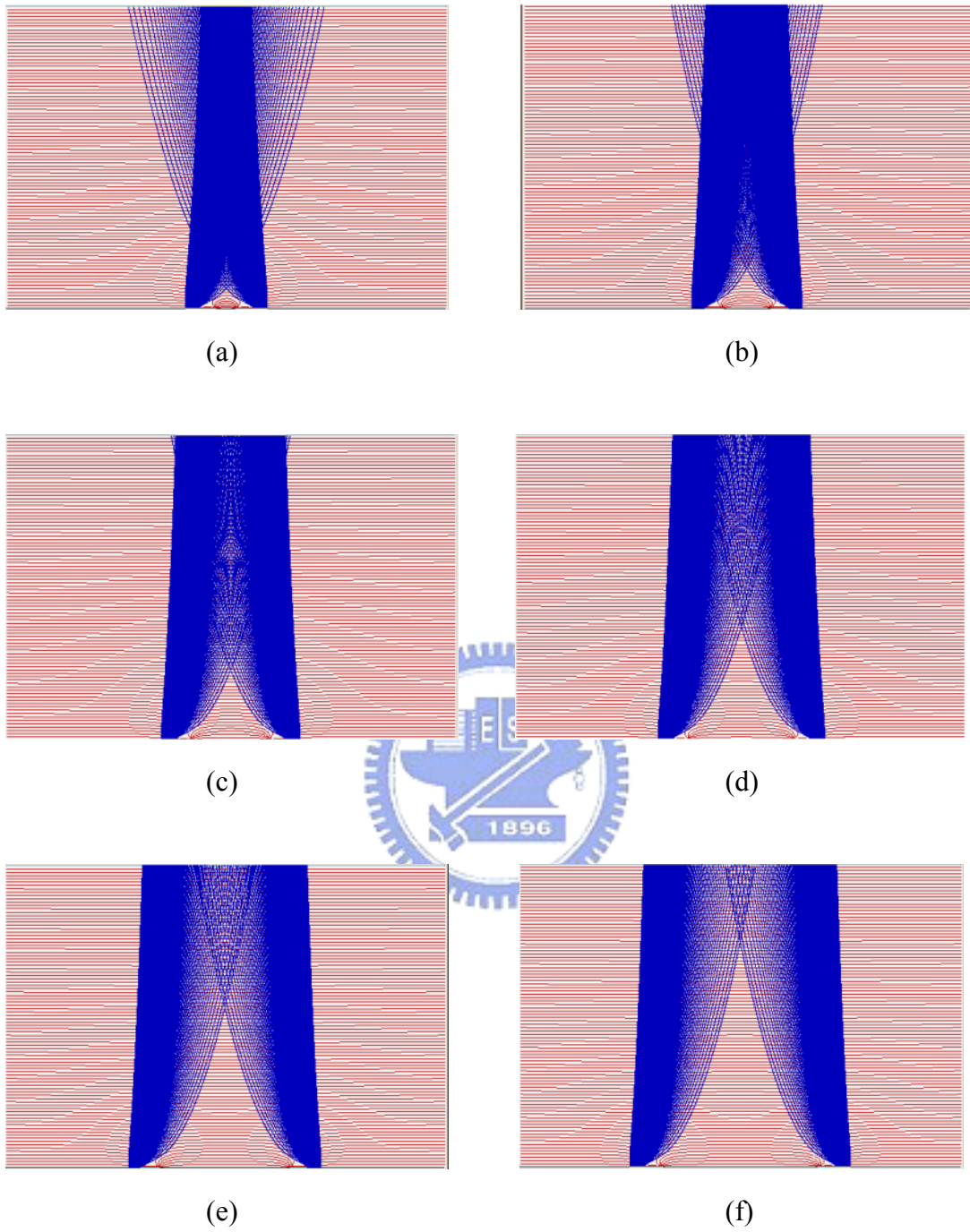
Figure 4.6 The trajectories of electrons emitting from self-focusing gate devices with different gate spacing: (a) 100, (b) 150, (c) 200, (d) 250, (e) 300, and (f) 350 μm.
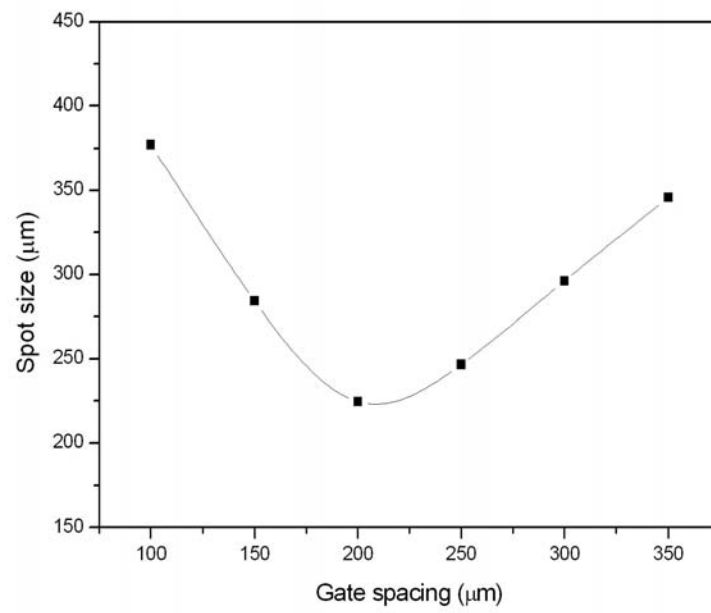
Figure 4.7   Spot size as a function of gate spacing in the self-focusing gate structure.
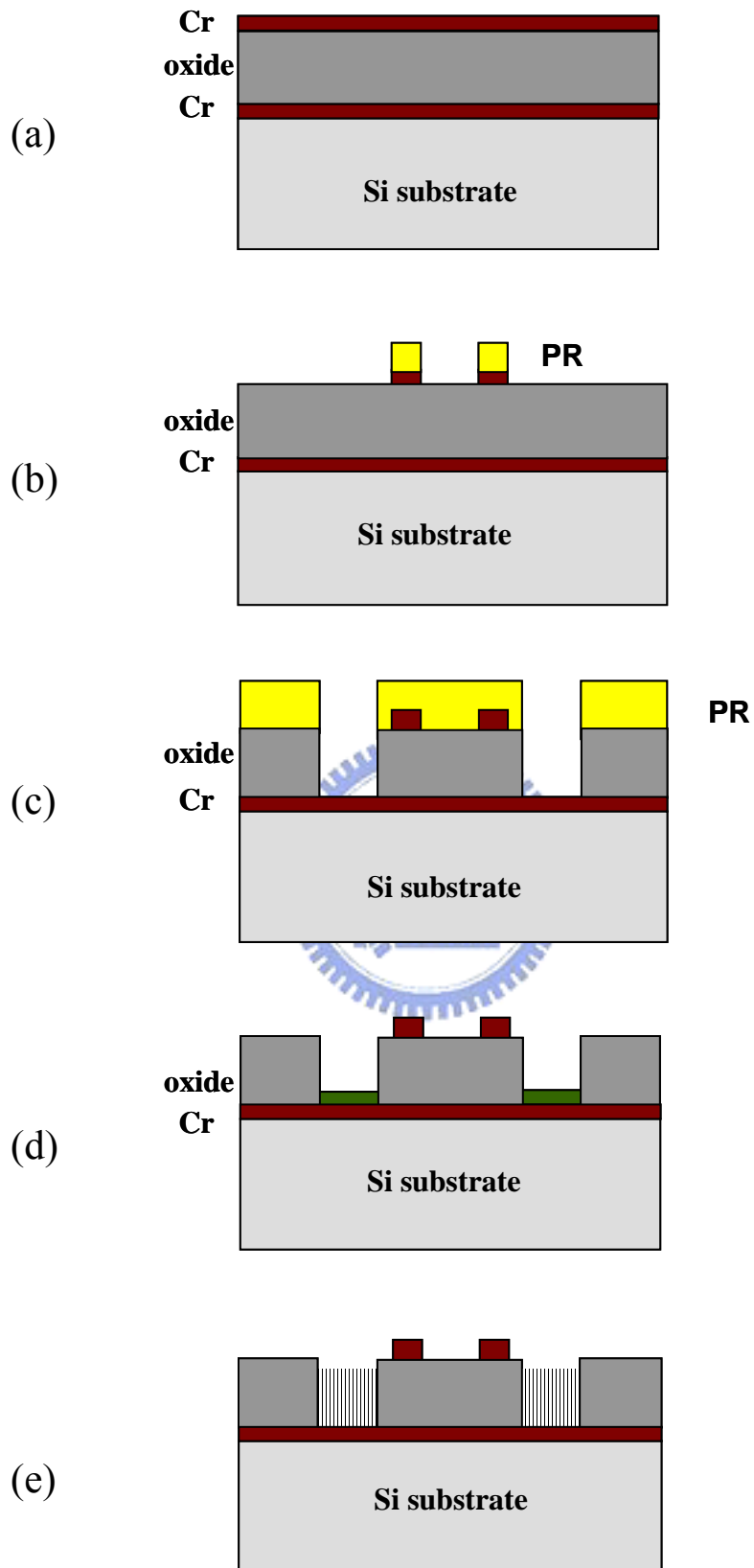
Figure 4.8   Schematic drawings for the process flows of the self-focusing gate devices.
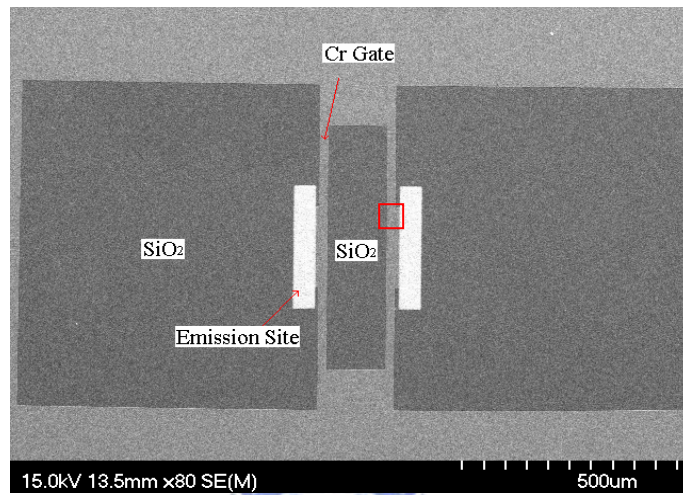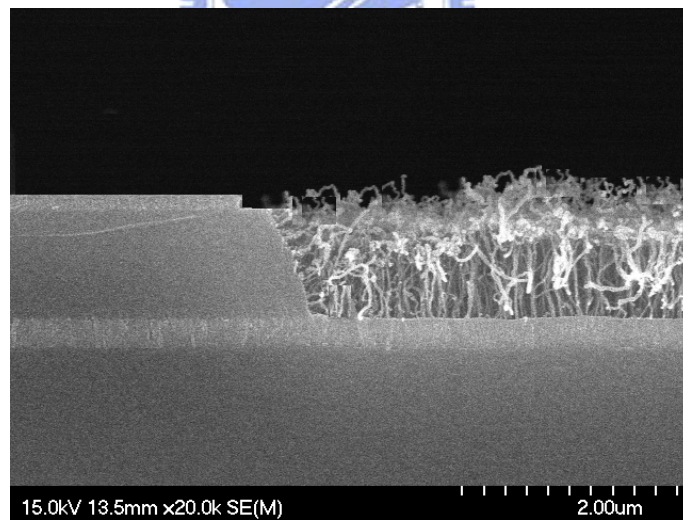
Figure 4.9 SEM images of the self-focusing gate device: (a) top view and (b) cross-sectional view.

139
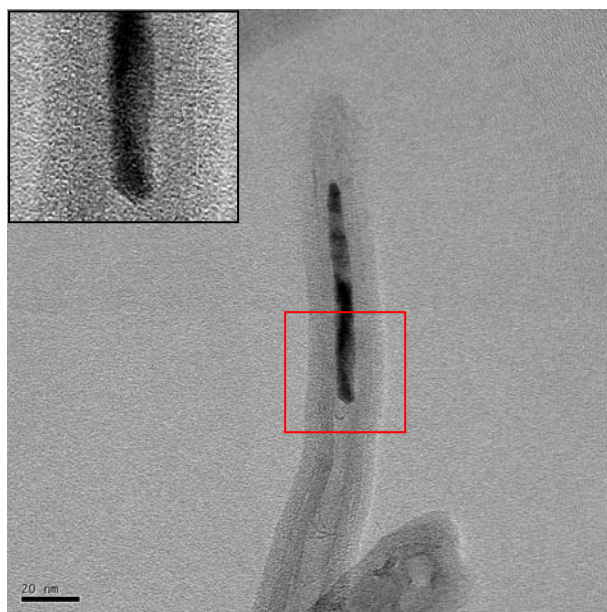
(a)
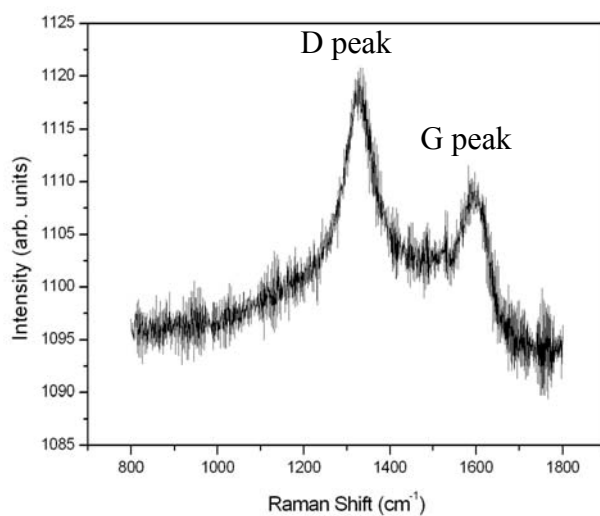
(b)

Figure 4.10   (a) HRTEM image of nanotubes grown with the multilayer catalyst at 500℃, and the inset is an enlarged partial image of the square region. (b) The correlative Raman spectrum of nanotubes.
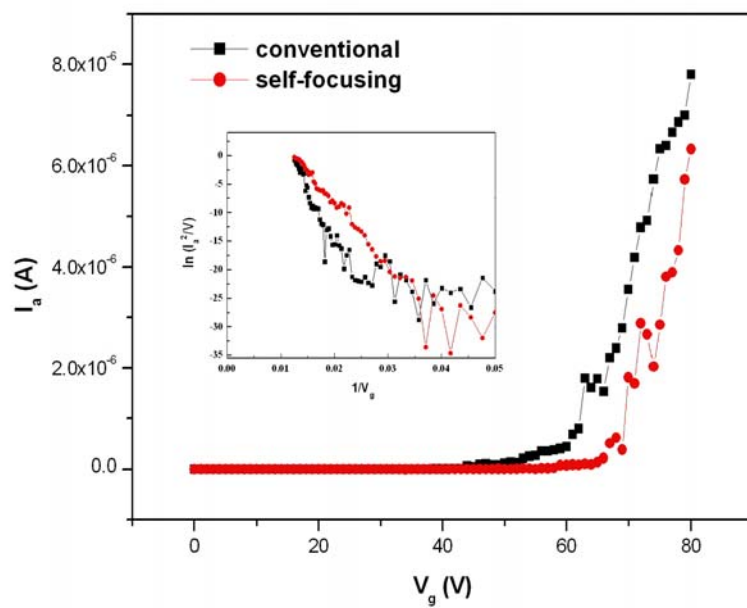
Figure 4.11 (a) Field emission characteristics of conventional and self-focusing gate devices and the inset shows the corresponding FN plot.
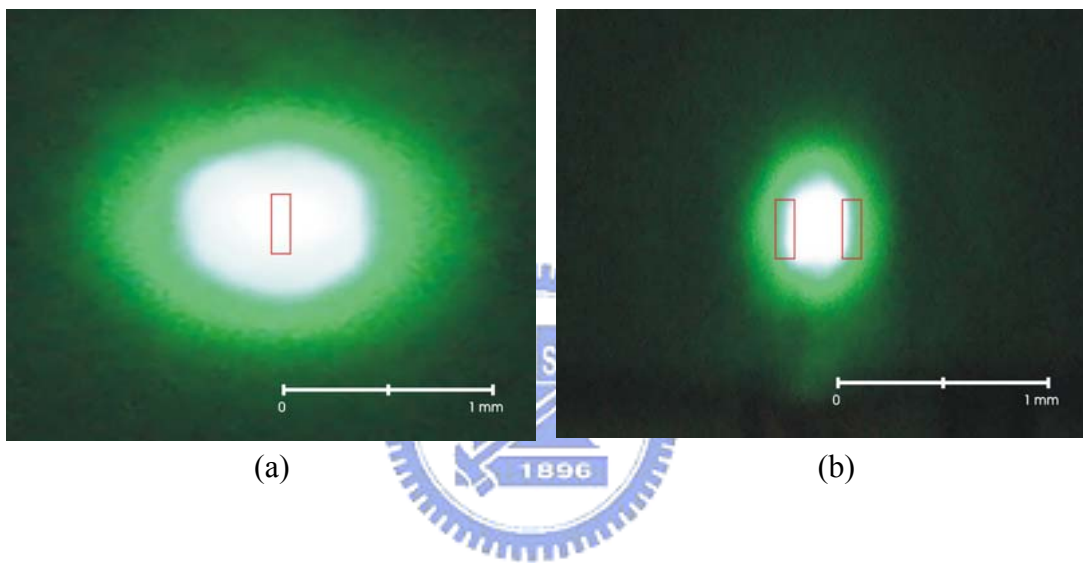
Figure 4.12   Photo-luminescent images of (a) the conventional and (b) the self-focusing gate structure. The squares shown in the images are the corresponding region of CNT emitters of the field emission devices.
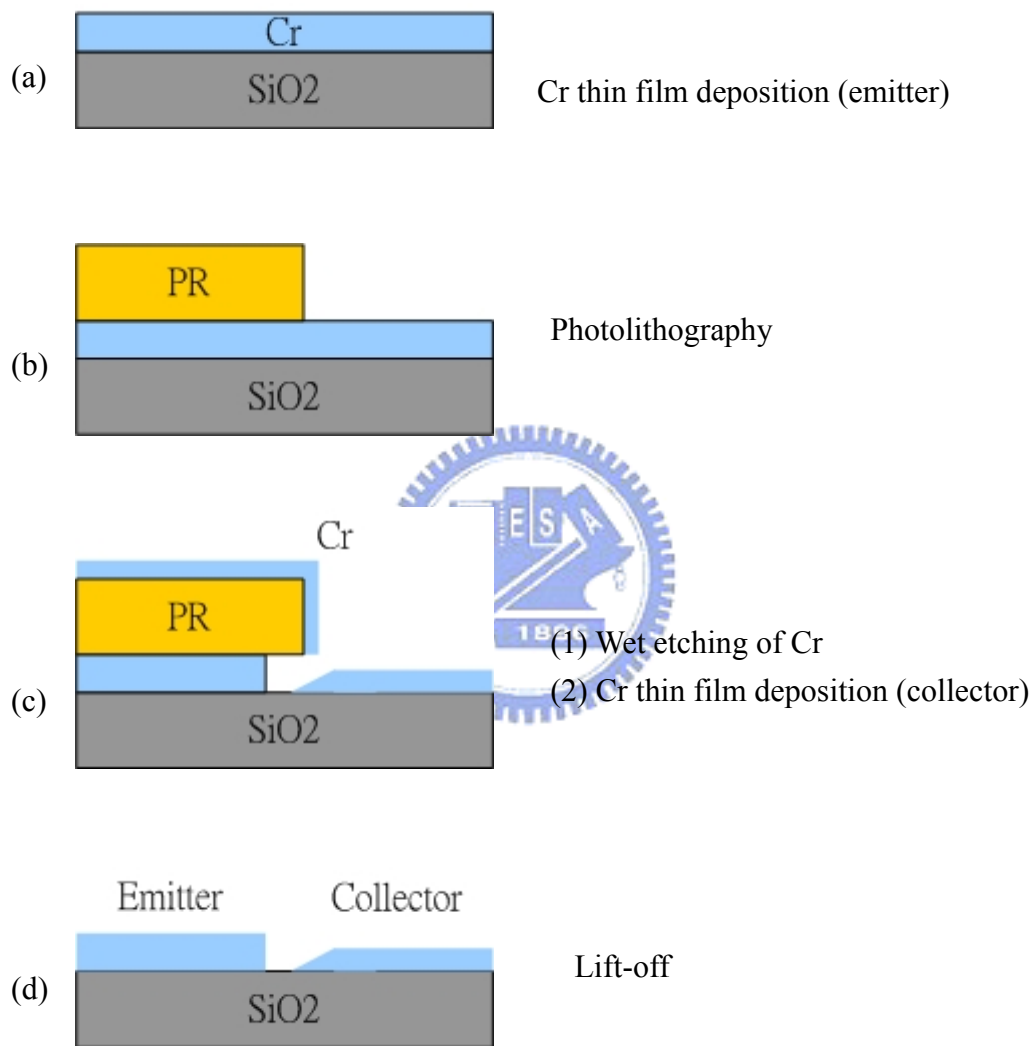
(a) Cr thin film deposition (emitter)

(b) Photolithography

(c) (1) Wet etching of Cr
(2) Cr thin film deposition (collector)

(d) Lift-off

Figure 5.1   Schematic drawings for the process flows of the planar field emitters.
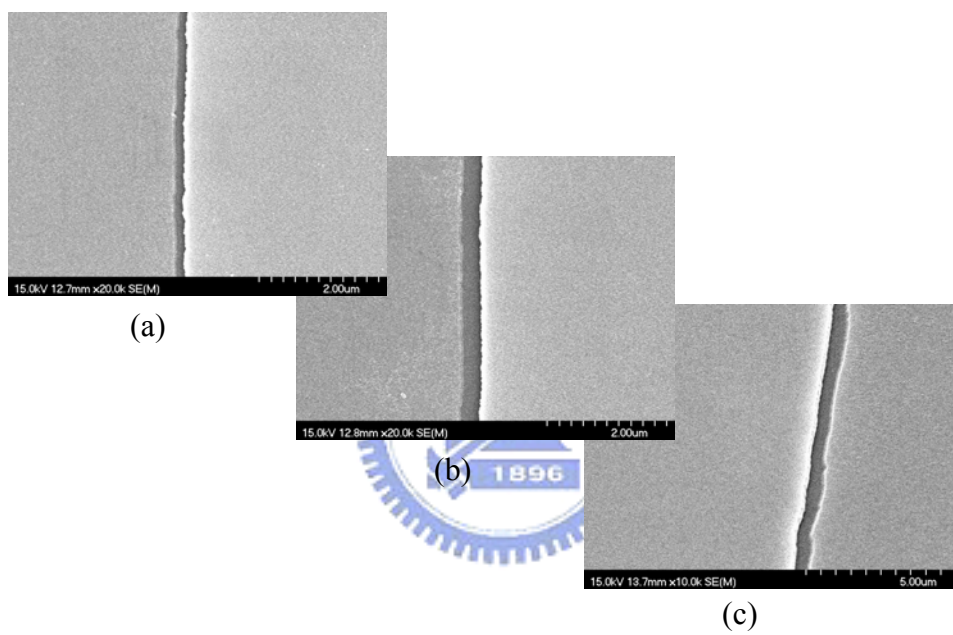
Figure 5.2   SEM images of submicron gaps of planar field emitters with spacing of (a) 200 nm, (b) 300 nm, and (c) 500 nm.
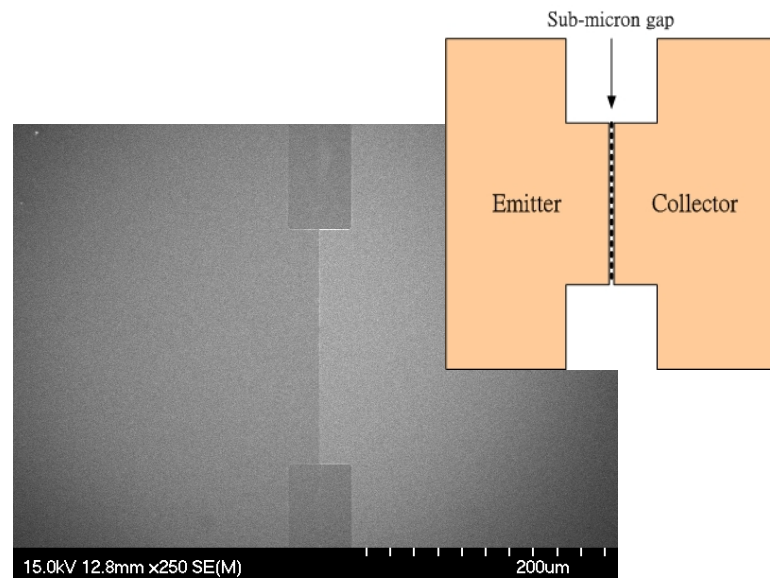
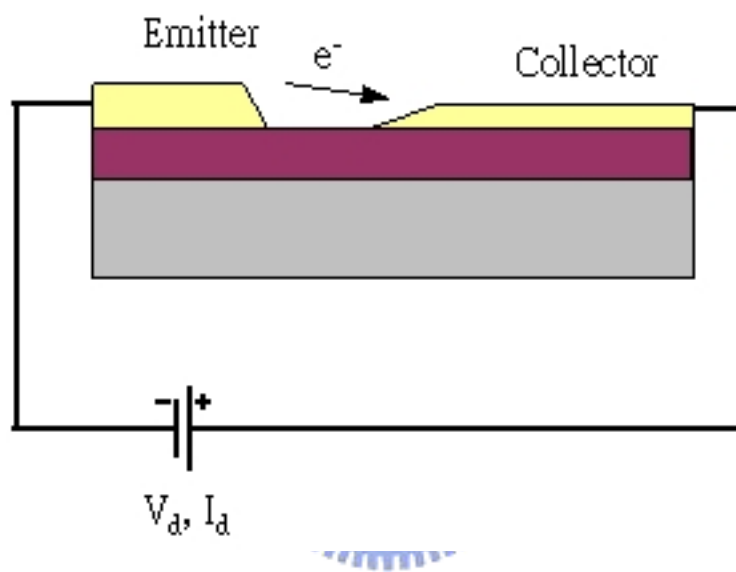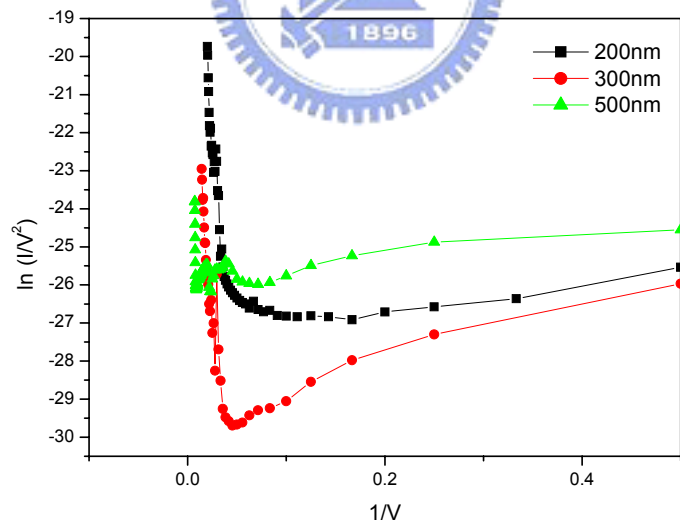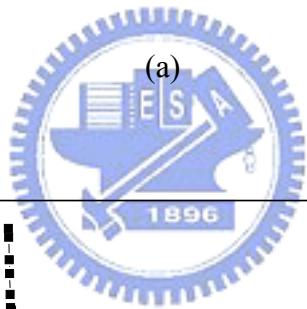Figure 5.3 The top-view SEM image of a planar field emitter and the schematic diagram shown in the inset.
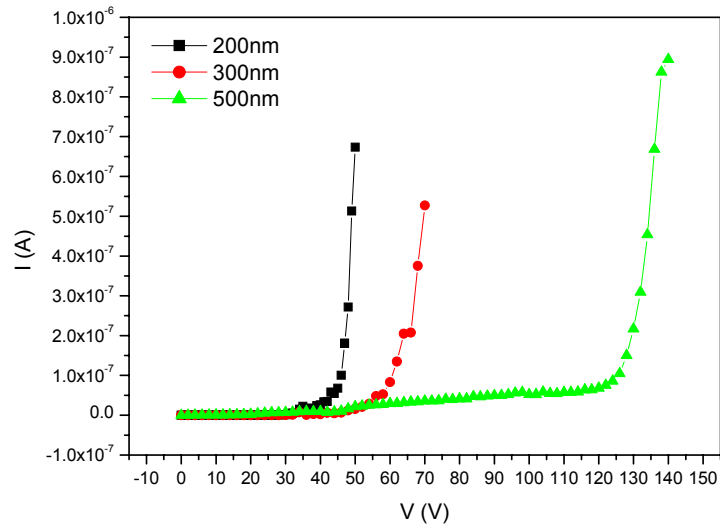
Figure 5.4   A schematic diagram of the field emission measurement of a planar field emission diode.

Figure 5.5 (a) Field emission characteristics of planar edge field emission diodes of different spacing between emitters and collectors and (b) the corresponding FN plot.

SiO₂ (500nm)
First Cr thin film
Silicon substrate

(a)

PR
SiO₂ (500nm)
Cr
Silicon substrate

(b)

SiO₂ (500nm)
First Cr thin film
Silicon substrate

(b)

Second Cr thin film
SiO₂ (500nm)
First Cr thin film
Silicon substrate

(c)

Second Cr thin film
SiO₂ (500nm)
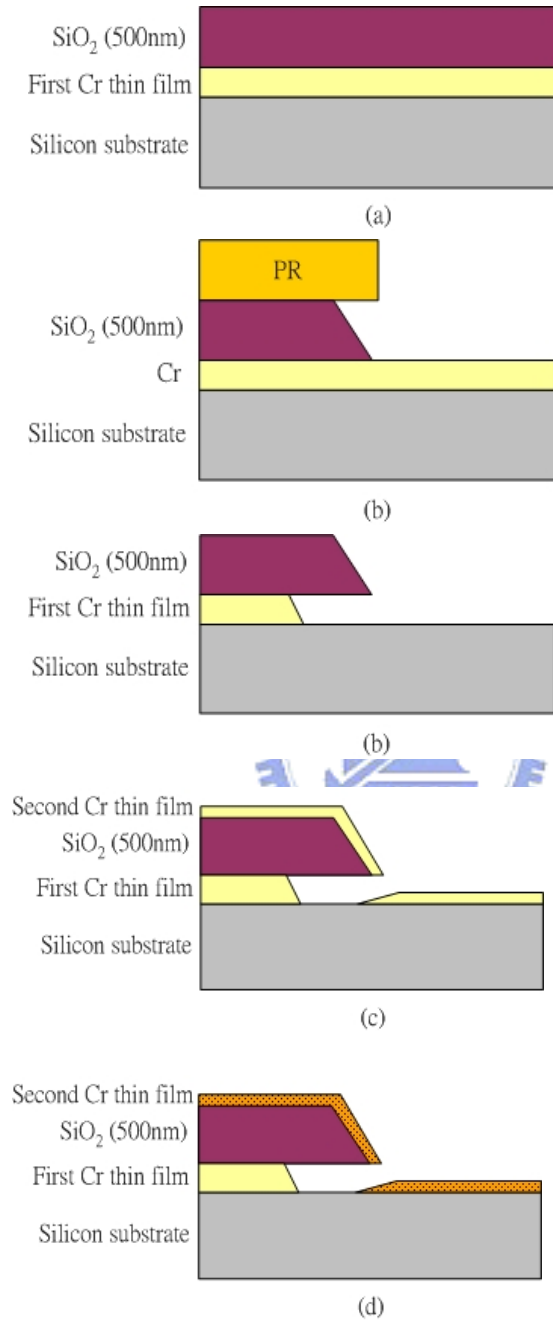First Cr thin film
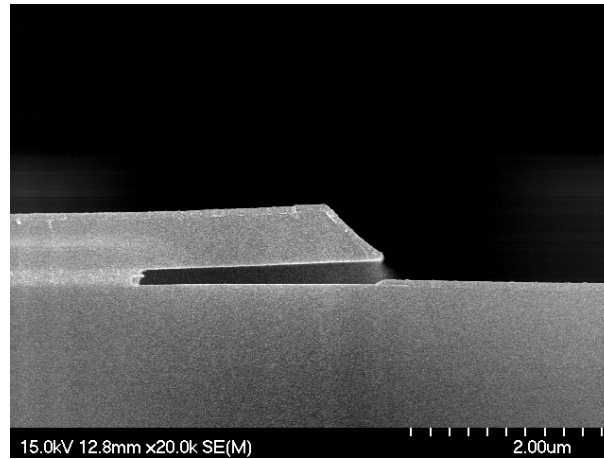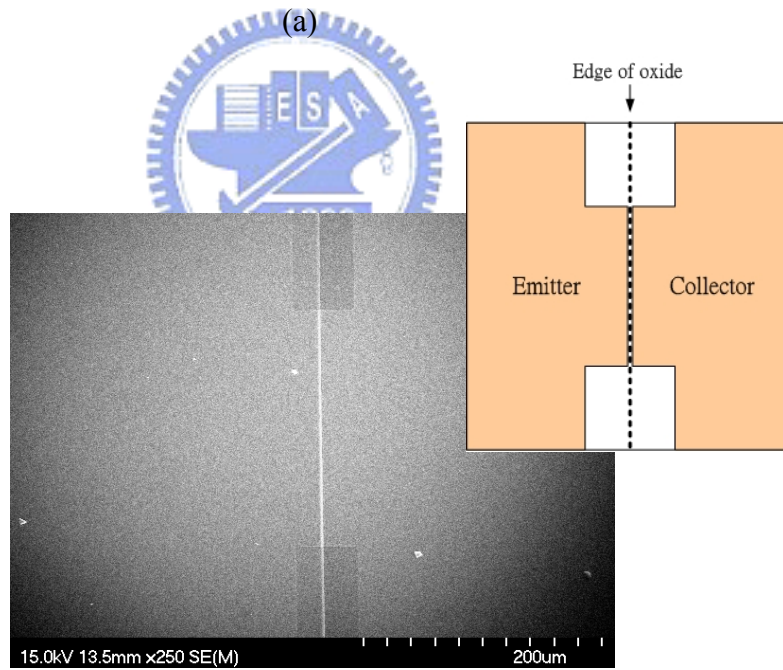Silicon substrate

(d)

Figure 5.6   Schematic drawings for the fabrication procedures of a quasi-planar field emission diode.

(a)

(b)

Figure 5.7   (a) The cross-sectional and (b) top-view SEM images of a quasi-planar field emission diode.

RMS=2.7 nm   RMS=5.7 nm

(a)   (b)

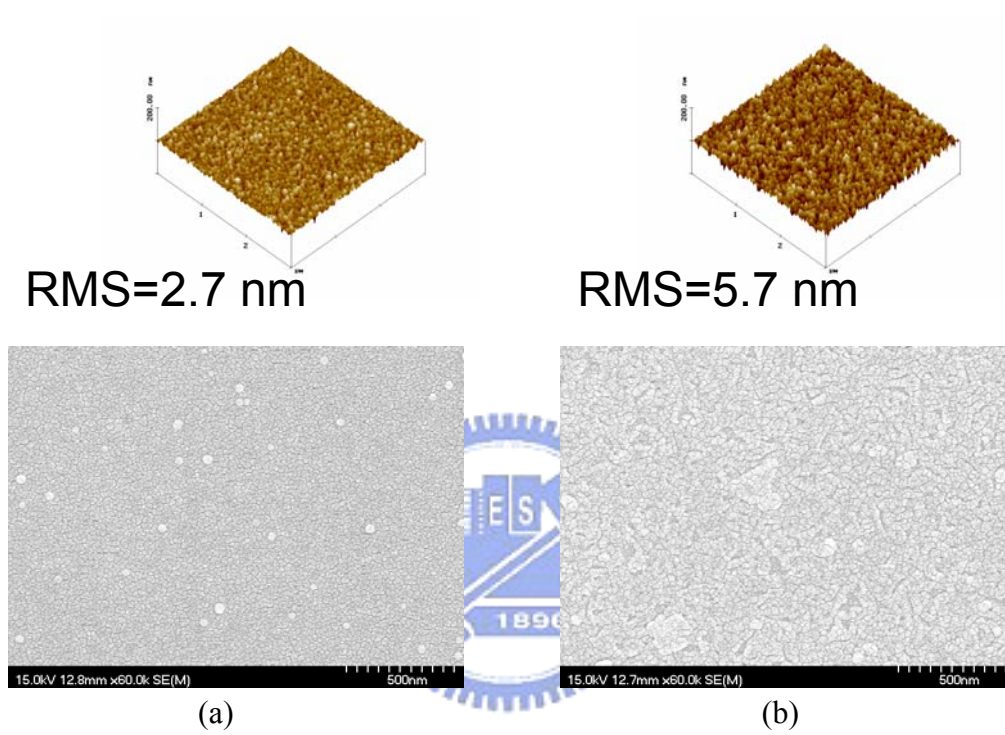Figure 5.8 SEM and AFM images showing the surface morphologies of Cr thin film (a) before and (b) after the forming process, respectively.
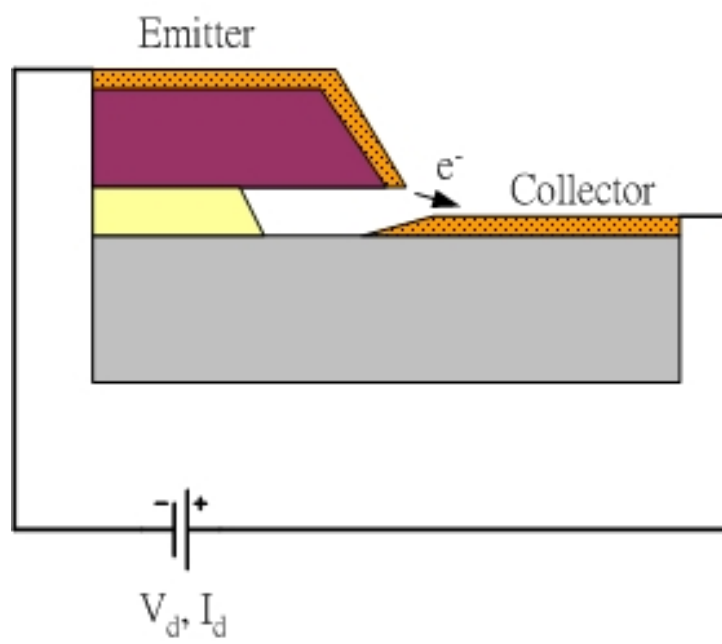
Figure 5.9 A schematic diagram of the field emission measurement of a quasi-planar field emission diode.
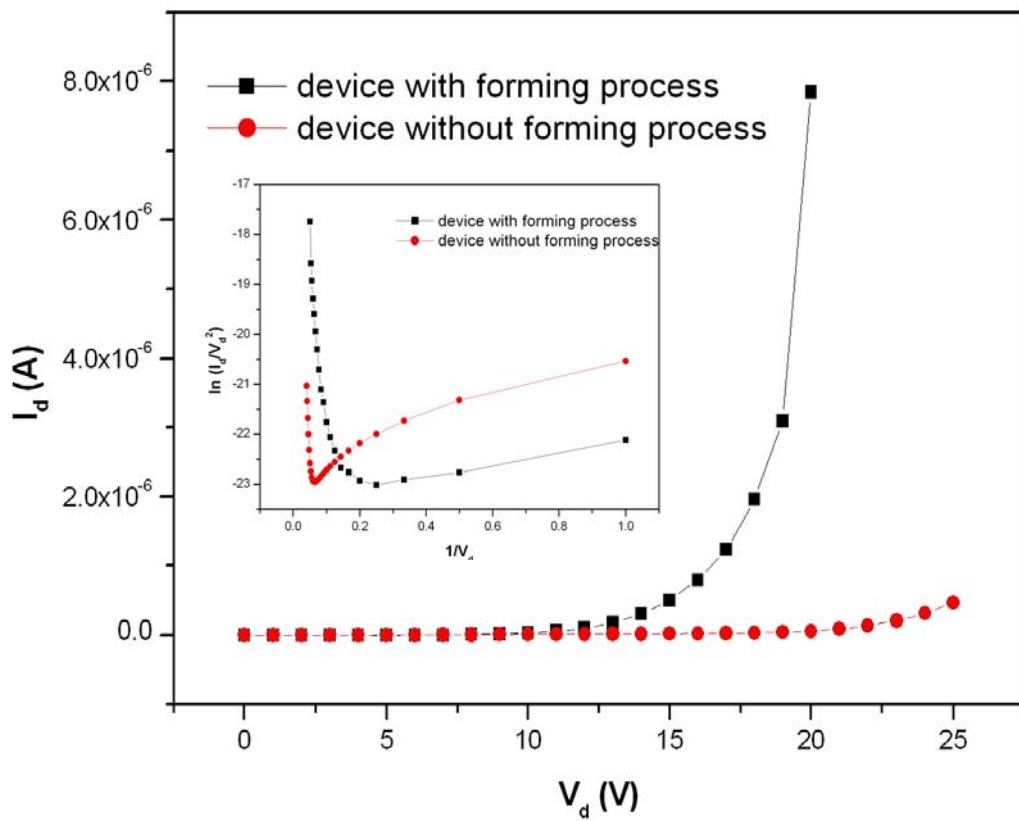
Figure 5.10 Field emission characteristics of quasi-planar field emission devices with and without forming process; the corresponding F-N plot shown in the inset.
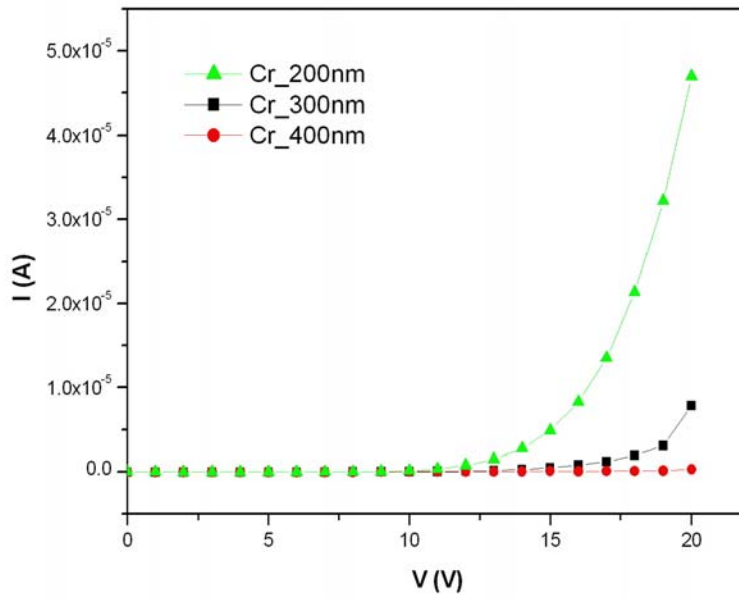
(a)
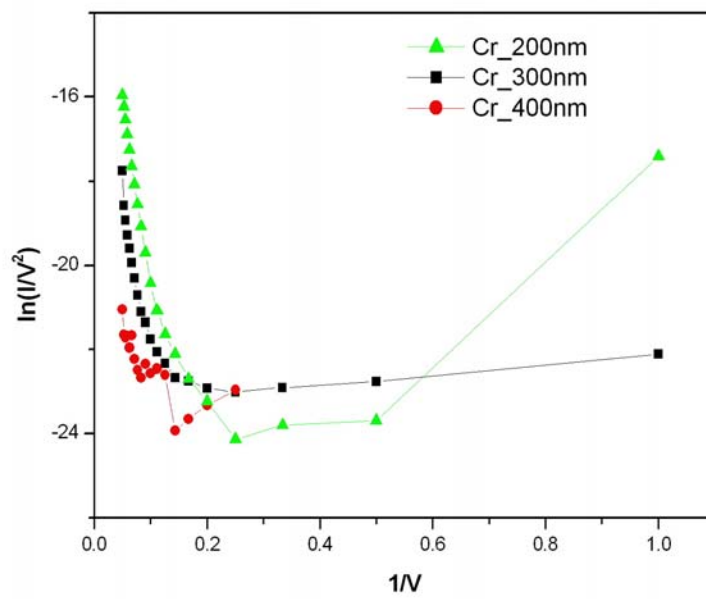
(b)

Figure 5.11   The field emission characteristics of quasi-planar devices with different
thickness of the first Cr layers; (a) I-V curve, and (b) F-N plot.

簡　　歷

姓　　　名: 林高照

性　　　別: 男

出生年月日: 民國六十八年七月七日

籍　　　貫: 台灣省嘉義縣

地　　　址: 嘉義縣番路鄉番路村 8 鄰番路 37-11 號

學　　　歷: 台灣省嘉義高級中學

（83 年 9 月～86 年 6 月）

國立交通大學材料科學與工程學系

(86 年 9 月～90 年 6 月)

國立交通大學電子工程研究所碩士班

(90 年 9 月～91 年 6 月)

國立交通大學電子工程研究所博士班

(91 年 9 月～97 年 6 月)

低溫合成之奈米碳管與薄膜側向場發射子之場發射特性研究

Study on the Field Emission Characteristics of

Low-Temperature-Synthesized Carbon Nanotubes and Thin Film Edge

Field Emitters

Publication Lists

A. International Journal:

[1] Chuan-Ping Juan, Kuo-Ji Chen, Chun-Chien Tasi, **<u>Kao-Chao Lin</u>**, Wei-Kai Hong, Chen-Yu Hsieh, Wen-Pin Wang, Rui-Ling Lai, Kuei-Hsien Chen, and Huang-Chung Cheng, "Improved Field-Emission Properties of Carbon Nanotube Field-Emission Arrays by Controlled Density Growth of Carbon Nanotubes," ***Jpn. J. Appl. Phys.***, Vol. 44, No. 1A, pp. 365-370, 2005.

[2] Rui-Ling Lai, Jiun-Kai Shiu, Yao-Ran Chang, **<u>Kao-Chao Lin</u>**, Pei-Chi Chang, Chuan-Ping Juan, Han-Chung Tai, and Huang-Chung Cheng, "Properties of Carbon Nanotubes via a Ti Capping Layer on the Pretreated Catalyst," ***J. Electrochem. Soc.***, Vol. 154, pp. J109-J115, 2007. (also be collected in the ***Virtual Journal of Nanoscale Science & Technology***)

[3] Chuan-Ping Juan, **<u>Kao-Chao Lin</u>**, Rui-Ling Lai, Kuo-Ji Chen, and Huang-Chung Cheng, "Field Emission Improvement through Structure of Intermixture of Long and Short Carbon Nanotubes," ***Jpn. J. Appl. Phys.***, Vol. 46, No. 2, pp. 859-862, 2007.

[4] Huang-Chung Cheng, Rui-Ling Lai, Yao-Ran Chang, **<u>Kao-Chao Lin</u>**, Chuan-Ping Juan, Pei-Chi Chang, Chien-Ying Lee, and Jiun-Kai Shiu, "Improvement of Luminescent Uniformity via Synthesizing the Carbon Nanotubes on a Fe-Ti Co-deposited Catalytic Layer," ***Jpn. J. Appl. Phys.***, Vol. 46, No. 2, pp. 863-866, 2007.

[5] Huang-Chung Cheng, **<u>Kao-Chao Lin</u>**, Han-Chung Tai, Chuan-Ping Juan, Rui-Ling Lai, Yaw-Shine Liu, Hsia-Wei Chen, and Yu-Ying Syu, "Growth

and Field Emission Characteristics of Carbon Nanotubes Using Co/Cr/Al Mutilayer Catalyst," ***Jpn. J. Appl. Phys.***, Vol. 46, No. 7A, pp. 4359-4363, 2007.

[6] Rui-Ling Lai, Jiun-Kai Shiu, Yao-Ran Chang, **Kao-Chao Lin**, Pei-Chi Chang, Chuan-Ping Juan, Chien-Ying Lee, Hsia-Wei Chen, and Huang-Chung Cheng, "The Reliability Improvements of Carbon Nanotubes Emitters by Using an Fe-Ti Codeposited Catalyst," ***Jpn. J. Appl. Phys.***, Vol. 46, No. 8A, pp. 5367-5372, 2007.

[7] **Kao-Chao Lin**, Chuan-Ping Juan, Rui-Ling Lai, Hsia-Wei Chen, Yu-Ying Syu, and Huang-Chung Cheng, "A Quasi-Planar Thin Film Field Emission Diode," ***Jpn. J. Appl. Phys.***, Vol. 46, No. 11, pp. 7446-7449, 2007.

[8] **Kao-Chao Lin**, Hsia-Wei Chen, Chuan-Ping Juan, Rui-Ling Lai, Yu-Ying Hsu, and Huang-Chung Cheng, "Carbon-Nanotube-Based Field Emission Devices with a Self-Focusing Gate Structure," ***J. Electrochem. Soc.***, Vol. 155, pp. K38-K41, 2008.

B. International and Local Conference:

[1] Chuan-Ping Juan, Chun-Chien Tsai, Kuo-Ji Chen, Wei-Kai Hong, **Kao-Chao Lin**, Chen-Yu Hsieh, Wen-Pin Wang, Rui-Ling Lai, and Huang-Chung Cheng, "Controlled Density Growth of Carbon Nanotubes and its Improvements on Fied-Emission Properties," the ***8th Asian Symposium on Information Display***, pp. 420-423, 2004.

[2] **Kao-Chao Lin**, Rui-Ling Lai, Yao-Ran Chang, Chuan-Ping Juan, Tsung-Ting Chuang, Jiun-Kai Shiu, Han-Chung Tai, and Huang-Chung Cheng, "Constraining the Direction of Carbon Nanotubes by Oxide Capping

Layer," *the 2005 International Conference on Solid State Devices and Materials*, pp. 752-753, 2005.

[3] Rui-Ling Lai, Yao-Ran Chang, Chuan-Ping Juan, Tsung-Ting Chuang, **Kao-Chao Lin**, Jiun-Kai Shiu, Han-Chung Tai, Kuei-Hsien Chen, Li-Chyong. Chen, and Huang-Chung Cheng, "Improvement of Breakdown Field of Carbon Nanotubes by a Ti-Capping Layer on Catalyst Nanoparticles," *the 2005 International Conference on Solid State Devices and Materials*, pp. 832-833, 2005.

[4] Jiun-Kai Shiu, Rui-Ling Lai, Yao-Ran Chang, Chuan-Ping Juan, **Kao-Chao Lin**, Tsung-Ting Chuang, Han-Chung Tai, and Huang-Chung Cheng, "Density Control of Carbon Nanotubes by Ti-Fe Co-deposition," *Taiwan Display Conference*, 06-019, 2006.

[5] **Kao-Chao Lin**, Tsung-Ying Chuang, Han-Chung Tai, Chuan-Ping Juan, Rui-Ling Lai, Yao-Ren Chang, Jiun-Kai Shiu, and Huang-Chung Cheng, "Low Temperature Growth of Carbon Nanotubes by Thermal Chemical Vapor Deposition using Novel Catalyst," *Taiwan Display Conference*, 06-018, 2006.

[6] Huang-Chung Cheng, Rui-Ling Lai, and **Kao-Chao Lin**, "Carbon Nanotubes-Based Field Emission Deisplays," *the International Electron Devices and Materials Symposia 2006*, invited talk, 2006.

[7] Han-Chung Tai, Tsung-Ying Chuang, Chuan-Ping Juan, Yao-Ren Chang, Rui-Ling Lai, **Kao-Chao Lin**, Jiun-Kai Shiu, Wen-Pin Wang and Huang-Chung Cheng, "Relatively Low Temperature Growth of Carbon Nanotubes by Thermal Chemical Vapor Deposition using Novel Catalysts," *the Material Research Society 2006 Spring Proceedings*, Vol. 922E, U7-16, 2006.

[8] Chuan-Ping Juan, **Kao-Chao Lin**, Rui-Ling Lai, Jung-Yen Yang, and Huang-Chung Cheng, "Field Emission Improvement from Pillar Array of Aligned Carbon Nanotubes," *the 2006 International Conference on Solid State Devices and Materials*, pp. 722-723 (P-9-4), 2006.

[9] Hsia-Wei Chen, **Kao-Chao Lin**, Yaw-Shing Leou, Yu-Ying Hsu, Rui-Ling Lai, Pei-Chi Chang, Chien-Ying Lee, Chuan-Ping Juan, and Huang-Chung Cheng, "Study on Carbon Nanotubes Synthesized at Low Temperatures Using Multilayered Catalytic Films," *the International Display Manufacturing Conference 2007*, P2-02, 2007.

[10] Pei-Chi Chang, Rui-Ling Lai, **Kao-Chao Lin**, Hsia-Wei Chen, Chuan-Ping Juan, Chien-Ying Lee, Yu-Ying Hsu, Chia-Hao Chang, and Huang-Chung Cheng, "Pillar-shaped Carbon Nanotubes by Ti-Fe Codeposition," *the International Display Manufacturing Conference 2007*, P2-03, 2007.

[11] **Kao-Chao Lin**, Hsia-Wei Chen, Rui-Ling Lai, Chuan-Ping Juan, Yu-Ying Hsu, and Huang-Chung Cheng, "A Quasi-planar Thin Field Emission Diode," *the 2007 International Conference on Solid State Devices and Materials*, pp. 618-619, 2007.

[12] Hsia-Wei Chen, **Kao-Chao Lin**, Chuan-Ping Juan, Yaw-Shing Leou, Yu-Ying Hsu, and Huang-Chung Cheng, "A Field-Emission Device with Novel Self-Focus Gate Structure," *the 2007 International Conference on Solid State Devices and Materials*, pp. 1178-1179, 2007.

C. Local Journal:

[1] 林高照、陳國基、鄭晃忠，"場發射顯示器技術介紹"，電子月刊第 85 期，2002 年八月號

[2] 賴瑞霖、**<u>林高照</u>**、鄭晃忠,"平面顯示器新星-淺談奈米平面顯示器",零組件雜誌 2003 年四月號

[3] 阮全平、**<u>林高照</u>**、賴瑞霖、謝振宇、傅珍貴、莊宗穎、張耀仁、鄭晃忠,"奈米碳管場發射顯示器",電子月刊第 109 期,2004 年八月號

[4] **<u>林高照</u>**、賴瑞霖、鄭晃忠,"奈米碳管場發射顯示器元件技術",電子月刊第十二卷第八期,2006 年八月號

[5] 賴瑞霖、**<u>林高照</u>**、鄭晃忠,"場發射顯示器應用之奈米碳管技術",電子資訊第十二卷第二期,2006 年十二月

[6] Rui-Ling Lai, **Kao-Chao Lin**, Pei-Chi Chang, Jiun-Kai Shiu, Yao-Ren Chang, Chuan-Ping Juan, Jien-Yin Lee, and Huang-Chung Cheng, "Improvements of Uniformity and Reliability for the Electron Emission of Carbon Nanotubes in High Vacuum Environment," 真空科技,2007 年十九卷第四期